Bismuth Ferrite Sensitization of Nanostructured Titanium Dioxide and/or Zinc Oxide-based for Photovoltaic Device Applications

A Thesis

Submitted to the Faculty

of

Drexel University by

Jonadan Ando Burger

in partial fulfillment of the requirements for the

degree

of

Master of Science in Materials Science and Engineering

2010

Dedications

'For freely you have received, so freely shall you give'
Lord Jesus Christ in Matthew 10:8[trans., Bible]

Advisor: Dr. Jonathan Spanier

MML Labmates: Terrence, Stephen, Eric, Eitan, Mike, Jennie, Stephanie, Greg, Guannan, Dominic, Brian, Chris, Mark, Oren

NEAT Collaborators: Dr. Jason Baxter, Hasti, Kevin, Ishai

BNL: Dr. Charles Black, Jon, Chang-Yong, Raluca, Danvers; Dr. Widera's FaST team; other CFN, BNL, and SULI staff, and other summer program participants

Family: Mom, Dad, Brother (Daniel), Sunshine, Tibbs, Freckles, Chippies, Chiperoo, Granny(RIP, PLGB God Willing, Bless, And Glory Always Be), Papa, Uncle (Nick), paternal grandparents, uncles, and cousins, and the multitude of relatives on the maternal side as well

Neighbors: All the good folk I grew up 'paling around' with, particularly the Blazowskis, Demorys, and Biegels, but all of them really have had some impact on my life somewhere

Friends: especially the sustainable energy and 'nerding out' fans among them, and those that got the 'brunt' or 'blunt end' of my hard times, and the roommates past and present, judo friends and frat bros, and the church-folk and priests around St. John's and St. Agatha-St. James

Judo: Judo instructors and teammates and particularly in memory of Kurokawa-sensei

PSP: fraternity "bros", especially my 'big' Tiff and 'adoptive big' Regina, but all of the "brothers" of the Gamma Xi chapter of Phi Sigma Pi

MSE, etc.: faculty and staff who have helped along the way, as well as any other *Drexel* professors and staff and *grade school* and *high school* teachers and staff along the way, along with *martial arts* and *religion* teachers; your devotion, teaching, assistance, etc. mean so much to me still

The folks at the boatyard (Kreuters, etc.) and the farmstand (Rottkamps, etc.), those 'honest work, honest pay' type jobs that I've had in between here and there

Many others of all kinds and callings, esp. those on 'trial', for one never knows whose lives make a difference in theirs or theirs could make a difference in

And Very Most Importantly Always All Good Unto The Lord God Up Above †<3^^
Peace, Love, And God Bless, All And Every, And Forever May His Glory Be…!

Acknowledgements

The folks of the MML; My advisor Dr. Jonathan E. Spanier, for his continued guidance, tolerance, backing, and mercy, as well as the initial ideas that spurred this project to ‘life’, I likely would not have known or thought of it without his assistance.

Labmates Terrence(nominal grad. mentor), Stephen(may as well at some point have been my grad. mentor), Eric (‘adopted’ grad mentor and IV-guy), Eitan, Mike, Jennie, Stephanie, Greg, Guannan, Dominic, Brian, Chris, Mark, Oren; for sharing the lab-space, training me on various techniques and equipment, continued assistance, ordering stuff for me, and helping out and creating the dynamic and production that is the MML at Drexel.

The NEAT lab group in ChE; Dr. Baxter, Hasti, Kevin, Thinh, Glenn, Ishai; for sharing your lab-space and training me on dip-coating and thin-film synthesis, ‘spotting me’ some solution/precursors, FTO glass, etc., literature, past thesis work, and ideas. For basically being those ‘good neighbors’ that [metaphorically] ‘lend [one] some sugar’ ☺. Thanks much Ishai for the thesis from which my ‘outline’ and ‘ordering’ was initially based, and some reference(s) and protocol came from, though I’m not sure we ever met. Dr. Baxter for being on my committee; sharing advice, space, time, and resources. Kevin for dip-coating lit. and know-how. Thihn and Hasti for dealing with my ‘shenanigans’ of science and screw-ups and scheduling and such, and Hasti’s advice/help from time to time, whether she knows it or not, plus assistance with solar simulator IV measurements.

Various folk at BNL; Electronic Nanomaterials Group: Dr. Charles Black, Jon, Chang-yong, Raluca, Danvers. Prof. Widera’s FaST team; for really ‘piquing’ my interest in and driving my [current] research towards sensitized photovoltaics. Rest of the CFN, SULI, and BNL Staff; Sensei Mark; and other program participants.

The MSE department faculty and staff; Dr. Z. on my committee, Judy upon her retirement and all her great service to the dept. as a whole, and professors/teachers, in this and other departments/schools, for I’ve had many great classes, teachers, and academic experiences, among other things, at Drexel as a MSE student as well as on the roads to there and now beyond. Keiko, Dorilona, Yeneeka for dealing with my ‘shens’ [again]. And Dr. Wegst for insight and feedback. Also thanks for the recommendation letters team! And other folks in labs around here (‘Johnson’, Wei (Dr. Shih’s Lab), Volker (Dr. Gogotsi), and Babak (Dr. Barsoum), and Zakiya (Dr. K. Lau) to name a few ‘fairly direct’ (at least ‘attempted’ ^.^t) contributors of some sort.

CRF Staff for their training, availability, guidance, etc., and maintenance of the facilities. Jay Bhatt and the other library folk for database access and re-access….

My judo friends, instructors and teammates, other students, and the art itself; for the good times, great fights, excellent training, and lifestyle of maximum efficiency, strength and service, and mutual benefit and welfare for all.

My family, each and every one, particularly those ‘closest to home’ and providing continued support, tolerance, and guidance in many ways (Mom, Dad, Daniel, Sunshine, Tibbs, Freckles, Chippies, Chiperoo, Granny, and Papa). You know how you’ve been there, words may not be ample to describe all the familial support and contributions I’ve received ‘across the board’.

My supervisors and co-workers at previous jobs and the ‘honest work, honest pay’ types of things done in the past.

My ‘nerd’ and other friends, here and abroad, and classmates and their continued shenanigans, sharing, good times, and great support. And the Wikipedia/Google Scholar/MS Office(+help)+Paint/etc.

Priests and church friends, as well as anyone and everyone throughout who may benefit from my work or I’ve benefited from something of theirs God-given and used well.

And Very Most Importantly Always All Good Unto The Lord God Up Above For His Many Gifts And Blessings And All That He Does And Continues To Do For All Creation, Always And Forever, Alleluia, and Amen! †<3^^!!!! Peace, Love, God Bless, to all and every, And Unto the LORD, May Glory Always Be….

Table of Contents

List of Tables

Abstract

Bismuth Ferrite Sensitization of Titanium Dioxide Nanowire-based Photovoltaic Devices
Jonadan A. Burger
Jonathan E. Spanier, Ph.D.

Bismuth ferrite (BFO) is a 'mid-range' band gap, multiferroic (ferroelectric, antiferromagnetic) material of interest in numerous applications[39,96,100-106]. Though its use in photovoltaic applications has been investigated[39,96,100-102,104,105] with interesting result, such a material has not yet been used as a photovoltaic sensitizer/thin absorber in sensitized solar cell (SSC) or extremely thin absorber solar cell (eta-SC) devices. A band gap (E_g~2.2-2.8eV) [40,100,103,105,117,139,147] within the visible light range (albeit high) makes BFO a potential candidate for such application. Moreover, BFO is ferroelectric (E_c ~500-600kV/cm, $P_r = 60\mu C/cm^2$)[100,159], which provides the material with an internal electric field (which can be directed/'poled' towards one electrode or another in a(n) SSC/eta-device), which may provide an additional mechanism for either or both charge separation and transport.

CuSCN/ZnO, CuSCN/TiO_2, CuSCN/Bi-Fe-Zn-O/ZnO, CuSCN/BFO/TiO_2 thin-film 'sandwich-like' structures were fabricated on transparent-conducting-oxide-glass (TCO) substrates, via combinations of electrodeposition and suspension or sol-gel (requiring 'high temperature' for crystallization) dip-coating, and characterized at various stages of production to assess material/phases present, optical absorbance characteristics, and preliminary electronic device performance. 'High-temperature' heat treatments in air or N_2 of Bi-Fe-Zn-O/ZnO samples result in films yielding crystalline non-BFO phases, while O_2 annealing of similar samples appear promising. BFO has been successfully

crystallized on nearly-pure anatase TiO_2 synthesized/deposited two ways, as well as on F:SnO_2-glass. Moreover, BFO is found to enhance absorbance in at least a portion the visible portion of the electromagnetic spectrum. Such are promising signs that thin-absorber-PV devices based on either TiO_2 or ZnO may be viable for development in the near future.

CHAPTER 1: INTRODUCTION

1.1 Background and Motivation

The United States Department of Energy (US DoE) Energy Information Administration (EIA) predicts, as of 2006, that world energy consumption is expected to increase by over 18% (85 quadrillion Btu) by the year 2015 and almost 45% by 2030 (Fig. 1.1.1)[1]:

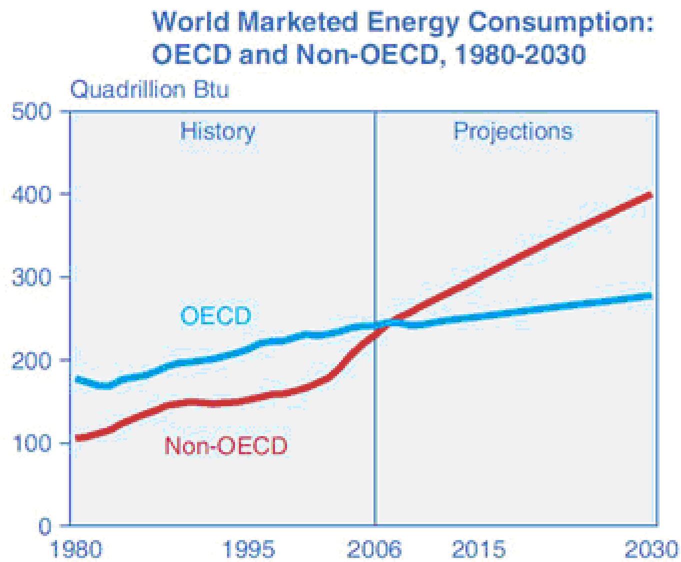

Figure 1.1.1[1]: World marketed energy consumption, historical and projected (OECD is Organization for Economic Cooperation and Development)

Electricity is a major and vital part of energy production and consumption throughout much of the world today. From 2006 onward, electrical power generation is expected to jump by approximately 31% (~5.5 trillion kWhr) by 2015 and by almost 78% (~13.8-13.9 trillion kWhr) by 2030 (Fig. 1.1.2)[1]:

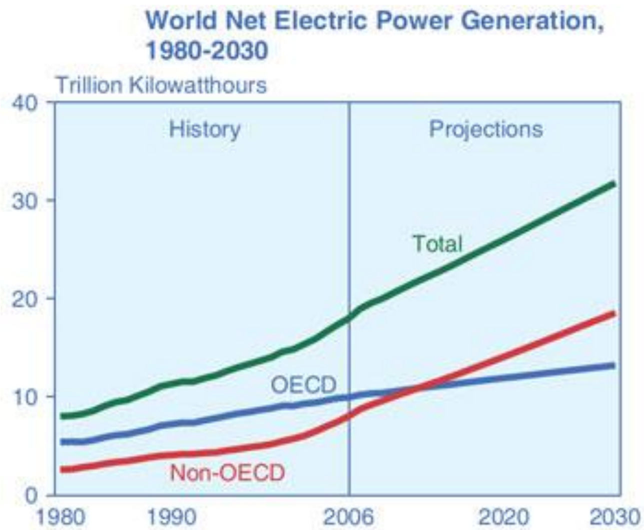

Figure 1.1.2[1]: World electricity generation, historical and projected

The supply of fossil fuels is non-renewable and decreasing with increased consumption of and demands for energy. Undesirable byproducts from and environmental consequences of the combustion of such for energy production have become more profound and realized[2]. Carbon dioxide and other greenhouse gas emissions from human activities have markedly increased since the onset of industrialization in the 19th century[4], correlated with and likely leading at least somewhat to climate change and consequences of global warming[4]. Moreover, NO_x and SO_x gasses are also byproduct emissions from the burning of fossil fuels, which can cause respiratory sensitivity/irritation[5], as well as acid rain (from NO_x and SO_2 gasses forming the strong acids HNO_3 and H_2SO_4, respectively[2,6], NO_x gasses have also been shown to contribute to O_3 formation/pollution[5]) and its consequential environmental hazards/destruction to organisms and the landscape, ecosystem "shifts"/"unbalancing"/disruption[2,6]. Other unfavorable byproduct air pollutants include CO and particulates (which also lead to some degree of respiratory sensitivity/ailment/issues[5], as well as smog). Figure 1.1.3[3] illustrates the contributions of various human activities to such air pollutants.

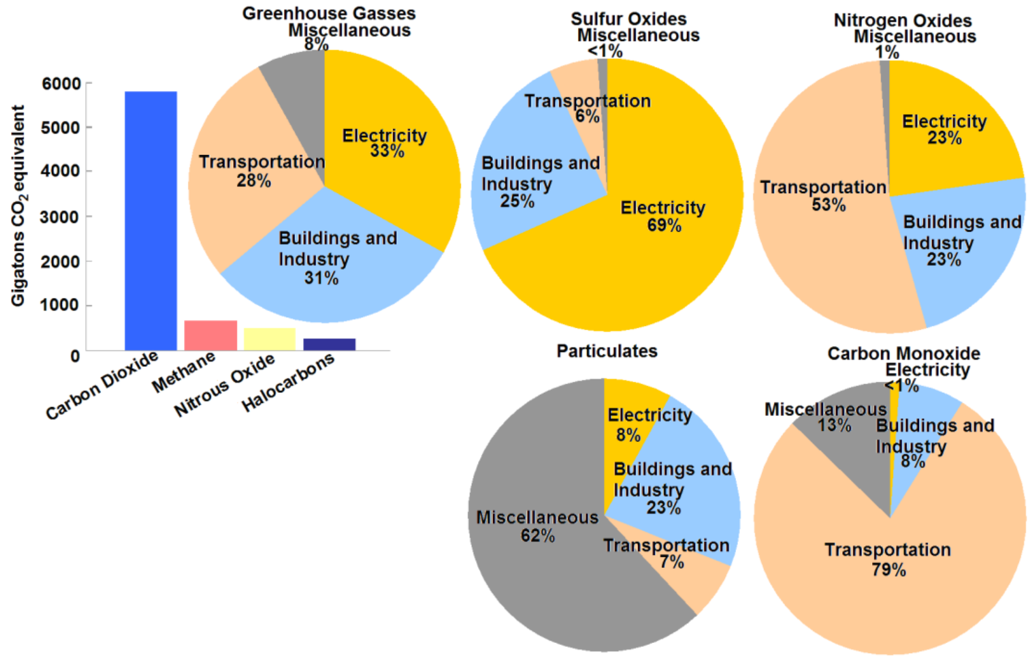

Figure 1.1.3[3]: a) Amount of greenhouse gasses produced annually (by species) for all sectors b) Contribution of each sector to various greenhouse and irritant byproduct gasses and pollutants

As shown in the above figure, electricity generation is a major source of several undesirable air pollutants and undesirable byproducts such as greenhouse gasses, acid-rain-forming compounds, and general air pollutants/irritants. However, the demand for energy and particularly for electricity (seen previously in Fig. 1.1.2) is on the rise, and a vital part of current technology and society, as well as future development. Clean, renewable/sustainable production of electricity is therefore a requirement for the sustenance of modern civilization, infrastructure, and technological progress, coupled with the conservation and/or rebuilding of our surrounding environment, throughout present-day society. In 2002, the International Energy Agency (IEA) determined that increased government involvement in the promotion of clean, renewable energy solutions in lieu of fossil-fuel burning plants and facilities *significantly* above their current efforts to do so could lead to a 16% *decrease* in CO_2 emissions alone by the year 2030 (not to mention the likely marked decreases in other emissions such as other greenhouse gasses, NO_x, SO_x, CO, and particulates as a result of burning less fossil fuels to meet energy demands), *despite* a predicted population increase of ~2 billion people (and hence a higher energy/electricity demand worldwide)[7] between now and that time.

The US DoE EIA lists five major energy sources that fit this category: biomass, geothermal, hydroelectric, solar, and wind power[8]. According to the EIA, “renewables” are the fastest-growing ‘class’ of energy sources, with an annual ‘jump’ in consumption of ~3.0% annually[1]. Solar-harvesting technologies (solar thermal energy (STE) and photovoltaic (PV) devices and plants) are a favorable alternative energy solution, particularly for electricity generation, for a number of reasons. For one, though in varying amounts, solar energy is, quite fortunately and remarkably, widely available throughout the entire world[7] (Fig. 1.1.4)[9-11]:

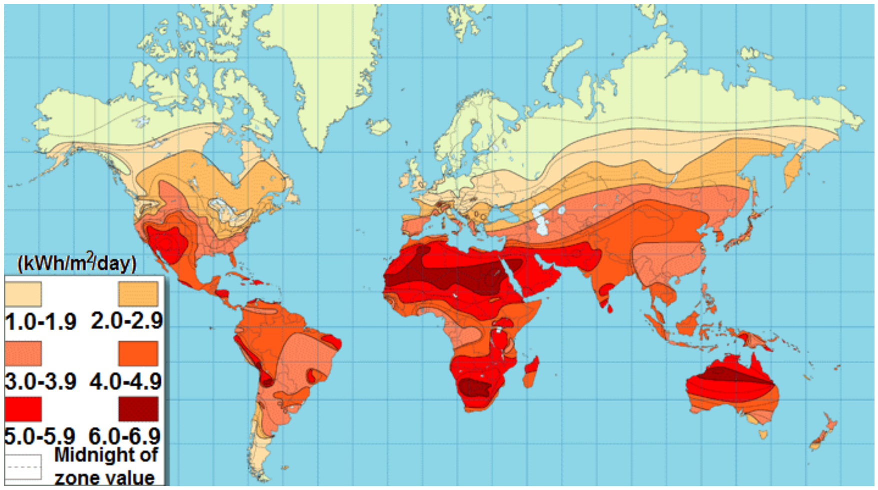

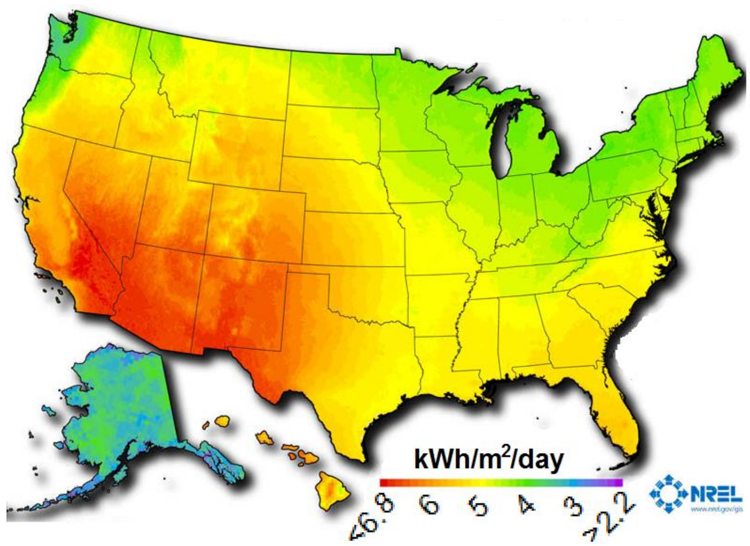

Figure 1.1.4[9-11]: Average daily solar insolation for the world [during the month of least sunlight] (top) and the US [averaged over the course of a year] (bottom)

Furthermore, using a few strategically "high intensity" sunlight areas based on the above map, it has been shown that the energy demands of the world could be, at least hypothetically, completely met by photovoltaic power, assuming 2000 hours (out of 8760 hours total) per year of 1,000W/m^2 striking intensity on 20% efficiency panels (Fig. 1.1.5)[12]. Note that the total projected area required for such a project by 2030 (496,805km^2) is less than the total land area of the country of Spain[13](~98.6%) or the state of Texas[14] (~71.4%).

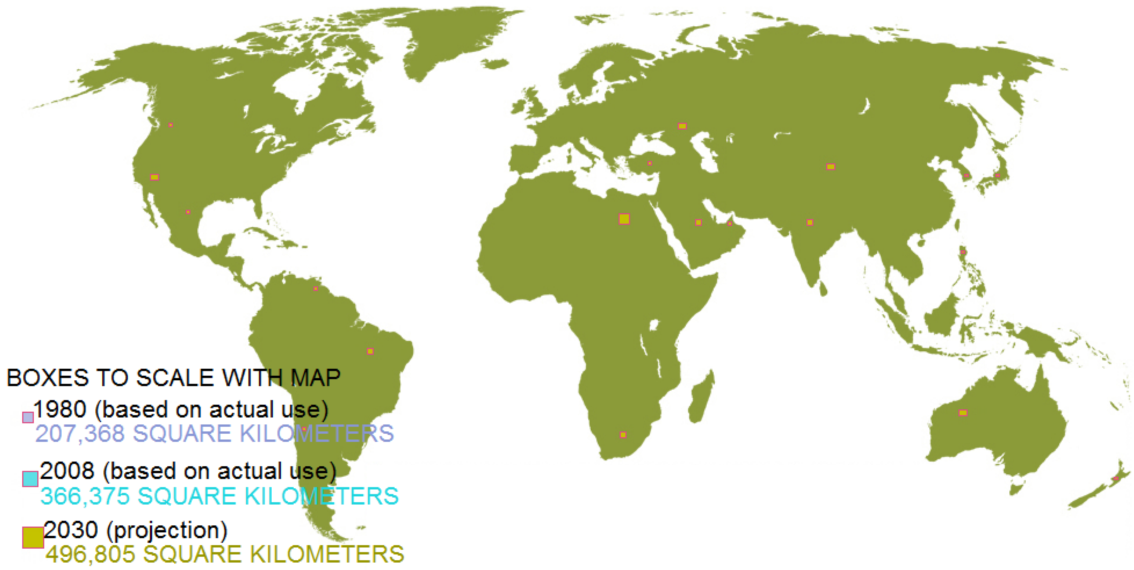

Figure 1.1.5[12]: Strategic placement of 20% efficient photovoltaic panels such that photovoltaic energy conversion could power the entire world, with zero carbon emissions.

It is also noteworthy that photovoltaic power would be, directly at least, a carbon neutral and emission-free technology[12], because no fuels are combusted or consumed during photovoltaic electricity generation. Finally, photovoltaic research and development is undergoing a period of recent accelerated growth, in terms of both financing as well as generation capacity and consumption, as seen in Figure 1.1.6[9,10,15,16]. According to statistics from the Renewable Energy Policy Network for the 21st century (REN21), electrical “grid-connected” photovoltaic power “continues to be the fastest-growing power generation technology in the world, with 50 percent annual increases in cumulative installed capacity in both 2006 and 2007...”[14]

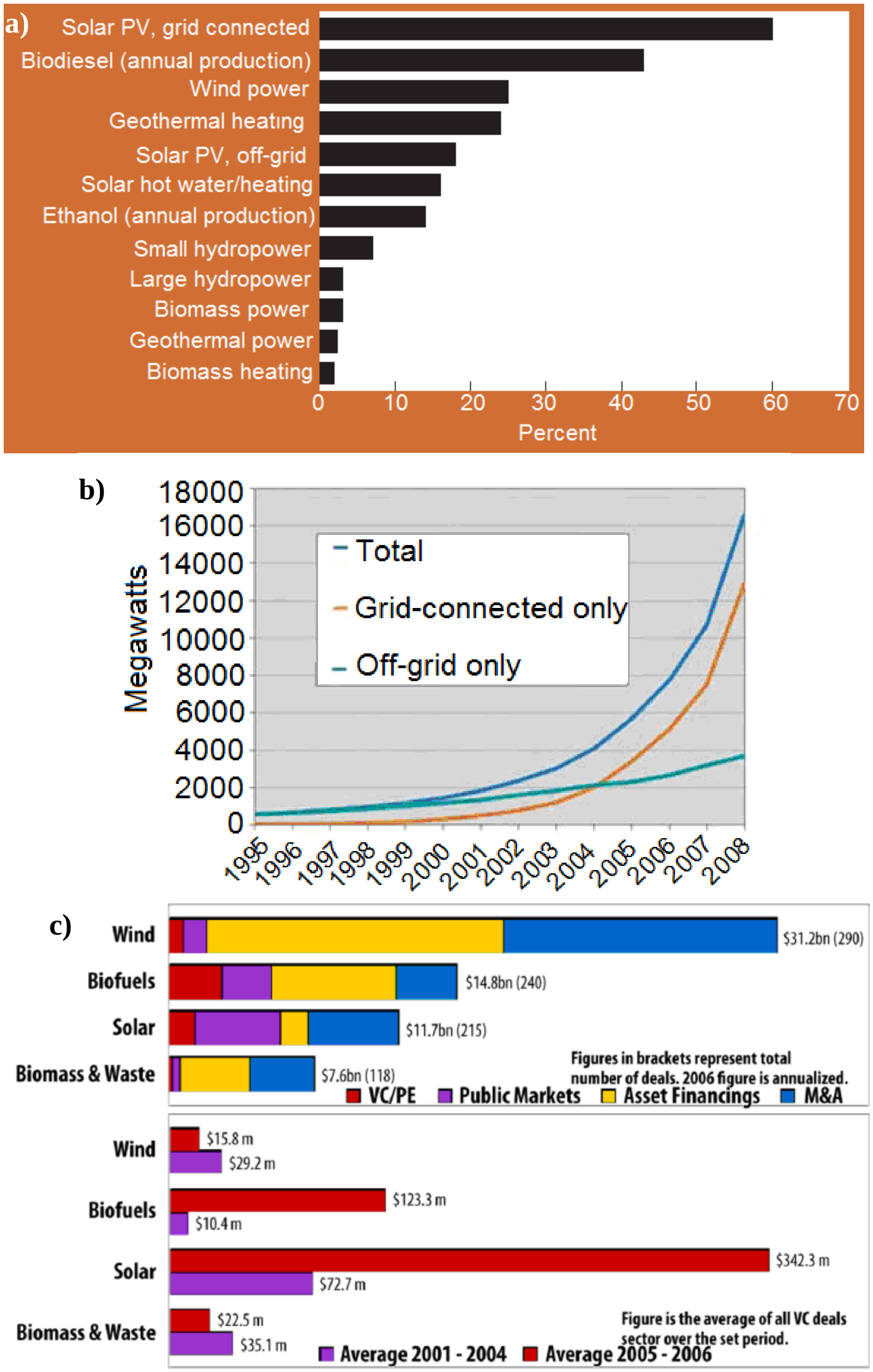

Figure 1.1.6[9, 15,16]: Recent growth of PV technology in terms of a) energy capacity and b) power capacity while c) illustrates funding of and investment growth in solar power technology compared to other "renewables"

Furthermore, both the Earth Policy Institute and recent thin film PV start-up company Nanosolar predict that photovoltaic power will become "competitive with coal-fired electricity" within the next couple of to few years (i.e. around 2012) with a price of ~$0.99-$1.00 per watt by that time[17,18].

1.2 Photovoltaic Cells

Photovoltaic cells are semiconductor-based devices able to absorb light ("capture") energy through the excitation of electrons into conduction ("conversion"). Based on material choices and arrangements, photovoltaic devices exposed to light experience an electronic potential difference across them without any externally applied electric field, driving the movement of charge carriers (i.e. current) from the device into a load circuit (Fig. 1.2.1)[20,21]. As semiconductor diode-based devices, upon the excitation of charges by absorbed photons, photovoltaic cells are then able to separate excitons (i.e. electron-hole pairs), and then maintain this separation and allow charge carriers to travel via a potential gradient, thus facilitating conduction[19].

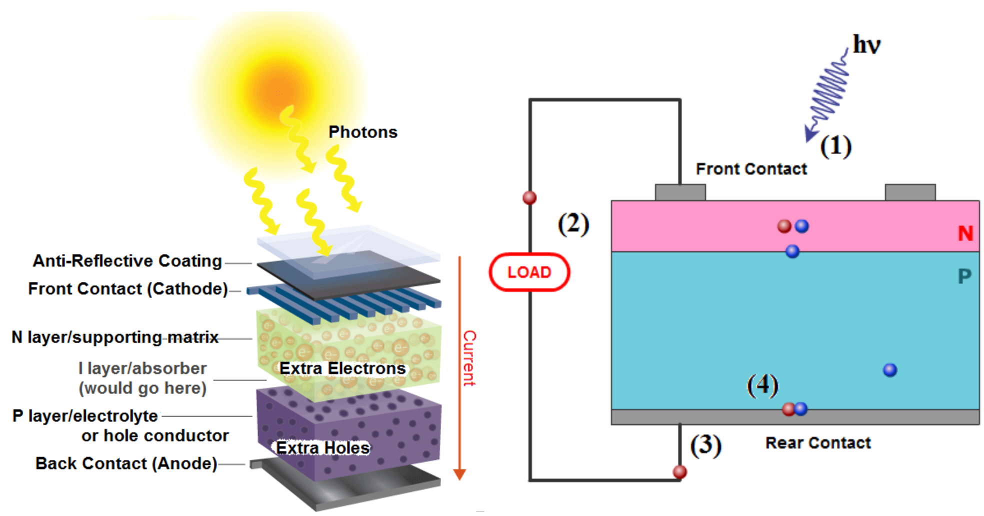

Figure 1.2.1[modified from 20, 21]: Generalized schematic of a photovoltaic cell (left) and a PV device in a simple load circuit (right), steps described ahead

The photovoltaic effect is the primary working principle behind solar cells, which utilize light from the sun to generate electrical power. Light with energy above the material's band gap generates additional carriers in each layer (1). Since it is energetically favorable for these excess carriers on both sides to recombine, they are likely to do so. Attaching a load circuit to a PV device gives electrons from the n/'emitter' side of the device a route to travel to the p/'base' side and recombine with holes (4), while generating a useful current(2,3). Meanwhile minority carriers (i.e. holes photogenerated in the n-layer and electrons in the p-) flow in the same direction as their current-carrying counterparts, and often diffuse towards and perhaps meet up at the p-n junction, recombining and hence creating a depletion region between the p- and n-type materials.

Photoconductivity was noted initially by Becquerel in 1839 in liquid electrolytes[19]. Then, in 1873, Smith observed photoconductivity in solid Se, followed later by Adams' and Day's (1877) observation of the PV effect in Se tubes[19]. The first noted functional solar cells were made by Fritts in 1883, and were composed of solid Se on metal foil top-contacted with Au[19]. The "modern era" of solar cells is considered to have started in the mid-1950's, when researchers at Bell Labs [accidentally] discovered that, when under illumination, voltage generation occurs across a p-n junction[19]. Over time, three different and distinct classes or "generations" of photovoltaic devices have emerged (Fig. 1.2.2)[22]:

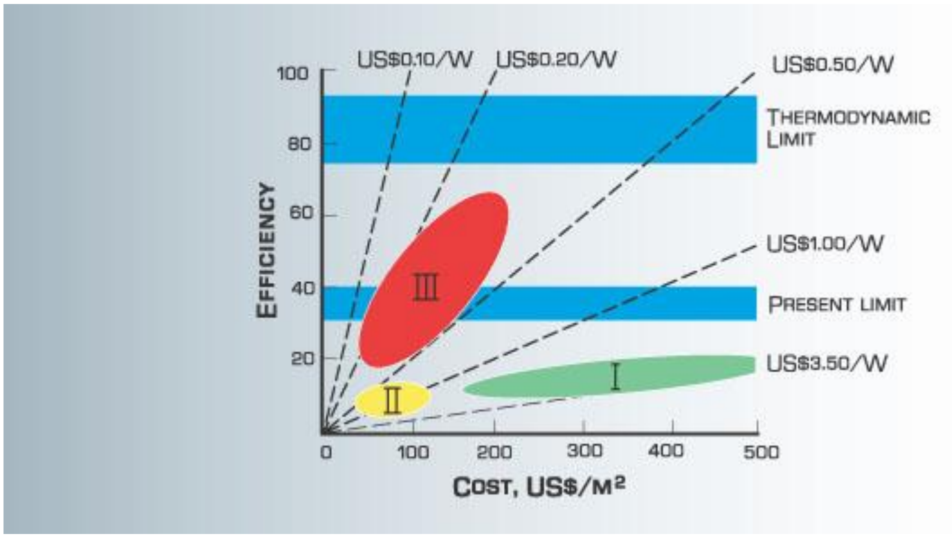

Figure 1.2.2[22]: Schematic illustrating the differences in cost vs. efficiency of the three generations of solar cells

1.2.1 Overview of Different Generations of Photovoltaic Cells

1.2.1.1 First Generation

“First generation” solar cells are often crystalline-Si based, composed “high-quality” (“low-defect”) material in order to minimize potential additional recombination sites and ‘traps’ for charge carriers than inhibit carrier diffusion through the material to conduction in an attached load circuit[23]. Such devices still dominate the marketplace[7,8,24], and are approaching the theoretical Shockley-Queisser[25] limit established for single band-gap devices[22]. However, due to the cost of processing such quality material, such devices are relatively expensive (and hence their cost to power is fairly high, at ~$3-4 per watt)[22], and therefore are not intrinsically (i.e. without favorable legislation, subsidy, etc.) economically favorable (i.e. ~$1 per watt for coal-fired electricity)[17,18] on the market as of yet, despite the “clean energy” they provide.

1.2.1.2 Second Generation

"Second generation" solar cells are based on polycrystalline or even some amorphous semiconductor thin films (i.e. amorphous Si, CdSe, CdTe, $CuInSe_2$, etc.)[23], as opposed to "high quality" bulk materials from the first generation. Because they require less material, they are cheaper to produce. Moreover, with the "defect free" requirement relaxed, they can be fabricated by less expensive means (i.e. vapor deposition techniques and electrodeposition/plating). However, "lower quality" material yields lower efficiencies for such devices, albeit making their cost per unit energy much more competitive (~$1 per watt).

1.2.1.3 Third Generation

"Third generation" solar cells refer to a compilation of "up and coming" researched and developed technology in photovoltaic. Such devices are basically divided into two categories, following, to some extent at least, along the ideas of the previous two generations. Multi-junction, multi-material solar cells, often coupled with concentrators upwards of thousands of suns, are following 'in the same vane' as first generation solar cells in that they are crafted from expensive, high-quality materials and processing, but are composed of several different semiconductor compounds in layers of varying sizes, unlike first-generation cells which were primarily Si-based[26]. Such devices, especially when coupled with concentrated sunlight, are designed for "maximum efficiency" to counter their expense, and can and have achieved efficiencies upwards of 40%[26]. Organic/polymeric and nanocrystalline/nanostructured devices, as well as/in conjunction with extremely thin absorber and sensitized solar cell technologies are following with the basic idea of their second generation counterparts, meaning 'simpler' synthesis techniques and cheaper materials and processing are utilized to make devices that are cheap, flexible, and relatively simple to create[23]. Although efficiencies of such devices have improved with research and development over time thus far, organic solar cells have yet to reach or surpass an efficiency of ~8%[27], and sensitized photovoltaic device efficiency has thus far 'peaked' between 11-12%[28,29]. Improvements upon such devices while maintaining their relative inexpensiveness is desired in the future.

1.2.2 Sensitized Photovoltaics

The class of photovoltaic devices known as sensitized solar cells were pioneered by Michael Grätzel in the mid-1990's with the concept and creation of dye-sensitized solar cells (DSSC)[24,30,31] (which were 'inspired' both by photosynthesis (and the related electron transport chain) as well as photography[24,30,31]). Figure 1.2.3[24] shows a schematic of the working principals of sensitized photovoltaics.

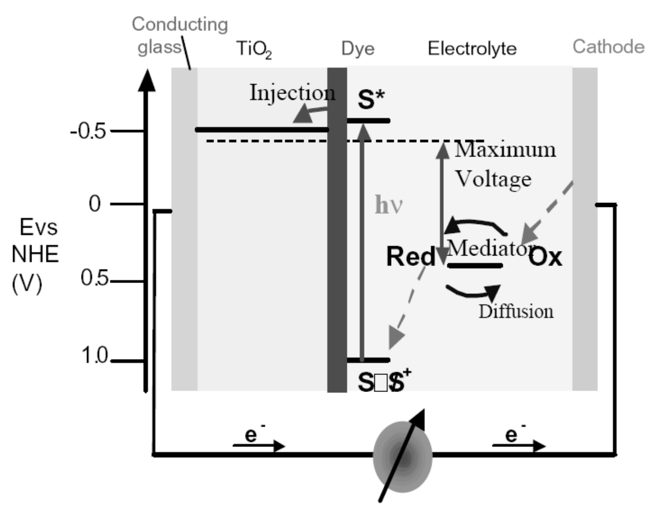

Figure 1.2.3[24]: Working schematic of a [dye] sensitized solar cell

Briefly, [visible] light passes through a transparent substrate and electrode (i.e. a transparent conducting oxide (TCO)). The light then passes through a wide-band gap semiconductor (TiO_2 both originally and for the work presented in this thesis) material, due to it's band gap (E_g) being outside of the range for which visible light absorption could occur (i.e. E_g>3.1eV, which is the energy of "blue" light) to a sensitizer layer (dye shown, otherwise may be semiconductor thin films a/o nanocrystals, bismuth ferrite (BFO) films for the work presented in this thesis). The sensitizer material can absorb visible light, either due to its molecular orbital energy level separation (i.e. in organic materials and conventional dyes) or band gap (in semiconductors/crystalline materials) being of sufficiently low "separation", energetically, to absorb some or all visible light (i.e. ~1.8eV(red)-3.1eV(blue)). Absorption of visible light then excites electrons to an excited molecular state (dye) or the conduction band (semiconductor), depending on the type of material used. Rather than "falling" back down to the ground state (dye) or valence band (semiconductor) of the sensitizer, the electron "falls" into the conduction band of the wide band gap semiconductor, where it is then "fed" into the load circuit via the contacted TCO electrode on the glass substrate. Meanwhile, the dye or semiconductor material either "gains back" the lost electrons (from the oxidation of an electrolyte, as shown, or from the departure of "holes" left behind from the lack of electrons into a "hole conductor", as in the work to be presented in this thesis). After the electrons proceed through the load circuit back up to the metallic cathode, they are then 'fed' back into the electrolyte (thus reducing it, as shown. Alternatively, in a system with a hole conductor (i.e. copper(I)thiocyanate (CuSCN), as in the work presented in this thesis) holes move the reverse direction through the hole conductor, which is essentially the same as electrons moving the forward direction within the material) solution to complete the circuit, and, in the presence of light, the cycle continues, provided the sensitizer material remains 'in tact' and chemically, electronically, and mechanically photostable.

1.2.3 Extremely Thin Absorber Cells

Fabrication of extremely thin absorber (eta) solar cells began in the mid-1990s with theoretical studies of parallel multijunction systems by Green and Wenham (1994)[32], and in practice by Konenkamp, et. al with completely solid-state TiO_2 nanocrystalline film-based devices (1996)[33]. Similar to their sensitized counterparts, eta solar cells often consist of a wide-gap semiconductor, some thin layer of 'absorber' material (low-gap inorganic semiconductor, as opposed to dyes or organics), and a layer that serves to complete the circuit (i.e. a 'hole conductor'). Also, similar to second generation and sensitized photovoltaic devices, eta solar cells are fabricated via cheaper processing roots and/or materials. Figure 1.2.4[34] shows a schematic of an eta solar cell:

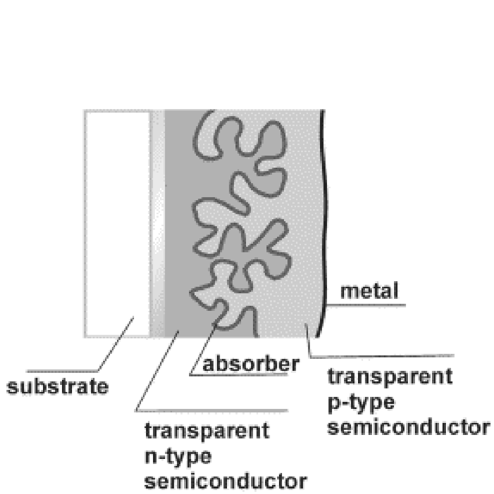

Figure 1.2.4[34]: Schematic of an eta solar cell (left) with band diagram (right)

In eta cells, similar to their first- and second-generation counterparts, a p-n (or p-i-n) junction setup allows for charge separation and transfer due to the generated photovoltage in the presence of light. Moreover, similar to sensitized solar cells, eta-devices are also based on favorable, staggered (type-II) band alignment[34].

1.3 Ferroelectric Materials

Ferroelectricity, the electronic analogue to ferromagnetism, occurs in materials that can exhibit spontaneous polarization in the absence of an electric field[35]. Figure 1.3.1[35-37] illustrates the working principles of ferroelectric behavior:

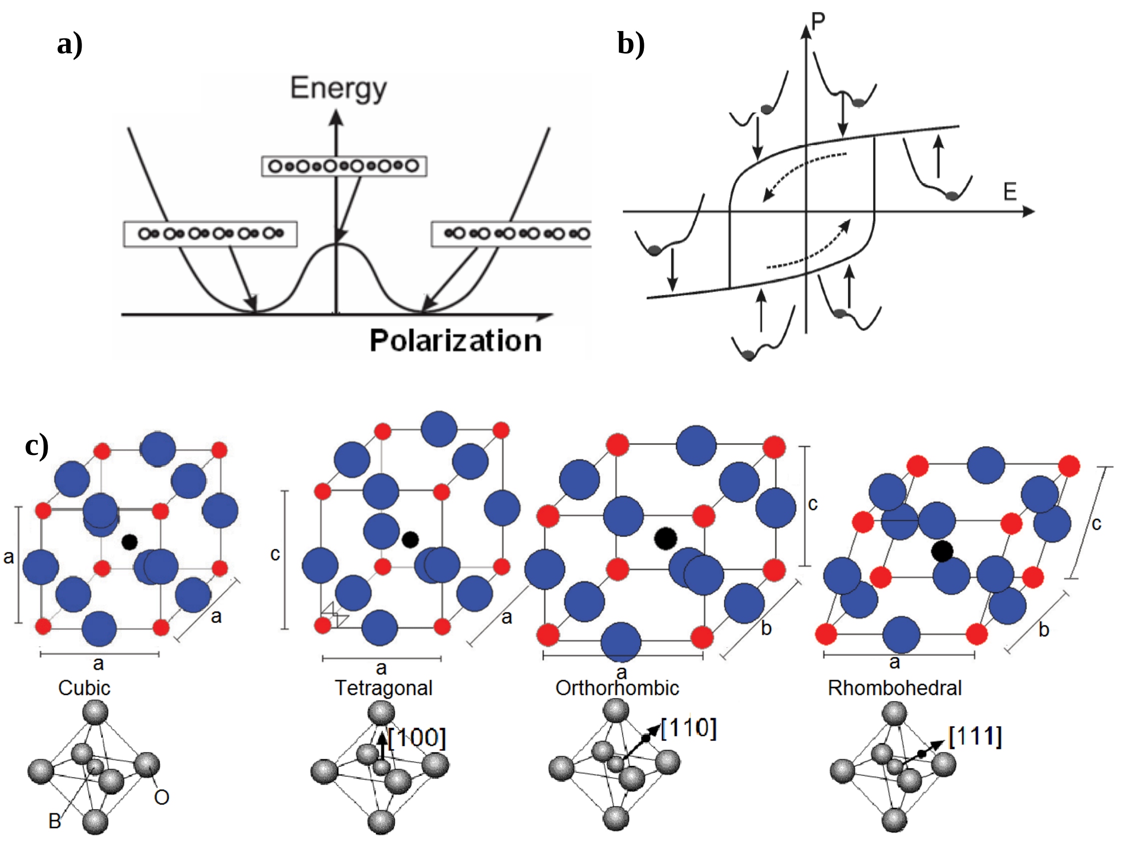

Figure 1.3.1: a) Favorable energy states for a ferroelectric material in the absence of an external field[36], b) Ferroelectric hysteresis[36], and variation in the energy-polarization/location curve with externally-applied field, , and c) Perovskite (cubic) unit cell and possible corresponding 'asymmetric' distortions of atoms in such (shown in the BO_6 octahedra below each unit cell), which lead to ferroelectric behavior[35,37]

Ferroelectricity in perovskites (i.e. ABO_3 oxide materials) originates from the distortion of a unit cell due to the motion central ("B") cation slightly off-center, and subsequent (rotational a/o translational) "shifts" in position from the surrounding "O" anion octahedron the "A" corner cations (Fig. 1.3.1c), below a critical temperature T_c. In this situation, one of three distortions (tetragonal, orthorhombic, or rhombohedral) from cubic symmetry can occur, depending on the comparative sizes of the atoms and the direction the "B"-cation displaces. In turn, due to the asymmetry, the unit cell adopts a slight electronic polarization. The off-center position of one central cation couples to that of its neighboring unit cells, causing their central cations to also take a similar, preferentially off-centered position[35]. Perovskites have at least two distinct distortions, and hence opposite polarizations, below T_c. Figure 1.3.1b illustrates how these 'poled states' are energetically favorable (below T_c), and an energy contribution is required to 'switch' between them. Applying an electric field across a ferroelectric material causes one polarization state to be favorable over the other, depending on the direction of the applied field (Fig. 1.3.1b+c). At a temperature less than the critical temperature, placing an electric field (i.e. applying a 'coercive field' (E_c)) across a perovskite allows one to switch between these polarization states by switching the direction of the applied field. Also, under the critical temperature, upon removing the applied electric field, some 'remnant polarization' (P_r) remains, despite the absence of an external electric field (Fig. 1.3.1b). This remnant polarization is again due to the "B"-cation displacement and subsequent cell asymmetry, and creates an internal electric field within the material.

Similar to ferromagnetic materials, ferroelectric materials also exhibit domain structure and domain walls. Under an applied electric field, domains polarized in the direction of the field may grow at the expense of those not polarized the same direction, similar to ferromagnetic domains[35].

Also similar to their ferromagnetic counterparts, these materials follow the Curie-Weiss Law (eqn. 1.3.1)[35]:

$$P = \frac{C}{T - T_C} \qquad \textbf{(1.3.1)}^{35}$$

where P is polarization, C is a material-based constant, and T_C is the Curie (critical) temperature denoting the ferroelectric-parelectric phase transition[35].

Above T_c, the thermal/entropic contribution to free energy in the material overcomes the driving force for electronic ordering and spontaneous polarization[38]. Therefore, above T_C ferroelectric materials lose their spontaneous polarization. So above T_C such materials require a field to be electronically polarized and are then parelectric[35,37], as shown in Figure 1.3.2[37]:

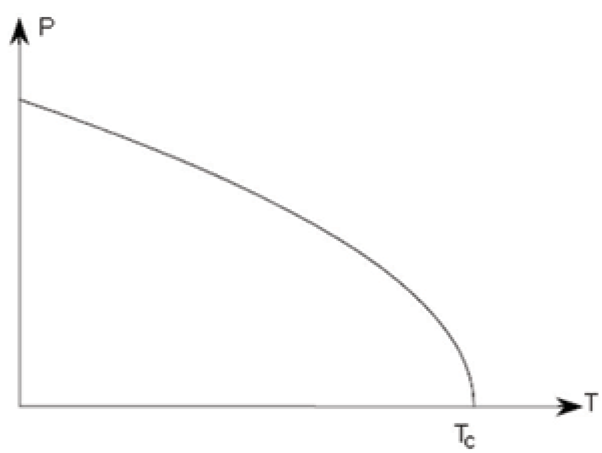

Figure 1.3.2[37]: Ferroelectric to parelectric phase transition, illustrated by a marked decrease in (saturation) polarization

Ferroelectric materials have been used and/or are being researched for use in a wide variety of applications, such as memory[37], actuators/sensors[35] (because they are piezoelectric as well), and recently photovoltaics as alternatives to conventional semiconducting materials[39,40].

CHAPTER 2: EXTREMELY THIN ABSORBER/SENSITIZED SOLAR CELLS

2.1 Historical Development

2.1.1 Sensitized Solar Cells

Sensitized solar cell technology was first developed in the mid-1980's via Michael Grätzel[41,42], working on optical 'sensitization' of the wide-gap semiconductor TiO_2 (anatase) using organic dyes, meaning that, since TiO_2 intrinsically cannot absorb much light in the visible range, it is coated with a dye that does, which can transfer it's electrons from an excited state into the conduction band of TiO_2. The first 'fully realized' dye-sensitized solar cell (DSSC) was published about in 1991, again by Grätzel[30]. Such devices were initially inspired by the electron transport chain in photosynthesis, and meant to separate the processes of light harvesting and carrier transport to enable the use of inexpensive materials to produce solar cells. The original sensitized solar cells (and still many today), were TiO_2-based (a quite prevalent and relatively inexpensive wide-gap semiconductor material) sensitized with organic dyes and/or metallorganic 'complexes' (able to absorb light due to the narrow energy gap between ground and excited molecular electronic states, allowing them to 'mimic' the light-absorbing functionality of chlorophyll in photosynthesis), and a liquid electrolyte (at first the iodine/iodide system, later on typically the iodine/triiodide system)[30,31]. Similar to their photosynthesizing counterparts in nature (i.e. stacks of thylakoids called grana), these devices work best with rough and/or porous, perhaps even hierarchically-structured, films for increased surface area for light absorption and charge transfer.

The first-published DSSC from Gratzel in 1991 was composed of a rough, porous, colloidal-based TiO_2 film sensitized by a thin, bound layer of Ru-metallorganic complex, and a liquid iodine/iodide (I_2/I^-) redox couple or lithium iodide/iodine/ethanol solution as an electrolyte. Two transparent electrodes (composed namely of FTO-glass, one of which was coated with Pt as an electrocatalyst) finalized the device[30]. Figure 2.1.1[30] shows a schematic of the original DSSC:

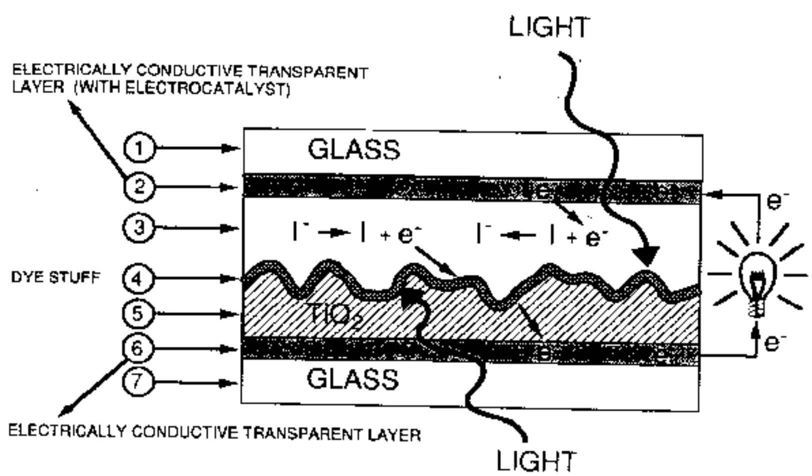

Figure 2.1.1[30]: Schematic of the 'original' DSSC

Much of the research in sensitized solar cells has gone into improving sensitizer absorption properties/efficiency, photostability, or both. Panchromatic (i.e. 'black') dyes, absorbing light in the visible range and into the near infrared, to better match the incident solar radiation spectrum, are most favorable as absorbers[24,42]. Mixtures ('cocktails') of dyes have also been tried, in order to better match the solar spectrum[24], as well as semiconductor quantum dots[24,42,43]. N3, a organocomplex Ru-thiocyanate-based dye, had proven to be a top sensitizer for around 8 years, eventually beat by a black dye of similar variety, N749[24,42,43]. Eventually, both of these were beat out by new Ru-based organocomplex dyes, which though having a lower wavelength absorbance onset, have high extinction coefficients and enhanced absorbance response in the 'red' area of the solar spectrum[42]. Much organic chemistry goes into creating dyes with favorable light absorbance, photostability, and favorable adsorption to wide-gap semiconducting materials (i.e. TiO_2), and several alternative organocomplexes have been found, and ~10% efficient devices are expected to be readily reproducible[42]. Strictly organic (as opposed to organometallic) dyes also gained interest in recent years, albeit still have issues with photostability outdoors[42].

Quantum dot (QD) sensitizers on TiO_2 followed after Grätzel's work leading up to and on DSSCs, the first of such devices which appears in the literature in 1990 from Vogel, et. al.[44] using CdS QDs(achieving overall efficiency >6%), with the rationale that QD band-gaps were more tunable to the solar spectrum via changing their size, and that functionalizing such particles could make them more photostable than dyes[44-47]. Moreover, due to quantum confinement effects, it may be possible to generate multiple electron-hole pairs per incoming photon due to impact ionization[47]. Vogel, et. al. continued such work into mid-1990s, using varying quantum dots and photoelectrode materials[45]. Hotchandani and Kamat achieved efficiencies of >2% with CdS QDs on ZnO in the early 1990's, albeit they were still able to study charge transfer and several trends in open-circuit voltage and short-circuit current in such systems[46], which was likely important work for the progress of that field. Shalom, et. al. made devices with a dye/QD ‘bilayer’ absorber, and were able to reach efficiencies >1.5%, which was a 263% improvement vs. their solely QD-SSCs[49]. Kongkanand, et. al. studied variations in CdSe QD size (and hence band gap) on device performance, and implications of perhaps making a ‘rainbow’ solar cell by using ordered combinations of QD-sizes on TiO_2-NT arrays[50]. Though recent work on QDSCs often still produces overall efficiencies of one to a few percent at best, though new insight into QDSCs is being found via these experiments[47-50].

Though TiO_2 is the dominantly found matrix/photoelectrode material for DSSCs[24,42,43] (also prevelant in eta-SC research[51]), other materials have been incorporated into DSSCs for this purpose. ZnO and SnO_2 are found quite often in DSSC research[24,42,52,53], and extremely thin absorber[51] devices. Other materials, such as Nb_2O_5[24,52], Ta_2O_5[45], etc. have also been assessed for such applications, as well as combining wide-gap semiconductors in the photoanode of a given device[52].

Aside from strictly materials-based changes and composites, photoanode structure/architecture/morphology has also been researched somewhat thoroughly. The first nanotube-based (TiO_2) DSSCs appeared in the literature around 2002, from Uchida[54] and Idachi[55] independently. Such devices were found to have improved charge-collection efficiency[56] over their random-NP-based counterparts, as well as enhanced light scattering effects[56], and overall conversion efficiencies over 3% were eventually achieved[56]. Ordered arrays of nanowires were used first by Law, et. al. in 2005[57]. Nanowire (NW) DSSCs are favorable to nanoparticle-based ones due to faster electron transport in NWs (often single crystalline) vs. random, porous (and polycrystalline) networks of particles, while still maintaining favorable characteristics such as high surface area (for absorbance and possible light trapping/scattering) as well as a low amount of material utilized/required[57]. Although these first NW-DSSCs had low fill factor (0.36-0.38) efficiency (1.2-1.5%) values, this issue was attributed to poor dye loading/adsorption on nanowire surfaces[57]. Branched a/o hierarchically structured nanostructures are also being studied and integrated into DSSC. The former a/o NW-based hierarchical structures, like their NW counterparts, such structures still provide straighter, less random, more definitive conduction pathways, while providing further increased surface area and potential light-scattering effects when compared to plain nanowires[58,59] and inhibiting "back-reaction" of electrons into liquid electrolytes[58]. Device efficiencies of ~5% have been achieved with such structures[58]. Zhang, et. al. in 2008 were able to increase overall device efficiency by using hierarchically-structured, polydisperse, spherical ~100-500nm-sized aggregates of smaller ZnO nanoparticles (~2.4% for 'regular' nanocrystals compared to ~5.4% for NP-aggregates), due to enhanced light scattering and harvesting in aggregate-based films[60]. Also, TiO_2 NW-based and 'composite' nanowire/nanoparticle TiO_2 architectures produced by Tan and Wu were found to have >6% and >8% conversion efficiencies, respectively, with photoanode films up to ~17μm thick prevented from cracking by NW-reinforcement[61]. Composite structure photoanodes, similar to their hierarchically structured counterparts, have multiple levels of structure, providing possible light scattering benefits along with increased surface area[61].

Also, a significant amount of research has gone into 'circuit-completing' materials such as liquid electrolytes, and eventually solid-state hole conductors, for DSSCs[42,48]. Volatile liquid electrolytes are undesirable due to leakage and evaporation issues, so ionic liquids[42], non-volatile electrolytes[42], better sealing methods[42], and solid-state hole conductors[48] have all been researched and improved as viable alternatives, and much confidence in improved service life (up to ~20 years) has been found in recent DSSC research[42].

Solid-state hole conductors for DSSC (and eta-SCs) came about in 1995 from Tennakone, et. al using p-CuI as a hole conductor, as opposed to liquid electrolytes[62,63]. However, these first solid-state DSSCs were fairly inefficient (~0.8%), at least in part due to the likely deterioration of the CuI hole conductor due to humidity[62,64]. Tennakone, et., al. managed to make a more efficient CuI-containing DSSC by changing dyes (achieving ~2.4%[53,62]), and, later, Meng, et. al. (~3.8% with a TiO_2(ZnO)/CuI+molten salt-based device)[64]. However, issues with the deterioration of CuI (along with photo-oxidation/stability[48,62] and excess I^-, as well as poor pore penetration/filling[48,62]) were comparable to, if not worse than, those associated with liquid electrolytes at the time[62]. MEISCN[62,63], an organic compound, was found to inhibit crystal growth in CuI while still allowing for hole conduction, but is expensive to produce[62]. However, CuSCN was then found to be the next viable hole conductor candidate, and was much more stable than

CuI[62]. Moreover, using dilute solutions of CuSCN in n-propyl sulfide led to better pore filling in a TiO_2 matrix, and it could also be electrodeposited[62]. However, poor device performance was still noted with this compound due to its lower hole conductance than CuI[62]. Grätzel and others were found to have some deal of success with organic p-type semiconductors as hole conducting materials, which are relatively cheap and easy to form into films, but again efficiencies still seemed limited[62]. In 2004, a conversion efficiency for "solid-state" DSSC was estimated at ~7%, achieved by Kaneko, et., al. using solid polysaccharide-based electrolytes, though the solid polysaccharide matrix contained liquid I^-/I_3 electrolyte[65]. As noted in 2008 by Nazeeruddin, et. al., the record for a 'fully' solid state DSSC is ~5%, achieved by Snaith, et. al., using spiro-OMeTAD, an organic p-type semiconductor, as a hole conductor[66,67].

2.1.2 Extremely Thin Absorber Cells

Eta-solar cells (Fig. 2.1.2[68]), similar to DSSCs, place an absorber layer on an often nanostructured, rough, a/o porous (for enhanced light absorption via high surface area and light scattering/trapping) wide-gap (n-type) semiconductor matrix in order to absorb the light that the matrix cannot. Again, such devices function best with similar, type-II staggered band structure so electrons favorably 'fall' into the n-type and holes favorably 'climb' into the p-type layers, respectively. However, similar to their second-generation thin-film solar cell counterparts, these devices are often solid-state, and also include the 'conventional' p-n (or p-i-n) junction mechanism of photovoltage establishment, as well as charge separation and transport.

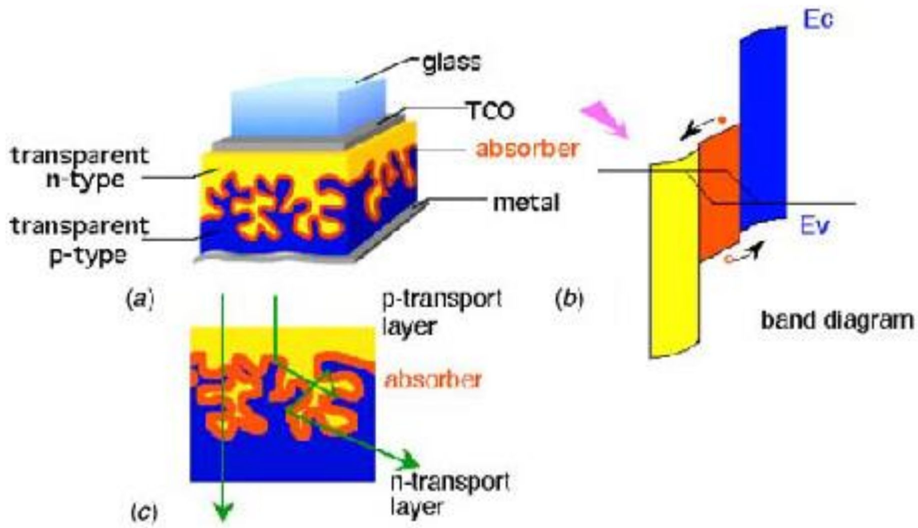

Figure 2.1.2[68]: a) Schematic of a fully-fabricated eta-solar cell, b) Favorable band structure/alignment for such a cell and c) Schematic of the path length enhancement of light due to the rough/nanostructured/highly structured nature of an eta-cell photoanode

The 'prelude' to eta-solar cells likely began in 1994 with Green publishing on model, theory, and calculation for efficiencies of multi-junction, thin-film solar cells, a paper in which he emphasized the benefits of multi-junction device setups for use with 'poorer quality' (i.e. cheaper processing a/o material) materials[32]. The first among, or perhaps predecessors to (because they were single junction and not p-n or p-i-n junction-based) eta-devices appears to be from Könenkamp, et. al. in 1996, an a-Si or PbS-QD absorber on a TiO_2 matrix, on a SnO_2-glass substrate back contacted with a thin layer of Pt[33]. However, the former of these devices at least failed to have absorber conformation to the porous TiO_2 matrix, thus limiting its efficiency and possible benefits from internal light scattering effects[33].

The term 'extremely thin absorber' (eta) solar cell appears to have been first used in 1997 by Könenkamp, for nanoscale-thickness CdS or CdSe-thin film-based devices[51,69,70]. The next year, at the same conference, both Könenkamp, et. al.[71] and Möller, et. al.[72] had work presented on the use of $CuInS_2$(CIS) as an extremely thin absorber due to it's low band gap (E_g~1.5eV) and decent absorption potential (α~10^5), as well as lower toxicity than potential counterpart $CuInSe_2$[73]. In 1999, Könenkamp, et. al. fabricated and studied a β-CuSCN/TiO_2 rectifying p-n junction[74], considered instrumental in future eta-cell fabrication, as these two materials are seen, combined or separately, throughout solid-state DSSC and eta-literature[34,51,62] (as well as in this particular work).

In 2004, Taretto and Rau established a model for eta-solar cells (discussed later, in section 2.2.1), which approximates eta-solar cells, due to their sandwich structure and roughness, as a multijunction system, and illustrating enhanced absorption due to layer surface area/folding, and predicting the potential of CdTe- and $CuInS_2$-based eta-devices up to 15% (enhanced by up to 5% by photoanode structuring and subsequent light trapping)[75].

Nanowire-based eta-solar cells begin to appear in 2005, from Tena-Zaera, Levy-Clement, and colleagues at the LCMTR-CNRS in France[76,77]. These devices were based on ZnO NWs and CdTe or CdSe absorbers, respectively, the latter of which achieved a conversion efficiency of ~2.3%[77]. Kieven, et. al. created ~2.5% efficiency eta-solar cells (ZnO/In_2S_3/CuSCN) and studied the effects of internal structure on such devices, finding that effective absorber thickness is enhanced by high internal surface area[78]. In 2005, Nanu, et. al.[79,80] achieved record efficiency at ~4% with $CuInS_2$/TiO_2-based devices, utilizing an Al_2O_3 buffer layer to protect the TiO_2 layer from contamination a/o reaction with the Cu-compound[80]. Record efficiency for eta-solar cells appears to be at slightly greater than ~4% currently, achieved by Krunks, et., al. with a ZnO-NW/In_2S_3/$CuInS_2$ device[81].

2.1.3 Ferroelectric Materials/Perovskites

The term 'ferroelectricity', was apparently first 'coined' and utilized in 1912 by Erwin Schrödinger[82-84] (likely due to the comparability of this phenomenon to ferromagnetism). Ferroelectricity (described previously in section 1.3 and further in section 2.2), a hysteretic, non-linear dielectric behavior analogous to the prior discovered phenomenon of ferromagnetism, was discovered in Rochelle salt in 1921 by Valasek while investigating the piezoelectric (electronic response of a strained material) properties of the same material[82-85] Eventually, through the mid- to late-1930's, Mueller would publish four papers, hence creating the first 'complete phenomenological theory' for ferroelectric behavior in Rochelle salt[86]. Meanwhile, in the mid to late 1930's, Busch and Scherer discovered and subsequently reported on ferroelectricity in KH_2PO_4 (KDP) and H_2AsO_4, thus investigating a new class of ferroelectric materials[86]. Though these crystals were more stable and less complex than Rochelle salt, they had very low (~-150^{o}C) transition (Curie) temperatures[86]. Theories and models on ferroelectricity were further developed in the 1930's and 40's[86]. In 1937, Jaffe proposed that ferroelectric materials underwent a symmetry-based phase transition at some critical temperature[86]. Landau, in that same year, proposed that such phase transitions were both thermodynamically- and symmetrically (group theory)-based[87]. $BaTiO_3$ and a 'flurry' of other perovskite (ABO_3) ceramics were also discovered to be ferroelectric, during the 1940's-60's[82-84,86-88].

Studies of ferroelectric perovskite materials began with $BaTiO_3$, first synthesized in 1941 by Thurnaurer and Deaderick, (noteworthy for it's high dielectric constant)[88] and later described by Wainer and Salomon(US, 1943)[86,88], and later Wul and Goldman (Russia, 1944)[83,85], and Ogawa and Waku (Japan, 1945)[88]. Ferroelectricity in $BaTiO_3$ was described in 1945 by von Hippel[86]. Ginzburg (1946) and Devonshire (1949) also made stark contributions to the studies of phenomena in ferroelectric ceramics, particularly $BaTiO_3$[86]. In 1959-60, a considerable development in ferroelectric theory was made, with Cochran and Anderson, independently, describing 'soft modes' of ferroelectric transitions in such oxides, linking Mueller's early work on Rochelle salt with Davonshire's on $BaTiO_3$, all 'atomistic-based' theories on ferroelectricity[86]. In the 1960's, Ginzburg (describing phenomena microscopically) modified Landau (describing macroscopically) theory on thermodynamics/free energy and ordering in ferroelectric materials, particularly to more accurately describe/account for phenomena in "low-dimensional systems" and "systems with short-range interactions" near T_c[87]. Through the late 1960's, work by Aizu (1967, 1970) and Shuvalov (1970) led to a complete symmetry classification of ferroelectric materials[86].

Ferroelectric perovskite thin films were first synthesized and studied in the 1970's-80's, coincident with new processing techniques like sol-gel chemistry, chemical vapor deposition (CVD), and laser ablation[89]. Such films were considered favorable because they required little material, often lower processing temperatures, and less voltage required to 'switch' their polarization (because ferroelectric switching is done via a coercive electric field, E_c, and electric field $E = V/t$, where V is applied voltage and t is film thickness)[89]. However, *extremely* thin (i.e. on the order of a few nanometers or so) ferroelectric films experience issues due to a depolarizing field caused by charges accumulated at ferroelectric-electrode interfaces which oppose the polarization field within the ferroelectric material[90-92]. Overall, ferroelectric materials have found their way into a variety of applications, such as high-dielectric-constant(κ)-capacitors[84], sonar[84], computational memory[84], and transducers[84,85], and sensors[84].

Investigation of the photovoltaic effect in ferroelectric materials may date back as far as the late 1930's, when Brady and Moore published on what they referred to as 'actinoelectricity' in tartarate-based crystals[93,94]. Throughout the 1960's and 70's, a 'bulk photovoltaic effect' would be discovered in noncentrosymmetric crystals (i.e. piezoelectric and ferroelectric materials), that was not due to either of the previously two proposed mechanisms (the Dember effect (non-uniform lighting of a given material) or the separation of 'non-equilibrium carriers' (i.e. generally p-n junctions)), and unique to these materials, producing 'above band gap photovoltages', which were not seen in the prior proposed two mechanisms[94]. In 1974, after previous reports (~1960's)[95] of 'photocurrents in the absence of an applied field' in $BaTiO_3$ and $LiNbO_3$, Glass et. al.[96,97] decided to investigate doped versions of the latter, stating that 'bulk photovoltaic effect' in such materials was due to asymmetry in the c-direction, between the Nb and Fe (dopant) atoms in the crystal, and charge transfer between them[97]. In 1975, Brody and Crowne studied $BaTiO_3$, finding that in violet or UV-light (with energy above the band gap energy of $BaTiO_3$) photocurrents in the material peak and that photovoltage decreased with increasing temperature, until beyond the ferroelectric-paralectric phase transition temperature, at which point it and the photocurrents 'vanished'[93]. They believed that light-induced carriers 'screened' the internal electric field (intragranularly) caused by spontaneous polarization within the material, causing 'greater than band gap' photovoltages[93].

Overall, qualitatively, the theory behind photovoltage generation in ferroelectric materials appeared to be quite simple. Photo-induced charge carriers would flow their respective directions in a [poled] ferroelectric material, based on the material's spontaneous/remnant polarization to the lack of centrosymmetry, in perovskite materials often due to atomic displacements and subsequent lattice distortions, creating a dipole within the material[98]. Moreover, in mid-to-late 2000's, ferroelectric thin films were found to have such properties as well[98,99]. However, despite the promising signs of high (above band gap)-photovoltages possible in ferroelectric materials[93-99], the often high band-gaps (i.e. outside the visible range of the spectrum) limit how much light they can absorb[98,99], and hence their output, performance, and efficiency (i.e. Qin's report of 0.28% conversion efficiency from epitaxial PLZT films was considered very high, and orders of magnitude above such found in similar work)[98]. A narrower (i.e. energy in the 'visible' regime)-band gap ferroelectric material could present quite an improvement to such work and potential applications.

Bismuth ferrite ($BiFeO_3$, BFO) (E_g~2.2eV-2.8eV)[100,101] was such a material, a ferroelectric (rhombohedrally-distorted perovskite ($T_c = 825^{o}C$)) and antiferromagnetic (i.e. 'multiferroic') material, with band gap values often reported between the blue-green and yellow portions of the visible spectrum[100]. $BiFeO_3$ was synthesized and studied as early as the late 1950's by Smolenskii, et. al.[100]. Apparently, interest in the material was 'sparked' again in 2003, when Ramesh, et. al. published on its high remnant polarization (P_r ~60μC/cm^2)[100,101]. In 2008, Basu, et. al. published on the photoconductivity of BFO, stating that it was improved with increased oxygen vacancies, and increased when an applied field 'followed' the polarization direction of the material[102]. Furthermore, in 2009, Choi, et. al. demonstrated diode-like behavior in thick (~70μm and 90μm) BFO films, switchable in direction by switching the polarization direction of the material[39,101]. In the same year, Li, et. al. created $BiFeO_3$/α-TiO_2 core-shell nanoparticles that were successful as photocatalysts for dye degradation, but did not attribute these findings to nor investigate too much the ferroelectric nature of $BiFeO_3$[103]. In 2010, Yang, et. al. were able to achieve above band-gap photovoltages via yet another new mechanism for charge separation and transport in ferroelectric photovoltaic systems; domain wall engineering[96]. They found that the photovoltaic effect was not observed when IV measurements were taken parallel to domain walls, and was when perpendicular[96]. Moreover, they showed higher open circuit voltages occurred in smaller-domain width systems than larger, and got nearly zero open-circuit voltage for a single domain sample, believing that photoexcited charge carriers accumulate at domain walls due to the ferroelectric polarization across the material (and the upward-bent band structure theorized and modeled at the domain-domain wall 'interface')[96]. Similarly, also in 2009, Ji, et. al. were able to demonstrate the photovoltaic effect in BFO thin films[104]. Also that year, Wu, et. al. fabricated and characterized BFO-ZnO heterostructures, illustrating their theoretical type-II staggered band alignment (as between sensitizer and photoanode in DSSC/eta-solar cells) and demonstrating resistive hysteresis and diode-like behavior in such structures[105]. Interestingly as well, Kundys et. al. recently reported on the photostriction of BFO crystals in the presence of visible light[106]. Overall, these recent investigations[39,96,100-106] bring much excitement and potential into the field of ferroelectrics for photovoltaic applications[39,96,100-102,104,105] and photocatalysis[103].

2.2 Physical and Mathematical Description

2.2.1 Sensitized and Extremely Thin Absorber Solar Cells

2.2.1.1 General and Optimization/Efficiency Considerations

Two fundamental processes, the capturing and absorption of light along with the conversion of that energy into separated charges, which can be maintained as separate and carried/transported through a material into a load circuit as useful electrical current.

Upon the absorption of light and the excitation of electrons in the absorber layer, charges are separated, and their continued separation as well as their transport must be facilitated in order for the conversion from light to useful electrical current to be completed. In DSSC, and also favorably in eta-solar cells, this process is facilitated by a type-II band alignment, as seen previously in Fig. 1.2.3, and similar to the latter Fig. 4.5.1. It is energetically favorable for electrons to ‘fall down’, i.e. lose energy and attain a more stable ‘state’. In an absorber/sensitizer conduction band/excited molecular level should hence be higher in energy than the conduction band of the wide-gap semiconductor matrix, which electrons travel through to reach the ‘anode’ of the PV device and get carried through a load circuit. In the valence band of an absorber, remaining electrons 'falling down' in energy translates to the holes left behind 'climbing up' in energy, hence the absorber/sensitizer valence band/ground state/bonding molecular level of the absorber should be lower than that of the hole conductor or electrolyte (again, as shown in Figs. 1.2.3 an 4.5.1).

Charge separation and transport in eta-solar cells is further facilitated by a p-n junction setup (Fig. 1.2.1)[21], as in earlier generation photovoltaics, described previously in section 1.2.

In order to absorb light, a semiconducting material must have a band gap energy equivalent to or less than that of the photons of the incident light (i.e. this range is 1.8eV-3.1eV for visible light). In both sensitized and eta-solar cells, the 'capture' of light is primarily done by the sensitizer/absorber layer, due to its low molecular level energetic separation/band gap. Typically, for successful capture, two things must be true for the absorbing layer. For one, the absorber layer thickness (W) should be less than the length carriers typically travel prior to collection (L_c) (and, favorably, also lower than carrier diffusion length (average distance oppositely-charged carriers travel before recombining), L_D), (i.e. $W<L_c \rightarrow L_c/W > 1$), meaning as thin as possible an absorber layer would be most favorable[75,107,108]. This criterion functions in opposition to the second one, which states that a most effective absorber layer should be have a thickness equivalent to or greater than a material's absorption coefficient (α) in order to maximize the amount of light absorbed (and hence maximize capture, i.e. $W > 1/\alpha \rightarrow W\alpha > 1$), favoring a thicker absorber layer[75,107,108]. However a thicker absorber layer, particularly one thicker than L_c, has increased odds of carriers of getting trapped and/or recombining before they can be utilized in a load circuit, due to a higher probability of encountering traps, defects, and oppositely charged carriers, as well as an increase in the period of time carriers take to diffuse to an electrode (majority) or interface (minority) increasing due to the increased thickness and hence distance required for carriers to travel to reach these 'destinations'. However, keeping in mind that DSSC and eta-solar cells are often composed of higher surface area absorbers (due to absorber conformation with a rough a/o porous a/o nanowire-architectured wide-gap semiconductor 'matrix' layer), the criterion $W\alpha>1$ is often relaxed because the effective absorber layer thickness is increased due to roughness and 'folding' of the absorber throughout the photoanode of a device (which allows for modeling approximations similar to those used in multijunction solar cells[32,75], and perhaps also, due to light scattering and trapping caused by such a photoanode morphology[75].

2.2.1.2 Recombination

Traps and defects aside, the two main mechanisms of electron-hole recombination are bulk and surface recombination. In nanostructured- a/o high-surface-area-to-volume-ratio based-devices such as DSSCs and eta-SCs, the latter is often more prevalent, due to the high surface area of various layers as well as the number of interfaces available for such within a given device.

Bulk recombination in such devices is an issue if charges recombine in the absorber more quickly than they are injected into the photoanode, which is more likely to occur in a thicker absorber layer, due to the increase in L_c required for charges to reach the photoanode as well as a higher probability of them encountering, aside from traps and defects, oppositely charged carriers/sites along the way[75].

In DSSCs and eta-SCs, recombination at some interfaces is necessary and even favorable. For instance, after the absorber/sensitizer loses an excited electron to the photoanode, a new electron (from electrolyte or hole conductor) must replace it for a complete circuit, continued cell functionality, and prevention of absorber degradation[19]. However, there are instances of unfavorable surface recombination in such devices as well, such as at an undesired anode (TCO)-electrolyte interface which may exist due to holes/pores throughout the photoanode of such devices[109]. Also, fast recombination of electrons injected from absorber into the photoanode returning to the absorber is also problematic[110].

Extremely thin absorbers, at too low a thickness, may present another specific type of interfacial recombination[108], known as tunneling recombination, which occurs when majority carriers from either the p- or n- side of the device can 'tunnel' through a sufficiently thin 'tunneling barrier' presented by the absorber into the 'opposite' (n- or p-type, respectively) side and recombine with majority carriers still present there[75,108,111]. This problem is especially prevalent in systems with low diffusion lengths, and a high 'built-in' (due to band alignment) electric field across the absorber[75,111].

2.2.1.3 Light Trapping

In a 1974 publication, David Redfield appears to have first described the technique of light trapping to enhance solar cell efficiency[75,112]. He described the potential phenomenon for Si-based solar cells, in which he proposed they be engineered with a reflective material and periodic, angular geometry engineered to allow for total internal reflection of the light, thus maximizing the amount that would likely get absorbed, thus increasing efficiency[111]. Both DSSCs and eta-SCs are favorably designed with highly porous/rough or nanowire arrayed photoanode structures, which facilitate the internal scattering and reflection of light (Fig. 2.1.2[68])[68,75].

2.2.1.4 The P-I-N Junction Model for eta-SCs

Between 2003 and 2005, Taretto, et. al. developed a model for eta-solar cells based on a p-i-n junction, complete with equations describing the J-V characteristics of such[75,108,111,113]:

<u>Assumptions:</u>
-electric field (F) is homogenous throughout the absorber, based on the 'built-in' voltage (i.e. potential difference between p- and n-layers) and applied voltage on the cell:

$$|F| = \left|\frac{V - V_{\mathrm{bi}}}{W}\right| \qquad \textbf{(2.2.1)}^{114}$$

-photogeneration rate (G) are uniform throughout the instrinsic (absorber) layer, allowed if the solar cell is sufficiently thin a/o sufficient light trapping leads to 'uniform absorption' and subsequent carrier generation throughout the absorber:

$$\bar{G} = \frac{1}{NW}\int_{E_g}^{h\nu_{\max}} \Phi_{\mathrm{Sun}}(h\nu)A(h\nu)\mathrm{d}(h\nu) \qquad \textbf{(2.2.2)}^{114}$$

where h is Planck's constant, ν is photon frequency, A is absorbance, N is the # of absorber layers, and Φ_{Sun} is the incident solar photon flux

-carrier mobilities (μ) and life-times (τ) are the same for holes (p) and electrons (n), the latter given by:

$$\tau = \frac{\tau_0}{1 + \Gamma(\Delta E_{n,p}, m_{\text{tun}}, |F|)} \qquad \textbf{(2.2.3)}^{114}$$

where τ_o is the diffusion-based carrier lifetime, given as $\tau_o = (DL_d)^{1/2}$, Γ is the field-effect function, given by:

$$\Gamma = \frac{\Delta E_{n,p}}{kT} \int_0^1 \exp\left(\frac{\Delta E_{n,p}}{kT} u - K_{n,p} u^{3/2}\right) \mathrm{d}u \qquad \textbf{(2.2.4)}^{114}$$

where $\Delta E_{n,p}$ is the distance between trap/defect states in the absorber band gap and conduction band for electrons, or valence band for holes, m_{tun} is the effective tunneling mass, and $K_{n,p}$ is given by:

$$K_{n,p} = \frac{4}{3} \frac{\sqrt{2 m_{\text{tun}} \Delta E_{n,p}^3}}{q \hbar |F|} \qquad \textbf{(2.2.5)}^{114}$$

where ħ is the reduced Planck's constant, h/2π

-current density (J) is less than some critical current density (J_{CR}):

$$J_{\text{CR}} = q \mu_n N_{\text{d}} \frac{F}{\exp\left(\frac{FW}{V_{\text{t}}}\right) - 1} . \qquad \textbf{(2.2.6)}^{114}$$

where q is elementary charge, N_d is the dopant carrier density, and V_t is thermal voltage, given by the Boltzmann equation ($V_t = k_BT/q$, where k_B is Boltzmann's constant, and T is absolute temperature)

This model relies on solving the continuity equations for minority carriers (shown for electrons here):

$$G - \frac{n(x) - n_0(x)}{\tau} + D \frac{\mathrm{d}^2 n(x)}{\mathrm{d}x^2} + \mu F \frac{\mathrm{d}n(x)}{\mathrm{d}x} = 0 \qquad \textbf{(2.2.7)}^{114}$$

where the first term represents generation rate, the second recombination rate, the third diffusion, and the fourth is related to carrier mobility/drift in an electric field. A dimensionless form of this equation is given by:

$$G_s + \exp(-V_{s0}x_s) - n_s(x_s) + L_s^2 V_s \frac{dn_s}{dx_s} + L_s^2 \frac{d^2 n_s}{dx_s^2} = 0$$ **(2.2.8)**[114]

where quantities with the subscript s represent the following scaled quantities (Table 2.1.1)[113]:

Table 2.1.1[113]: Scaled quantities for use in the Taretto, et. al. p-i-n eta-SC model

Physical quantity	Scaled quantity	Range
Distance, x	$x_s = \frac{x}{W}$	$0 \le x_s \le \frac{1}{2}$
Electron concentration, n	$n_s = \frac{n}{n_{p0}}$	$1 \le n_s$
Diffusion length, L	$L_s = \frac{L}{W}$	$L_s \le 10^4$
Surface recombination velocity, S	$S_s = \frac{SW}{D}$	$S_s \le 10^4$
Potential drop $V - V_{bi}$	$V_s = \frac{V - V_{bi}}{V_t}$	$-V_{bi}/V_t \le V_s < 0$
Generation rate, G	$G_s = \frac{G\tau}{n_{p0}}$	$10^5 \le G_s \le 10^{13}$

The general solution of this equation is given as:

$$n_s(x_s) = G_s + n_s^* \exp(-V_{s0}x_s) + C_1 \exp(\lambda_1 x_s) + C_2 \exp(\lambda_2 x_s)$$ **(2.2.9)**[114]

where $n_s^* = \left(1 + (V_s - V_{s0}) L_s^2 V_{s0}\right)^{-1}$ and λ_1 and λ_2 are dimensionless eigenvalues given as:

$$\lambda_{1,2} = -\frac{V - V_{bi}}{2V_t} \pm \sqrt{\left(\frac{W}{L}\right)^2 + \left(\frac{V - V_{bi}}{2V_t}\right)^2}\,.$$

Figure 2.2.1[113] shows a diagram of the p-i-n junction with boundary conditions noted:

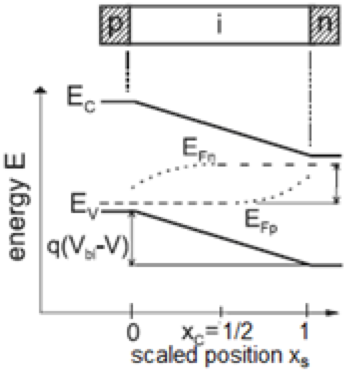

$$S_s(n_s(0)-1) = V_s n_s(0) + \left.\frac{dn_s}{dx_s}\right|_{x_s=0}.$$

$$n_s(1/2) = n(x_C)/n_{p0} = (n_i/n_{p0}) \times \exp(V/2V_t)$$

Figure 2.2.1[modified from 113]: p-i-n junction for the model (left) and boundary conditions noted (right) (n_{p0} and n_i are the electron concentration in the p- and i-layers, respectively)

The first boundary condition accounts for interfacial recombination at the p-/i- interface, and the second, from assuming μ and τ are the same for both electrons and holes in the absorber(i)-layer, the diffusion lengths for each carrier are equal, and their lifetimes are equal, so in the i-layer, n = p at x = W/2.

With these two boundary conditions established, solving for the constants C_1 and C_2 gives:

$$C_1 = -\frac{\exp(-\lambda_2/2)}{A_3} \times \left[A_1(\lambda_2 + S_s) + A_2 \exp(\lambda_1/2)\right]$$

$$C_2 = -\frac{\exp(-\lambda_2/2)}{A_3} \times \left[A_1(\lambda_1 + S_s) + A_2 \exp(\lambda_2/2)\right]$$

where

$$A_1 = n_s(1/2) - G_s - n_s^* \exp(-V_{s0}/2)$$

$$A_2 = n_s^*(S_s - V_s + V_{s0}) - S_s + G_s(S_s - V_s)$$

$$A_3 = -\lambda_2 - S_s + (\lambda_1 + S_s) \times \exp\left(\frac{\lambda_1 - \lambda_2}{2}\right)$$

with recombination current density (J_n) at the p-/i- interface given as:

$$J_n(x=0) = qS\left(n(0) - n_{p0}\right) \qquad \textbf{(2.2.10)}[114]$$

where S is recombination velocity

finally, plugging the general solution for n_s with constants, etc. into the continuity

equation (solved for current density, and scaled)

$$J_s = 2S_s(n_s(0)-1) + 2\int_0^{1/2} \frac{n_s(x_s) - \exp(-V_{s0}x_s) - G_s}{L_s^2}\, dx_s \qquad \textbf{(2.2.11)}[114]$$

gives

$$J_s = 2S_s(C_1 + C_2 + G_s + n_s^* - 1) + \frac{1}{L_s^2}\left[\frac{C_1(\exp(\lambda_2/2) - 1)}{\lambda_2/2} - \frac{C_2(1 - \exp(\lambda_1/2))}{\lambda_1/2} - \frac{(n_s^* - 1)(1 - \exp(-V_{s0}/2))}{-V_{s0}/2}\right] \quad \textbf{(2.2.12)}^{114}$$

and solving for actual current density gives

$$J = \frac{qn_{p0}D}{W} J_s \quad \textbf{(2.2.13)}^{114}$$

So, for dark current density:

$$J(0 < V < V_{bi}) = \frac{2qn_i W}{\tau} \times \left[\frac{1}{\lambda_1} + \frac{S\tau/W}{1 + SW/D\lambda_1} \exp\left(-\frac{\lambda_1}{2}\right)\right] \times \exp\left(\frac{V}{2V_t}\right). \quad \textbf{(2.2.14)}^{114}$$

and during illumination, particularly at two points of interest (V_{OC}, I_{SC})[111]:

$$J_{SC} = qGW \frac{\exp(\lambda_2/2) - 1}{\lambda_2/2}, \; V_{OC} \propto \ln\left(\frac{J_{SC}}{J_0}\right)$$
$$\text{where} \;\; J_0 = \frac{2qn_i V_t}{\tau F_0}.$$

where J_0 is the reverse bias saturation current density

The V_{OC} relation, in this case, is borrowed from Schottky a/o p-n solar cells[113], and holds only for low-W (i.e. "thin") i-layer p-i-n devices. *Reducing J_0 would improve thin absorber cell performance, and two proposed ways to do that are by increasing the built-in electric field (F_0) or carrier lifetime (τ) within the absorber material[113].* <u>Therefore, using a ferroelectric sensitizer such as BFO may be favorable to assist with the former at the very least, due to it's polarization-based 'built-in' electric field[105,114].</u>

Also worth noting is that the carrier collection efficiency (f_C) is given by J_{SC}/qGW, which gives[111]:

$$f_C = \frac{\exp(\lambda_2/2) - 1)}{\lambda_2/2}$$

and the diode 'ideality' factor (noted in section 4.6) as[113]:

$$n_{id} = V_t^{-1} \frac{d}{dV} \ln\left(\frac{J}{J_0}\right)$$

Calculations reveal that $n_{id} \sim 1.8$ for $W > L_D$, which makes sense considering $n_{id} = 1$ is for an 'ideal diode, and having a diffusion length less than the absorber thickness will likely result in much [bulk] recombination within the absorber. On the other hand, calculations run for $L_D > W$ yield $n_{id} \sim 1.2$, closer to ideal and again a sensible value[113].

Experimental data (on p-i-n Si devices) fit well to the model's predictions[113].

For the model to be utilized on eta-solar cells, the initial p-i-n model derived above is utilized in a multijunction system, which an eta-SC may effectively 'simplify' down to due to the roughness/folding of the anode and light trapping, meaning some light may pass through one junction and get absorbed at another, etc. Figure 2.2.2[75] illustrates this simplification:

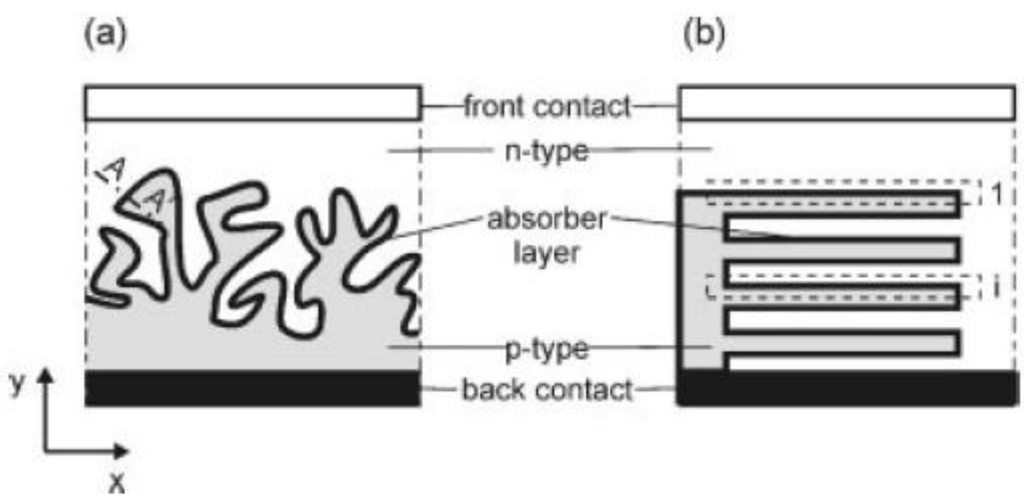

Figure 2.2.2[75]: a) Schematic of an eta-SC b) simplified multijunction system model for an eta-SC

In the case of an eta-SC, for eqn. 2.2.2, two different (i.e. ‘extreme’) absorbance cases were adopted to use in the model, that of no light trapping/scattering (eqn. 2.2.15)[75]:

$$A_a(h\nu) = 1 - \exp[-2\alpha(h\nu)NW] \qquad \textbf{(2.2.15)}^{75}$$

and that of ‘perfect’ internal reflectance; internal scattering of light off both front and back interfaces:

$$A_b(h\nu) = \left(1 - e^{-4\alpha NW}\right) / \left[1 - (1 - n^{-2})e^{-4\alpha NW}\right] \qquad \textbf{(2.2.16)}^{75}$$

where α is the absorption coefficient

Taretto, et. al. found that cells with light-trapping could improve conversion efficiency over their counterparts without light-trapping by a couple to few percentage points[75].

2.2.1.5 Ferroelectric Materials as Absorbers in eta-Solar Cells

The fundamental atomistic and physical nature and consequences were discussed at some length in section 1.3.

Thermodynamically speaking, ferroelectric materials follow the Landau function[91,114] (eqn. 2.2.17)[114]:

$$\hat{F} = -EP + \frac{1}{2}g_2P^2 + \frac{1}{4}g_4P^4 + \frac{1}{6}g_6P^6 \qquad \textbf{(2.2.17)}^{114}$$

where $\hat{F}$ is the Landau (Helmholtz) free energy density, E is applied electric field and P is polarization. The coefficients g_i vary with absolute temperature T.

Plotting this (i.e. $\hat{F}$ vs. P) at E = 0 (i.e. no external field) would yield a plot similar to the one shown in Fig. 1.3.1a. Plotting $\hat{F}$ vs. P at different values of E gives plots similar to the ‘representative’ ones shown at various points in the hysteresis loop of Fig. 1.3.1b.

Since equilibrium polarization for a given applied field E would result at a minimum in free energy, one must find locate this point by differentiating $\hat{F}$ and setting equal to zero (eqn. 2.2.18)[114]:

$$\frac{\partial \hat{F}}{\partial P} = 0 = -E + g_2 P + g_4 P^3 + g_6 P^5 \qquad \textbf{(2.2.18)}^{114}$$

For the ferroelectric state, one may assume that coefficient g_2 ‘zeroes’ (i.e. ‘transitions’) at some temperature T_o, giving:

$g_2 = \gamma(T-T_o)$, where γ is a positive constant and $T_o \leq T_C$

If g_2 is positive (i.e. $T > T_o$), then the unpolarized lattice is favored, and if g_2 is negative (i.e. $T < T_o$), polarization is favored.

Ferroelectric phase transitions may be either first- or second-order[37,114]. For a second-order phase transition, g_4 is positive, and neglecting the g_6, etc. terms, the condition for equilibrium polarization in field E can be rewritten as (eqn. 2.2.19)[114]:

$$0 = -E + \gamma(T-T_o)P + g_4 P^3 \qquad \textbf{(2.2.19)}^{114}$$

and at zero bias gives (eqn 2.2.20)[114]:

$$0 = \gamma(T-T_o)P + g_4 P^3 \qquad \textbf{(2.2.20)}^{114}$$

Solving for P (which is saturation polarization P_s for a single crystal) such a case gives either P = 0 or:

$P = \left(\frac{\gamma}{g_4}\right)^{\frac{1}{2}}(T_o - T)^{\frac{1}{2}}$, which is continuous at T_o (hence second order transition)[114], and T_o is equivalent to the Curie temperature T_C

For a first-order phase transition, g_4 is negative, and $|g_4|$ is taken because free energy is not likely to 'sink' to minus infinity ever, giving the equilibrium condition at zero applied field as (eqn. 2.2.21)[114]:

$$0 = E = \gamma(T - T_o)P - |g_4|P^3 + g_6P^5 \qquad \textbf{(2.2.21)}^{114}$$

Leaving (eqn 2.2.22)[114]:

$$0 = \gamma(T - T_o) - |g_4|P^2 + g_6P^4 \qquad \textbf{(2.2.22)}^{114}$$

At $T = T_c$, the free energies for the parelectric (P = 0) and ferroelectric (finite P) solution will be equivalent[114].

Similar to ferromagnetic materials, ferroelectric materials also tend to form polarization domains. A domain is a region of crystals with the same polarization direction. These domains in a crystal (often as synthesized/made) form in order to minimize the bulk crystal's energy by 'cancelling each other out', thus making the net polarization of the as-produced crystal equal to zero (outside of any externally-applied field)[35,114]. However, once a field of $E > E_c$(the coercive field) is applied, upon removal, leaves the crystal with a remnant net polarization in the direction of the field (P_r)[35].

In polycrystalline/polydomain ferroelectric thin films, Landau and Ginzberg alter the above equations/'framework' (which are more or less a 'bulk' expression) to eqn. 2.2.23:

$$G = \int_0^h \left[\frac{A}{2}P_r(r)^2 + \frac{B}{4}P_r(r)^4 + \frac{C}{6}P_r(r)^6 + \frac{1}{2}g(\nabla P_r)^2 - E_d(r)P_r(r)\right] r\,dr + \frac{D}{2\delta}\int_S P_r^2\,dS \qquad \textbf{(2.2.23)}^{91,116}$$

> where P_r is remnant polarization, G is the free energy, h is the film thickness, $A = g_2 = \gamma(T\text{-}T_o)$, $B = g_4$, $C = g_6$, D is another coefficient, g is an energetic cost to changing P_r near an electrode/FE interface, E_d is the depolarizing field, and δ is 'extrapolation length', a correction term which compensates for surface area. The dS term compensates for interface/surface effects, and E_d for the depolarizing field

Polarization P, atomistically, is caused by distortions of the center cation of the BO_6 octahedron and subsequent shift of that octahedron relative to the corner atoms of the initially cubic perovskite lattice, as discussed previously[35-38,111], and hence the consequential formation of electronic dipoles within the crystal. The total dipole moment $\vec{p}$ ($\vec{p} = \sum q_n \vec{r}_n$, where q_n is charge and $\vec{r}_n$ is position vector) of a polarized crystal leads to a built-in electric field at any given point($\vec{E}(\vec{r})$, which is based on Maxell's equations[114]) within it, given by (eqn. 2.2.24)[114]:

$$\vec{E}(\vec{r}) = \frac{3(\vec{p}\cdot\vec{r})\vec{r} - r^2\vec{p}}{4\pi\varepsilon_0 r^5} \qquad \textbf{(2.2.24)}^{114}$$

> where ε_0 is the electrical permittivity of free space

If $\vec{E}(\vec{r})$ is taken at various points $\vec{r}$ within the crystal, it may be referred to as 'microscopic field' $\vec{e}(\vec{r})$, which can then be plugged into eqn. 2.2.25 to find a net average 'built-in' electric field ($\vec{E}(\vec{r}_o)$)within a ferroelectric (or otherwise electronically polarized) crystal[114]:

$$\vec{E}(\vec{r}_o) = \frac{1}{V_c}\int_V d\vec{r}\,\vec{e}(\vec{r}) \qquad \textbf{(2.2.25)}^{114}$$

The calculations for the dipole moments (based on ion charges and displacements) as well as those for the microscopic fields, even within a single unit cell or bulk single crystal, can likely be quite cumbersome, and likely best solved numerically based on lattice models, distortions/displacements, and ion charges.

A semi-empircal approximation for the correlation between polarization and internal field is given by eqn. 2.2.26[115,116]:

$$E_{local} = \chi(E)E_{applied} + \frac{\gamma P}{\varepsilon_0} \qquad \textbf{(2.2.26)}^{115,116}$$

> where χ(E) is the electronic susceptibility of the material at field E γ is the Lorentz factor for 'coupling of dipoles', 'theorized'[115] as ~0.33 but in experiments found to be approximately two orders of magnitude less[115].

Taking the value of remnant polarization for BFO[100,101] as ~60μC/cm^2 (and hence the applied field is zero), and the approximation for γ as given above[116] yields an approximate 'built-in' electric field of ~2240kV/cm, meaning that in a 1μm thick film, the 'built-in' voltage of ~0.22V, which could potentially make ferroelectricity a significant contributor to 'built-in' field/voltage and photovoltaic devices.

Morevoer, it has been proposed[117] that the internal field (both switchable (ferroelectric, $|V_p|$) and non-switchable ($|V_{bi}|$) contributions) can be calculated via IV-characterization and open-circuit voltages (V_+ when the ferroelectric material is poled one direction, and

V_- when it is poled in the opposite direction), as noted in eqn. 2.2.27[117] and 2.2.28[117] below:

$$|V_p| = \frac{1}{2}(V_+ - V_-) \qquad \textbf{(2.2.27)}^{\textbf{117}}$$

$$|V_{bi}| = \frac{1}{2}(V_+ + V_-) \qquad \textbf{(2.2.28)}^{\textbf{117}}$$

Thin-films as those likely to be used as sensitizers (i.e. on the order of 100-200nm or less) may be significantly [negatively] impacted by a depolarizing field (E_d)[104], as discussed previously in section 2.1.3[91,92]. A depolarizing field occurs due to the accumulation of charges at electrode/FE interfaces, and their subsequent production of an electric field opposing the applied electric field a/o 'built-in' field created by FE-polarization, thus lowering the net/apparent polarization across the material[91,92]. At some critical thickness (usually on the order of a few to several unit cells), this field leads to the apparent 'cancellation' of ferroelectric behavior in a material altogether[91,92,118]. Surface chemistry alteration[36] and curvature/stress-strain effects[91] can assist in mitigating the depolarizing field by mitigating surface charge (the former) and assisting/adding to polarization via curvature and strain (the latter)[36,91].

2.3 Thin Film Deposition Techniques

2.3.1 Electrochemical Deposition

Electrochemical deposition, or cathodic electrodeposition, is a process by which material (often metallic or ceramic)[119-123] is deposited from pre-cursor solution(s) onto a conducting substrate (i.e. 'cathode' of an electrochemical cell) via an applied electrical potential. This process often utilizes a three-electrode setup, with the substrate serving as the working electrode where deposition occurs, a conductive and an (often but not always)[120] inert[121,122] counter electrode to 'complete the circuit', allowing for the flow of current to occur, and a reference electrode containing a redox reaction of well-known and established potential (often a hydrogen-based standard, Ag/AgCl or saturated calomel ($HgCl_2$)), to establish a comparative potential, which the deposition or measured potential is based on. Since this section work deals primarily with the electrodeposition of ZnO from $Zn(NO_3)_2$ precursor, the equations for such zinc oxide electrodeposition is given below[121,122]:

$$NO_3^- + H_2O \rightarrow NO_2^- + 2OH^-$$
$$Zn^{2+} + 2OH^- \rightarrow ZnO$$

Giving an overall reaction of[121,122]:

$$Zn^{2+} + 2NO_3^- \rightarrow ZnO + 2NO_2^-$$

Figure 2.3.1[based on 119,etc.] shows a schematic of the electrodeposition process:

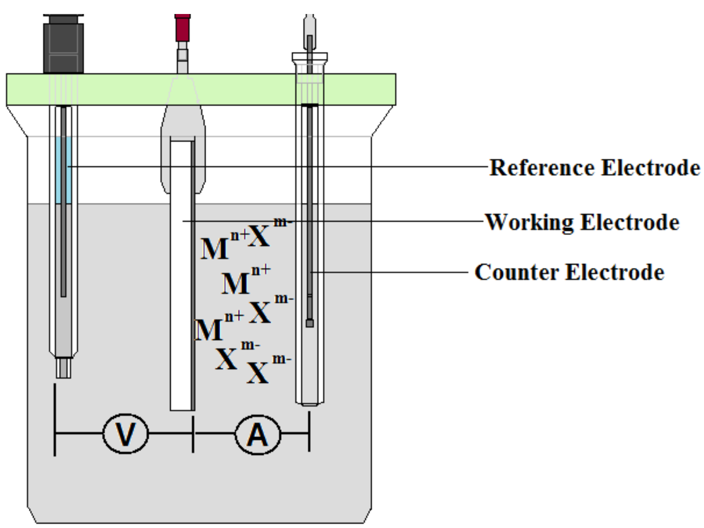

Figure 2.3.1[based on [119,etc.]]: Schematic of the electrodeposition setup/process

Deposition of material via electrodeposition is governed by Faraday's Law, a restatement of which is shown in eqn. 2.3.1[124] below:

$$h = \frac{M}{n\rho AF}\int_0^{t_f} I\,dt = \frac{M}{n\rho F}\int_0^{t_f} J\,dt$$ **(2.3.1)**[124]

where h is the film thickness, M is molecular weight of the deposited species, n is the number of electrons involved in the deposition reaction, ρ is the density of the deposited species, A is substrate deposition area, I is deposition current (or, as seen on the right, equation can be written in terms of deposition current density J), t is deposition time, and F is Faraday's constant (~96,500C/mol).

For simplicity, cathodic electrodeposition is often done as potentiostatic (constant voltage) or a galvanostatic (constant current) mode. Since the deposition current can be controlled by setting it (galvanostatic deposition) or known by measuring it (potentiostatic deposition), and the deposition species and charges are known, a desired thickness can be used to calculate deposition time required, or vice-versa.
Important parameters governing electrodeposition are the potential a/o current/current density, precursor solution, species and concentration, solution temperature, and deposition time. Increases in deposition potential (potentiostatic) or current (galvanostatic) increase deposition rate. Increased deposition time yields an increased deposition thickness.

In this work, electrodeposition was used to deposit rough ZnO films of ~several hundred nanometers to a few microns in thickness. However, the process has also been used to not only deposit ZnO nanowires[57,75,76,120,125] on 'pre-seeded'[57,125] substrates or via template assisted growth[120], but also more 'typical' sensitizer/absorber materials (CdSe[76], CdTe[105], etc.), and the hole-conductor CuSCN for other work on DSSC or eta-solar cells[62].

2.3.2 Atomic Layer Deposition

Atomic layer deposition (ALD) is a technique by which carefully-timed pulsed precursors, within a certain temperature and pressure window, can, via reaction and chemisorption, form many different metallic or ceramic/oxide compounds[126], as demonstrated in Fig. 2.3.2[127]:

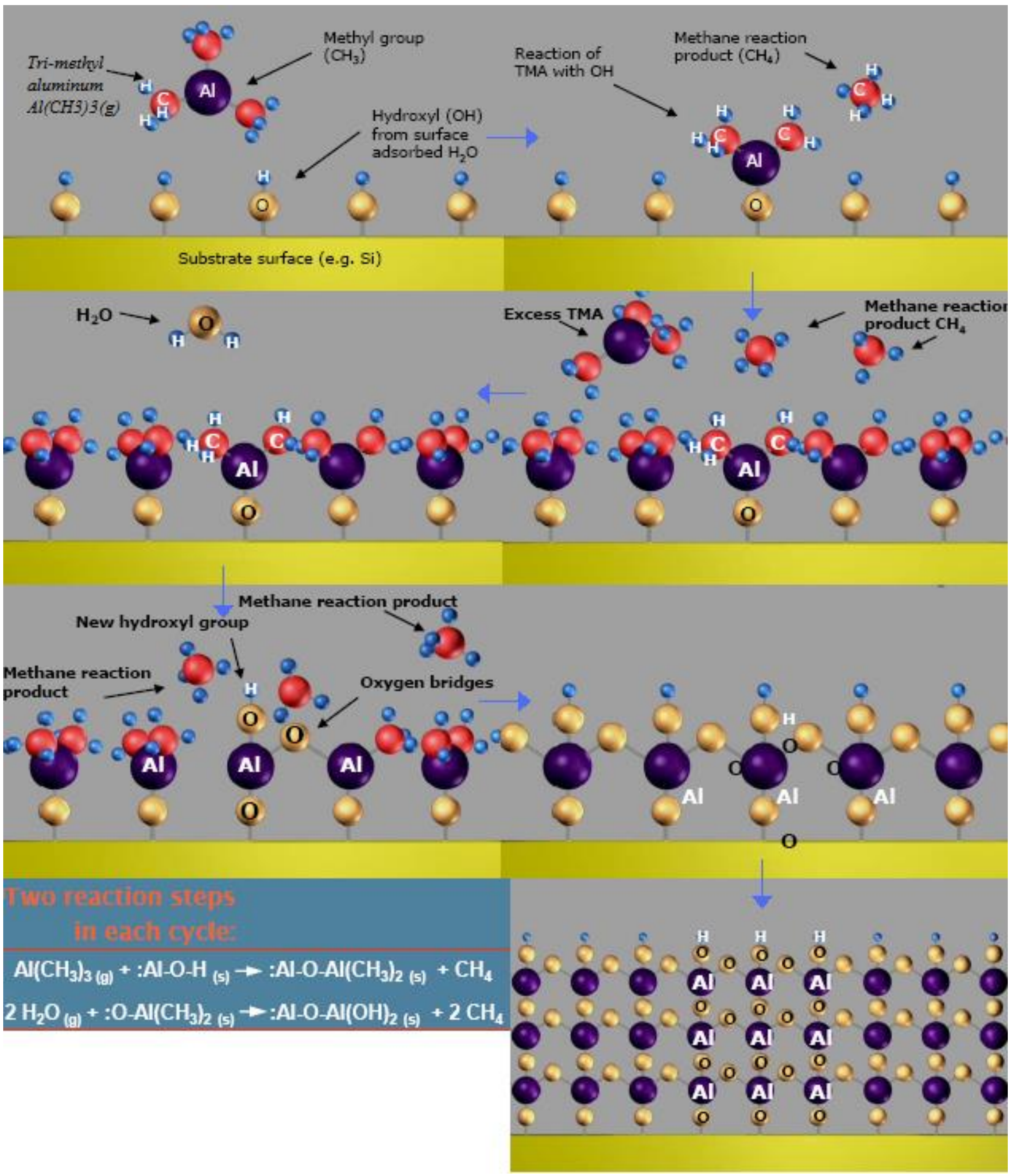

Figure 2.3.2[127]: Schematic of the atomic layer deposition process (for Al_2O_3 as displayed)

As shown in the diagram, appropriately chemically functionalized substrates allow chemisorption of a precursor based on reaction between the functional group and precursor ligand(s). Once the substrate is covered with the first precursor, which should not react or chemically bond with itself, excess precursor is flushed out of the chamber, and a second precursor flows, which does reaction with the ligands still attached to the later formed by the first precursor chemisorbed to the functionalized substrate, and a 'clean' layer of precursor 2 is then formed on top of precursor 1. This process can be repeated for several cycles depending on desired film thickness, etc., and can be used to fill over particles/features as well as in small a/o high-aspect ratio pores[126].

Well-established[128] protocol for ALD of TiO_2 films exist, when conformation to a substrate a/o extremely accurate film thickness is desired. Due to the ready availability of ALD to the group, ALD-based TiO_2 films were used in this work to initially determine the viability of using TiO_2 as a wide-gap semiconductor in conjunction with a $BiFeO_3$ sensitizer (more details in Ch. 5).

2.3.3 Dip-coating

Sol-gel chemical reactions, in general, have been used to deposit many ceramic, semiconducting, or even ferroelectric materials[129,130] previously. Metallic, non-metallic, or metalloid-based precursors for such processes often have organic or nitrate 'ligands' attached[130], which facilitate the sol-gel process, described generally by the hydrolysis and condensation reactions given[131]:

$$A(OR)_x + B(OR)_y + H_2O \rightarrow (RO)_{(x-a)}A\text{-}(OH)_a + (HO)_{(y-b)}\text{-}B\text{-}(RO)_{(y-b)} + ((x-a)+(y-b))R + xH_2$$

Hydrolysis (gel-formation)

$$(RO)_{(x-a)}A\text{-}(OH)_a + (HO)_{(y-b)}\text{-}B\text{-}(RO)_{(y-b)} \rightarrow (NO_3)_{(3-x)}A\text{-}O\text{-}B(NO_3)_{(3-x)} \ldots + xH_2O$$

Condensation (sol-formation)

Material ‘sols’ can be easily deposited on substrates by a variety of techniques, such as drop casting, spin coating, and dip coating. For this work, sensitizer/absorber material was [most] often deposited by dip-coating, due to the simplicity of the process and ease of layer thickness control when compared to the other two.

Moreover, nanoparticle suspensions can also be deposited via dip-coating, and subsequently heat treated to achieve desired morphology, thickness, and/or properties as well. Dip-coating wide-gap semiconductor nanoparticle suspensions onto conductive-glass substrates and subsequent sintering them can yield a rough and/or porous film, which, though perhaps not the most uniform and not flat, is often considered favorable for DSSC and eta-solar cell applications for the benefits of both additional surface area to absorb incident photons[58-61,75] and possible light-trapping[75], as discussed previously (Section 2.2.1.3).

Dip-coating is a simple, relatively inexpensive coating technique, where a vertically-oriented substrate is ‘dipped’ in a precursor solution bath (Fig. 2.3.1)[132] and retracted at a set speed.

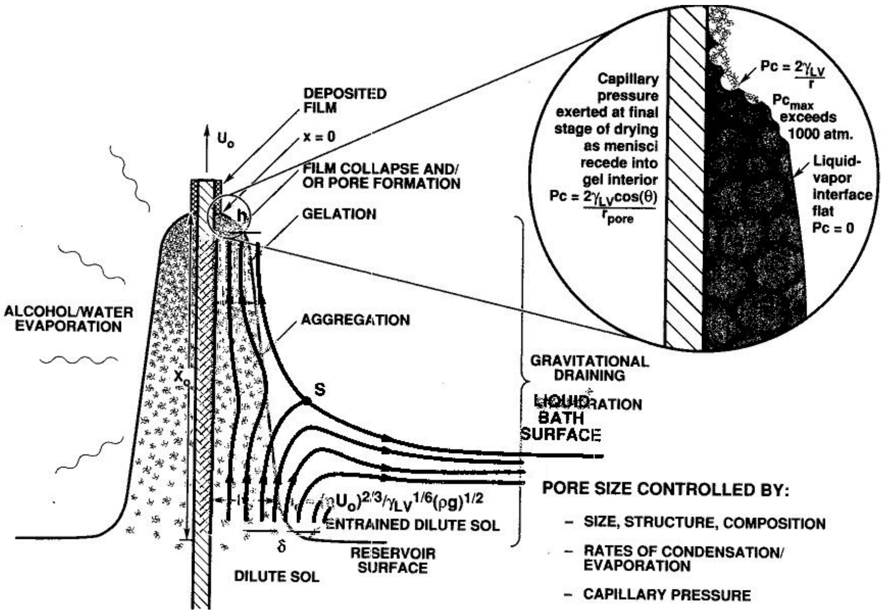

Figure 2.3.1[modified from 132]: Schematic of the dip-coating process, noting key parameters

As the substrate is removed, the desired inorganic material is deposited on the substrate surface and further concentrated by solvent evaporation, eventually forming a xerogel on the substrate.

Achieved film thickness can be controlled in the dip-coating process by three main parameters: withdrawal speed, sol/solution viscosity (namely dictated by solution concentration and solvent viscosity), and number of dipping ‘cycles’ performed on a given sample. Equation 2.3.2[132] shows the relationship between film thickness (h), sol viscosity (η), and withdrawal speed (U_o) first derived by Landau and Levich[132]:

$$h_o = 0.94(\eta U_o)^{2/3} / \gamma_{LV}^{1/6}(\rho g)^{1/2} \qquad \textbf{(2.3.2)}^{132}$$

Faster withdrawal speeds, higher sol viscosities, and more ‘cycles’ of dipping result in thicker films, and since all three of these parameters are easily tunable, dip-coating is a quite favorable, simple process for film/coating deposition. Also, coating porosity can be tuned by varying solvent species or evaporation rate[132].

2.3.4 Other Potential Deposition Techniques

TiO_2 has been, in [both] film and wire/nanotube form, successfully deposited by metallorganic chemical vapor deposition (MOCVD)[100,133], sol-gel synthesis[63,64,134,135], spray pyrolysis[110], electrochemical deposition[134], Ti-metal/foil anodization[56], pulsed laser deposition (PLD)[58,136], spin-coating[137], etc., as well as combinations of such techniques[64]. However, for the combination of simplicity, thicknesses control, and desired morphology (rough a/o porous)[30,58-61,68,,75], along with precursor and setup costs considered, suspension/paste deposition seemed to be the best technique for TiO_2 deposition for the ‘brunt’ of this work.

BFO thin films have been synthesized and deposited by sputtering[105], pulsed laser deposition (PLD)[101] and metallorganic chemical vapor deposition (MOCVD)[100] as well, but again for the sake of simplicity and maintaining low costs for precursors and processing (once again in the ‘spirit’ of DSSC and eta-solar cells in the ‘inexpensive and simple’ 3rd generation solar cells ‘camp’), as well as due to the control over thickness and conformation available to the process, sol-gel chemistry[138,139] and dip coating were chosen, respectively, as the synthesis and deposition routes for BFO. However, another possibility (utilizing the same nitrate-based precursors as the sol-gel technique), electrodeposition of BFO has also been proven possible and viable[140].

Aside from solution/drop-casting (section 3.5), the prevalent means of depositing CuSCN, especially for DSSC or eta-solar cells, is electrodeposition[62,141]. A method that allows for the fabrication of control devices as similar as possible to their sensitized counterparts (minus having an actual sensitizer/absorber layer) should be used, and solution casting of CuSCN can likely be done on ZnO, TiO_2, and BFO surfaces without any need for tuning/retuning process conditions for each material.

2.4 The ZnO or TiO_2/BFO/CuSCN System

The key semiconducting materials explored as a potential eta-solar cell device system in this thesis are TiO_2 (or ZnO), BFO, and CuSCN. These materials were chosen as a set based on their prospective, ‘idealized’ band alignment, found based on their electron affinities ($q\chi$) (conduction band locations relative to the vacuum level), work function (φ, to indicate location of E_f) and band gaps (E_g) (valence band energy relative to the conduction band)[142,143], as shown in Figure 2.4.1[40,59,76,100,103,105,108,117,140,142-150]:

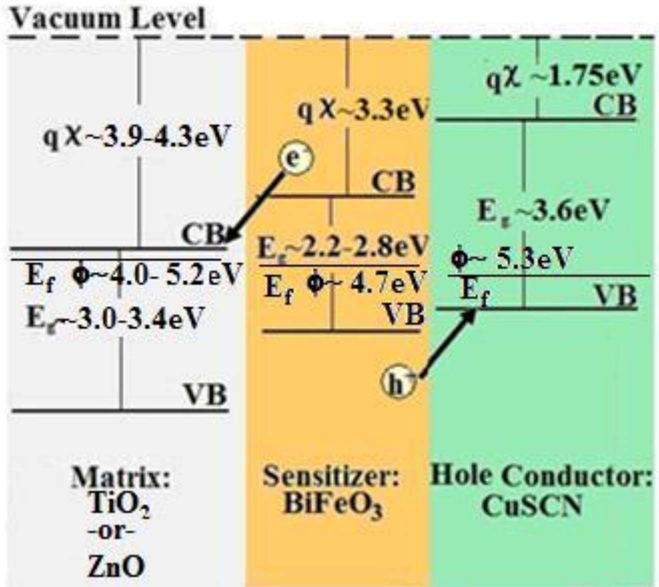

Figure 2.4.1[40,59,76,100,103,105,108,117,140,142-150] 'Idealized' band alignment for the TiO_2 or ZnO/BFO/CuSCN system

ZnO, due to its favorable band gap and predicted alignment (E_g ~3.3-3.4eV[59,76], $q\chi$~4.2eV[146]) with BFO and CuSCN, was also tried as a candidate wide-gap semiconductor photoanode matrix material in this work. ZnO is a II-VI oxide and wide-gap semiconducting material, which typically crystallizes in a hexagonal (wurtzite) structure[108,151,152], shown in Fig. 2.4.2[151]. It is often n-type as-synthesized likely due to oxygen vacancies[153], or potentially Zn-interstitials[153] or H-interstitial incorporation[154]. However issues arose with its sensitization via BFO (later described in section 5.1.3).

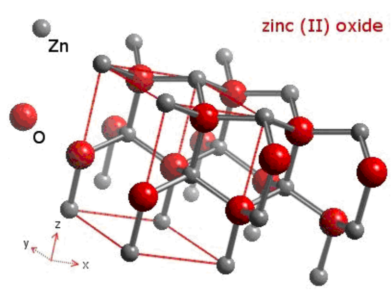

Figure 2.4.2[152] Schematic of the ZnO (wurtzite) crystal structure

TiO_2 has three distinct polymorphs[153,155-157]; anatase (tetragonal), rutile (tertragonal), and brookite (orthorohmobic), shown in Fig. 2.4.3[155-157]. Anatase, α-TiO_2 (E_g~3.1≲3.4eV[144,145], qχ~3.9eV[145]), is a wide-band-gap semiconductor used much throughout the literature[30-34,41-45,47-52,54-56,58,61-72,74,80,144,148] for DSSC and eta-PV applications.

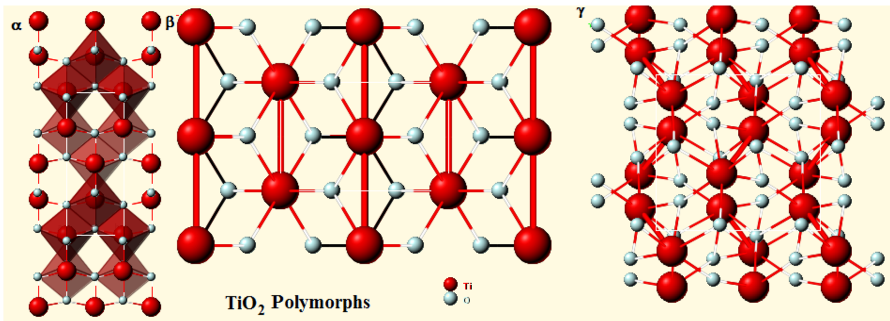

Figure 2.4.3[155-157]: Schematic of anatase (left), rutile (center), and brookite (right) crystal structures of TiO_2 polymorphs

Similar to ZnO, α-TiO_2 is often n-type ‘as synthesized’ as well, due to oxygen vacancies, and potentially Ti-interstitials[158].

$BiFeO_3$ is a multiferroic (ferroelectric (T_C ~ 850^{o}C, E_C >500-600kV/cm (50-60V/µm)(thin films) and ~17kV/cm(bulk)), P_R ~ 60µC/cm^2(for both))[100,159], antiferromagnetic (T_N = 370^{o}C)[100,159]) ternary oxide, which crystallizes in the perovskite structure, and is cubic above and rhombohedrally-distorted below its (ferroelectric) Curie temperature (Fig 2.4.3)[based on 160]. In addition, and fairly unique among perovskite materials, $BiFeO_3$ has a band gap well within the energy range of visible light (E_g~2.2-2.8eV)[40,100,103,105,117,139,147], hence allowing for its potential use as a photosensitizer or absorber.

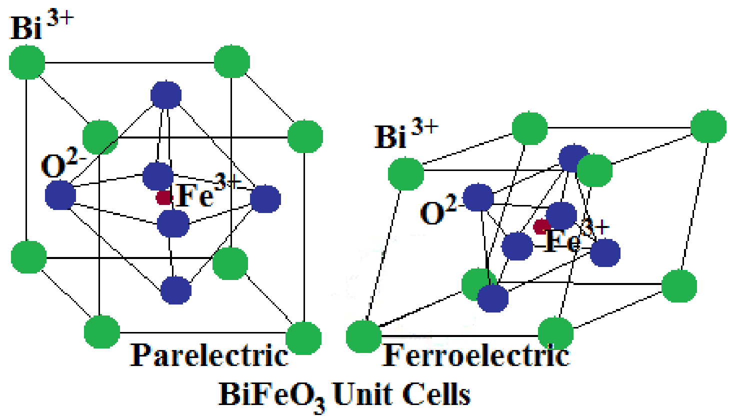

Figure 2.4.3[based on 160] Bismuth ferrite cubic-(left) and rhombohedrally-distorted-(right) perovskite crystal structures

Though its band gap is within the visible light energy range, the band gap of bismuth ferrite is 'higher than ideal' for sensitizer applications when compared to the energy required for absorption in many dyes or inorganic sensitizers/absorbers (i.e. ~1.4-1.8eV considered an 'ideal' range for sensitizer/absorber energy gap[108]) used in previous work. However, the use of a ferroelectric sensitizer, that is a material that can retain some electronic polarization within it despite the absence of an externally-applied electric field, may have novel effects on charge separation and/or transport that traditional dye-sensitizers or semiconductor absorbers would not have, possibly 'lending itself' to an increase in overall efficiency. Furthermore, the use of $BiFeO_3$ in photovoltaic applications may be favorable vs. many popular semiconductor absorber/quantum dot sensitizer materials due to the absence of carcinogenic or fairly toxic precursors and heavy metals (Cd, Hg, Pb, etc.), making this material a more 'environmentally-friendly' option for an already reasonably 'environmentally-friendly' application.

CuSCN is considered an inorganic p-type semiconductor (E_g~3.6eV) that crystallizes in a hexagonal[76,151], orthorhombic [151], or rhombohedral[151,161], or perhaps furthermore a trigonal[141] crystal structure, and serves as a solid-state hole conductor for the devices proposed and utilized in this work. As a solid, p-type material with favorable band alignment with both α-TiO_2 and BFO, and, as discussed previously, some possible stability advantages vs. CuI[], as well as it's usage for similar devices in previous literature[], CuSCN was selected as the representative hole conductor material for this work.

2.5 Novel Research in this Thesis

The central novelty in this thesis is the use of bismuth ferrite ($BiFeO_3$, BFO) as a "sensitizer"-type material in SSC/eta-type for TiO_2-based photovoltaic devices. Many groups in the literature already work on a variety of sensitizers and absorbers for such TiO_2-based devices[34,41-45,47-52,54-56,58,61-72,74,80] and ZnO-based[57,59,75,76,108,125], and others[39,40,100,104,106] have characterized BFO for potential "conventional"/"stand-alone" photovoltaic device properties and applications, and the use of ferroelectricity (as opposed to a p-n junction) for generating the electric field in PV devices necessary for charge separation and transport. Furthermore, Li et. al.[108], have coupled BFO with the wide-gap semiconductor TiO_2 in core-shell nanoparticles for catalysis of organic dye breakdown, but did not mention nor utilize such a system for photovoltaic applications, nor was the effect of ferroelectric polarization of BFO on such a system's performance investigated. Also, Wu, et. al., have investigated diode-like behavior in the BFO/ZnO system, though not noted for photovoltaic applications[105]. Despite the amount of somewhat related work in the literature, thus far none have published on the use of BFO as a thin-absorber or sensitizer material for photovoltaic applications. The synthesis and viability of a BFO-sensitized device, both TiO_2- and ZnO-based, are ‘talked’ about in this work, as well as structural, morphological, optical characterization of such devices at various stages of ‘production’ or ‘fabrication’, including comparison to ‘sensitizer free’ control devices. Also, attempts at and issues with ferroelectric polarization and characterization of BFO films on FTO-glass, as well as preliminary electrical measurements conducted on Bi-Fe-Zn-O/ZnO and CuSCN/BFO/TiO_2 devices are discussed. Assessment of such initial ‘pioneering’-type work on such systems of materials, as well future implications of and synthesis improvements for said systems, as well as related potential future systems, are also duly noted.

CHAPTER 3: SYNTHESIS AND FABRICATION TECHNIQUES

3.1 Synopsis of Synthesis/Fabrication

For 'complete devices', FTO-glass substrates were ultrasonically cleaned prior to TiO_2 film deposition via nanoparticle (NP)-based solution/suspension dip-coating. $BiFeO_3$ sols were produced via sol-gel chemical synthesis, and films were then deposited on FTO-glass substrates w/ TiO_2 films via dip-coating to 'sensitize' the TiO_2. CuSCN was then deposited as a 'hole conductor' via a solution deposition technique, and a metallic 'top contact' was then deposited on top of that layer to complete the device. Characterization was done (discussed further in chapter 4) on nearly-complete devices as well as samples at various stages of this fabrication process, including 'sensitizer-free' controls.

3.2 Substrate Preparation and Cleaning

F:SnO_2 (FTO)-glass substrates of sheet resistance ~10Ω/□ (Hartford Glass Co., Inc., TEC15, 25mm x 50mm) were probed via multimeter (Fluke 77III) in resistance measurement mode (i.e. ohmmeter) to find the FTO (i.e. 'conducting') side of the substrate. FTO-glass substrates were then scribed on the non-conducting (i.e. 'glass', to minimize potential damage to the FTO coating on the opposite surface) side to denote the conducting vs. non-conducting surfaces of the substrate. Substrates were then cleaned ultrasonically (Branson 3210) in small beakers containing an approximately 1:1:1 volumetric ratio of acetone to isopropyl alcohol (IPA) to deionized (DI) water, respectively, for approximately 15 minutes, and dried with N_2 prior to use [162,163].

3.3 Electrodeposition of ZnO

ZnO was cathodically electrodeposited on several ‘clean’ FTO-glass substrates (on the FTO (i.e. conductive) surface), either potentiostatically (between -0.95V and -1.10V) or galvanostatically (between -6.0mA and -10.0mA (~0.7-2.7mA/cm^2)) in ~0.1M $Zn(NO_3)_{2(aq)}$ solution at ~70^{o}C-90^{o}C (hot plate) for various times (~400-3600sec.), depending on the approximate desired [mean] film thickness, as described previously[119-121]. Potential was either established (potentiostatic) or measured (galvanostatic) via a potentiostat (PineWaveNOW) compared to an Ag/AgCl reference electrode (Pine Instruments Inc.). A Pt-wire (often contained in a glass frit) served as the counter electrode, and measurements were recorded by computer software (AfterMath).

3.4 Synthesis/Deposition of TiO_2 Films

3.4.1 Nanopowder Suspension-based TiO_2 Films

TiO_2 nanopowder (Alfa-Aesar, >99% anatase,~32nm average particle diameter) was dissolved, mixed/crushed manually with a metal spatula some, and subsequently magnetically stirred in deionized water for several minutes, yielding a suspension with final TiO_2 concentration of ~0.1g/mL. While stirring, ~ 4 drops (in ~30-40mL total suspension volume) of surfactant triton x-100 (Alfa Aesar (via VWR)) was added to the suspension, and it was then stored in a polypropylene bottle. This process was somewhat based on work by Kontos, et. al[164] and Arabatzis, et. al.[165,166], though they utilized a doctor-blade technique rather than dip-coating to achieve desirable thicknesses.

FTO-glass (Hartford glass TEC-15, 25mm x 50mm) substrates were subsequently dipped in the suspension via a LabView 7.0-controlled lead-screw linear actuator dip-coater, and retracted at selected rates in the range of 10mm/min-1500mm/min (see Fig. 5.1.17 following in Ch.5 for film thickness ‘detail’) for a ‘single cycle’ at each rate.

To achieve thicker films, multiple dip-coating ‘cycles’ could be performed on a given substrate, provided it was allowed to ‘properly dry’ in between each one. For instance, ~1.1μm thick TiO_2 films were achieved by dip-coating a clean FTO-glass substrate at 1500mm/min four times. Much of the discussed BFO/, CuSCN/, and CuSCN/BFO/TiO_2 work discussed later in this thesis utilized samples dipped in TiO_2 suspension at 1500mm/min dipped for one or four cycles, due to the potentially ‘desirable’ relatively ‘higher’ thickness achieved.

Post dip-coating, samples were placed in an oven (VWR) at ~100^{o}C for ~10min. (aqueous) to ensure drying, and then placed in a box furnace (Vulcan 3-130) at 500^{o}C for 1 hr to anneal and partially sinter the TiO_2 films.

3.4.2 Atomic Layer Deposition of TiO_2 Films

Atomic layer deposition (ALD, Cambridge Nanotechnology) of TiO_2 films was carried out on clean FTO-glass substrates. Titanium isopropoxide Ti(O-i-Pr)$_4$ (Strem Chemical, 98%) and deionized H_2O (via Millipore, Natural Polymers and Photonics Lab, Drexel University) were used in alternating pulses in the reactor at a base pressure of 0.5torr, and temperature of 200^{o}C, as prescribed by Cambridge[127]. Film thicknesses, estimated first via ellipsometry (w/ FilmWizard software) and later 'verified' via SEM cross section were between 200 and 250nm. Post-growth, films were heat treated in the furnace in ambient air at ~500^{o}C for ≳30 min, based on previous work/findings[167].

3.5 $BiFeO_3$ Deposition

The recipe for BFO sol via sol-gel chemistry was adopted from Park, et. al.[137,138]. 5mmol each of $Bi(NO_3)_3*5H_2O$(JT Baker, 98% ACS Reagent) and $Fe(NO_3)_3*9H_2O$(>99% ACS Reagent) were added to 12ml of ethylene glycol(VWR (BDH) 99% min.) and magnetically stirred on a hot plate (VWR) at ~80^{o}C for ~1hr. "Excess" ethylene glycol (a/o reaction 'byproducts' such as H_2O) was then evaporated via heating at ~200^{o}C for a few to several minutes on the same hot plate used previously. The following chemical reactions describe the formation of the BFO-sol (all in ethylene glycol in this case):

$$Bi(NO_3)_3 + Fe(NO_3)_3 + H_2O \rightarrow (NO_3)_{(3-x)}Bi\text{-}(OH)_x + (HO)_x\text{-}Fe\text{-}(NO_3)_{(3-x)} + xNO_2^- + xH^+$$

Hydrolysis (gel-formation)

$$(NO_3)_{(3-x)}Bi\text{-}(OH)_x + (HO)_x\text{-}Fe\text{-}(NO_3)_{(3-x)} \rightarrow (NO_3)_{(3-x)}Bi\text{-}O\text{-}Fe(NO_3)_{(3-x)}\ldots+xH_2O$$

Condensation (sol-formation)

After BFO sol was synthesized and, if necessary or desired, diluted, uncoated- or TiO_2 film-coated FTO-glass substrates were then typcially dip-coated into the BFO sol and retracted at a set rate between 1 and 1000 mm/min. 'BFO-sol'-coated substrates were then placed in an oven (VWR) at ~100^{o}C for ~1hr. to dry, and then heat treated (typically for TiO_2-based, not always for ZnO-based) at 400^{o}C for 30min. (to 'burn off' any excess organic, byproducts, ligands, etc.) and 625^{o}C for 1 or 2hr. (to crystallize BFO) in the furnace in air. Some Bi-Fe-Zn-O/ZnO samples were heat treated via rapid thermal annealing (RTA, Heatpulse 210) for 5-10min. between 400^{o}C-650^{o}C. For later analyzed CuSCN/BFO/TiO_2/FTO-glass, as well as the IV-characterized (Ch. 5.2) Bi-Fe-Zn-O/ZnO/FTO-glass sample, the BFO-sol retraction rate commonly used for samples discussed in this work was 200mm/min.

3.6 CuSCN Solution Bath Deposition

The procedure for simple solution deposition of CuSCN on FTO glass was adopted from Kumara, et. al. in 2001[168], with modifications similar to those done by O'Regan, et. al in 2002[161]. Briefly, ~0.2g CuSCN powder (Alfa Aesar, 96% min) in ~20mL (di-)n-propyl sulfide (Aldrich, 97%) was magnetically stirred "overnight" at room temperature, and allowed to 'settle' for several hours. Then, FTO-glass, TiO_2-FTO-glass, or BFO-TiO_2-FTO-glass substrates were placed on a hotplate at ~75^{o}C-85^{o}C until heated, and CuSCN solution (shaken sometimes prior) was then dropped on the 'top' surface of the substrate(s) and "lightly spread" (w/ a dropper) along the surface of the substrate(s), and the substrate(s) were allowed to dry on the ~80^{o}C hotplate (boiling point of propyl sulfide ~142^{o}C[161,162]), and the process was generally repeated ~8 times, for a thickness of ~3-8μm.

3.7 Electrical Contacting

Thermal evaporation (Lesker) of Ti-Au (on Bi-Fe-Zn-O/ZnO samples) or Au-Cr-Ag-Cr (CuSCN/BFO/TiO_2/FTO-glass, CuSCN/TiO_2/FTO-glass, BFO/TiO_2/FTO-glass, TiO_2/FTO-glass). However, due to CuSCN morphology as well as time required for evaporation, measurements were also done on samples contacted with silver paint (Ted Pella, Inc.; previously listed samples and similar as well as BFO/FTO-glass).

3.8 Electronic Polarization of $BiFeO_3$

A DC-voltage (V) may be applied (Radiant Technologies Precision LC 100V Ferroelectric tester) across the BFO layer or completely fabricated device equivalent to or greater than the coercive field (E_c) required to polarize BFO layer at its given thickness(t) (i.e. $V/t \geq E_c$). Measurement of E_c and hence further details on this process are discussed later in section 4.5.

CHAPTER 4 CHARACTERIZATION TECHNIQUES

4.1 Synopsis of Characterization Techniques

Characterization was performed on materials on FTO-glass substrates individually as well as combined materials/devices at varying stages and degrees of completion in the fabrication process. Samples were analyzed using scanning electron microscopy (SEM), sometimes coupled with energy dispersive x-ray spectroscopy (EDX), as well as x-ray diffraction (XRD), and UV-visible spectroscopy (UV-vis). Some finished devices and other samples were characterized by current-voltage (I-V) characteristics/curve measurements, and such curves were later further analyzed. Incident photon-to-electron-conversion-efficiency (IPCE), though not addressed in this work's results, is a useful consideration for the future.

4.2 Scanning Electron Microscopy (SEM)

SEM (Amray 1850) was used to view general morphology of films and material interfaces, as well as provide a general assessment of film thickness (cross section), microstructure, and grain sizes. Backscattered electron detection (BSE) was used when helpful to provide additional contrast between film/material layers (due to the difference in elemental sizes in each of the materials utilized at various stages of fabrication).

4.3 X-ray Diffraction (XRD)

XRD (Siemens D500) was used to assess material crystal structure, phase, and, if applicable, preferred orientation in the materials/films utilized in these devices. Typical scan parameters are a 2θ range of 20^o-60^o (or 15^o-85^o when such a range provides additional, useful information), scanned in 0.02^o-0.04^o 'steps', and a dwell time of 1.5-2.0 seconds.

Peak widths in XRD spectra vary with particle/crystallite size. This relation is given by the Debye-Scherrer formula (eqn. 4.3.1)[169-171]:

$$t = \frac{(K)\lambda}{B\cos(\theta_B)} \qquad \textbf{(4.3.1)}^{\textbf{169-171}}$$

> where t is crystal 'depth', λ is incident x-ray (Cu-Kα_1) wavelength, B is full-width at half-maximum (FWHM) for a given peak (in radians), and θ_B is the Bragg diffraction angle where that peak occurs. A 'shape' factor K is sometimes utilized to account for geometric, etc. considerations in crystallites/grains[169,170], but is simply set to 1 for the sake of simple approximation/confirmation in this work.

'True' FWHM is given by compensating for instrumental line broadening (B_{ILB}) within the measured FWHM ($B_{measured}$). B_{ILB} was found via XRD of a (111)-oriented Si wafer, and the FWHM (as that peak should be, in theory, as a δ-function in nature) of that peak[170]. 'True' FWHM (B) is given below (eqn. 4.3.2)[based on 170]:

$$B = \sqrt{B_{measure}^2 - B^2}$$ **(4.3.2)**[based on 170]

4.4 UV-visible Spectroscopy (UV-vis)

UV-vis (Shimadzu UV-2501 PC) was used in absorbance, reflectance (with integrating sphere/diffuse reflectance measurement capabilities) and transmittance modes to assess the absorbance of the wide-gap semiconductor, absorber/sensitizer, and hole conductor layers individually on FTO-glass, as well as wide-gap/absorber and wide-gap/hole conductor pairs, and the final 'sandwich structure' of the three materials. Light harvesting efficiency (LHE)[108,172,173] can be calculated from absorbance α by the following (eqn. 4.4.1)[108,172]:

$$LHE = 1 - 10^{-\alpha}$$ **(4.4.1)**[108,172]

The Tauc relations[172-174] can be used to determine the indirect(4.4.2a) and/or direct(4.4.2b) band gap(s) of a material based on UV-vis data:

$$(\alpha E)^2 \sim E - E_{g,direct}$$ **(4.4.2a)**[174-176]

$$(\alpha E)^{1/2} \sim E - E_{g,indirect}$$ **(4.42b)**[175,176]

Spectra were referenced to a piece of FTO-glass, similar to the ones samples were grown on.

4.5 Ferroelectric Poling and Characterization

A ferroelectric tester (Radiant Technologies Precision LC 100V) was used to measure the ferroelectric hysteresis of BFO on FTO-glass and TiO_2-FTO-glass, [as well as CuSCN-BFO-TiO_2-FTO-glass]. Based on 'estimated' BFO thickness and possible given hysteresis data, as well as the literature values for E_c[39,100,159] a voltage may be determined and then applied to 'pole' BFO, such that the electric field (E = V/t, where V is the poling voltage and t is the layer thickness) across the BFO layer is equivalent to or greater than the coercive field (E_c) 'required' for polarization direction 'switching' in the material.

4.6 I-V Characteristics and Overall Efficiency

IV measurements can be used to determine fill factor (FF) and overall device efficiency for PV devices (Fig. 4.6.1)[177]:

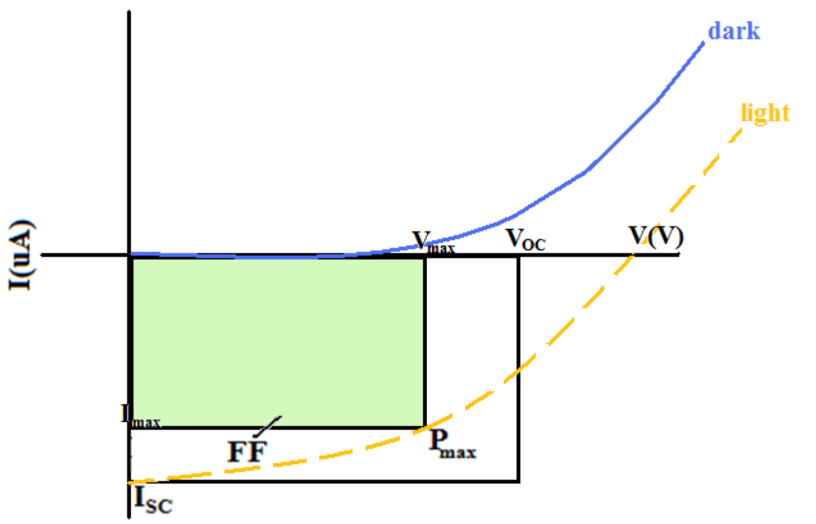

Figure 4.6.1[177]: Schematic example of IV-measurements, key values and parameters noted

PV-devices, as expected, often have a diode-like IV-characteristic (i.e. asymmetric IV characteristic, ideally with no current in the reverse bias direction (but often in reality with some leakage current this way), which follow the diode equation (eqn. 4.6.1))[19,21,178]:

$$I(V) = I_o(T)\cdot\left[\exp\left(\frac{qV}{n(T)k_BT}\right)-1\right] \qquad \textbf{(4.6.1)}^{19,21,178}$$

where $I_o(T)$ is the temperature-dependent dark saturation leakage current, n(I) is a current dependent 'ideality' factor, k_b is Boltzman's constant, and T is absolute temperature. Essentially, the exponential-shape of the IV-characteristics of diodes and PV devices (i.e. Fig. 4.6.1)[19,21,178] follows from this equation.

Overall device efficiency(η), using the parameters found from IV-measurements as noted above, is calculated as follows (eqn. 4.6.3-7)[177]:

$$\eta = \frac{P_{\max}}{P_{lamp}} \qquad \textbf{(4.6.3)}^{177}$$

where P_{max} is the maximum power generated by the PV device, given as:

$$P_{max} = V_{max}I_{max} \qquad \textbf{(4.6.4)}^{177}$$

where V_{max} and I_{max} are the current and voltage at the max power point, respectively. The fill factor (FF) is determined by:

$$FF = \frac{P_{\max}}{V_{oc}I_{sc}} = \frac{V_{\max}I_{\max}}{V_{oc}I_{sc}} \qquad \textbf{(4.6.5)}^{177}$$

where V_{oc} and I_{sc} are the open-circuit voltage and short-circuit current, respectively. Solving for P_{max} then gives:

$$P_{max} = V_{max}I_{max} = FF \cdot V_{oc}I_{sc} \qquad \textbf{(4.6.6)}^{177}$$

The overall efficiency is then given by:

$$\eta = \frac{V_{\max}I_{\max}}{P_{lamp}} = \frac{FF \cdot V_{oc}I_{sc}}{P_{lamp}} \qquad \textbf{(4.6.7)}^{177}$$

Preliminary IV-measurements were done on Bi-Fe-Zn-O/ZnO/FTO-glass samples via vacuum probe station, with 'light' measurements done under 'overhead' illumination upon the sample (i.e. illumination from the 'absorber' layer down, not (as favorable) from the glass substrate upward), and 'dark' measurements done with the sample chamber covered by paper. BFO/TiO_2/FTO-glass via potentiostat (PineWaveNOW) recorded by computer software (AfterMath) under controlled-sweep potential with current output measured. 'Light' measurements were done under diffuse/ambient light conditions in the room, and 'dark' measurements done with the sample under a black fabric cover.

4.7 Photon to Electron Conversion Efficiency

The incident photon to current conversion efficiency (IPCE) can be calculated using eqn. 4.7.1[modified from 19,108]:

$$\text{IPCE}(\%) = \frac{hc \cdot J_{sc}}{\lambda \cdot \Phi} \cdot 100\% = \frac{hc \cdot I_{sc}}{\lambda \cdot P_{lamp}} \cdot 100\% \qquad \textbf{(4.7.1)}^{19,108}$$

where h is Planck's constant and c is the speed of light (i.e. hc in this formula is commonly given as 1240eV-nm[19,179], to be used with wavelength λ in nm), J_{sc} is the short-circuit current density (I_{sc} would be short circuit current), and Φ is the incident light intensity (P_{lamp} would be incident light power).

Internal quantum efficiency (IQE) is a measure of a PV device's ability to convert *captured* incident photons of light into electrical power, and is given by eqn. 4.7.2[19,108,171]:

$$\text{IQE} = \frac{IPCE}{LHE} = \eta_c \varphi_{inj} \qquad \textbf{(4.7.2)}^{19,108,171}$$

where LHE is light harvesting efficiency (section 4.4), and η_c and φ_{inj} are the charge separation and injection efficiencies, respectively, and not directly measured or calculated here.

IQE can therefore be calculated from photon-to-electron conversion measurements coupled with UV-vis absorbance measurements.

External quantum efficiency (EQE) is a measure of the conversion of the *total* number of incident photons into charge carriers[21], and is calculated using eqn. 4.7.3[108,171]:

$$\mathrm{EQE} = \frac{\Phi \lambda q_e}{J_{sc} hc} = \frac{P_{lamp} \lambda q_e}{I_{sc} hc} \qquad \textbf{(4.7.3)}^{108,171}$$

where q_e is elementary charge (i.e. the charge on an electron).

CHAPTER 5: RESULTS AND DISCUSSIONS

5.1 Materials Characterization

5.1.1 ZnO

Polycrystalline (wurtzite) ZnO films were successfully electrodeposited on FTO-glass substrates, as confirmed by XRD measurements, as exemplified in Fig. 5.1.1:

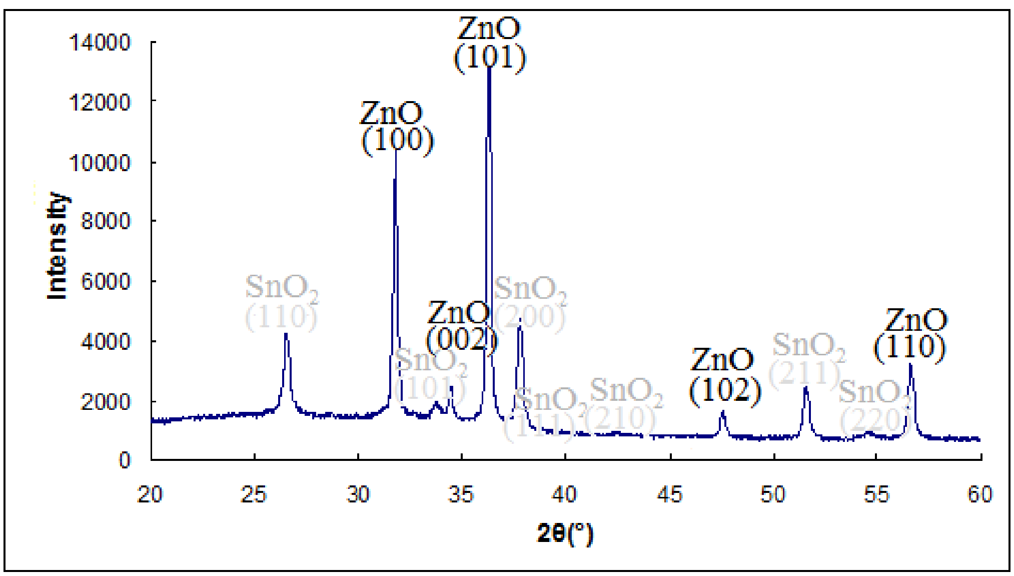

Figure 5.1.1 XRD spectrum (with peaks identified and indexed) of representative electrodeposited ZnO film on FTO-glass

Example SEM micrographs of such films are shown in Fig. 5.1.2 below:

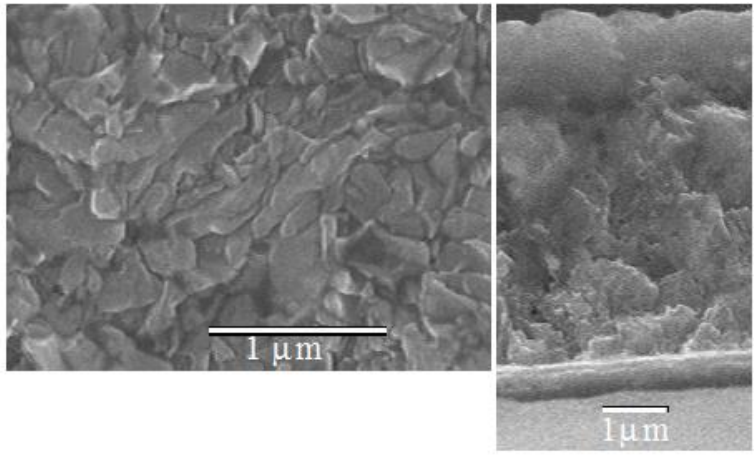

Figure 5.1.2: Top (left) and cross-sectional (right) views of an example electrodeposited ZnO (-10mA, 1800sec) film on FTO-glass

As seen in the micrographs, these polycrystalline ZnO films are rough in nature, which is favorable for eta- or sensitized-solar cell applications (as discussed previously in Ch. 2), and have a wide distribution of crystallite/grain sizes (~tens of nm to ~1μm). The SEM micrographs show, and XRD peak-width measurements run through the Debye-Scherrer equation (Section 4.3) for the first three peaks in Fig. 5.1.1 give a mean crystallite size of ~57nm, and indicate mild anisotropy ($\Delta d_{110} > \Delta d_{002} > \Delta d_{100}$).

UV-vis of electrodeposited ZnO films on FTO-glass is shown in Fig. 5.1.3. Extrapolating the band gap from these measurements yields a value of ~3.32eV, which is in good agreement with the literature on ZnO[76,121,122,171]. Moreover, this data and band-gap extrapolation fit the second Tauc relation (eqn. 4.4.2b), indicating (also in 'reasonably good' agreement with the literature[59,76,121,171]) that the ZnO is a direct-gap semiconductor.

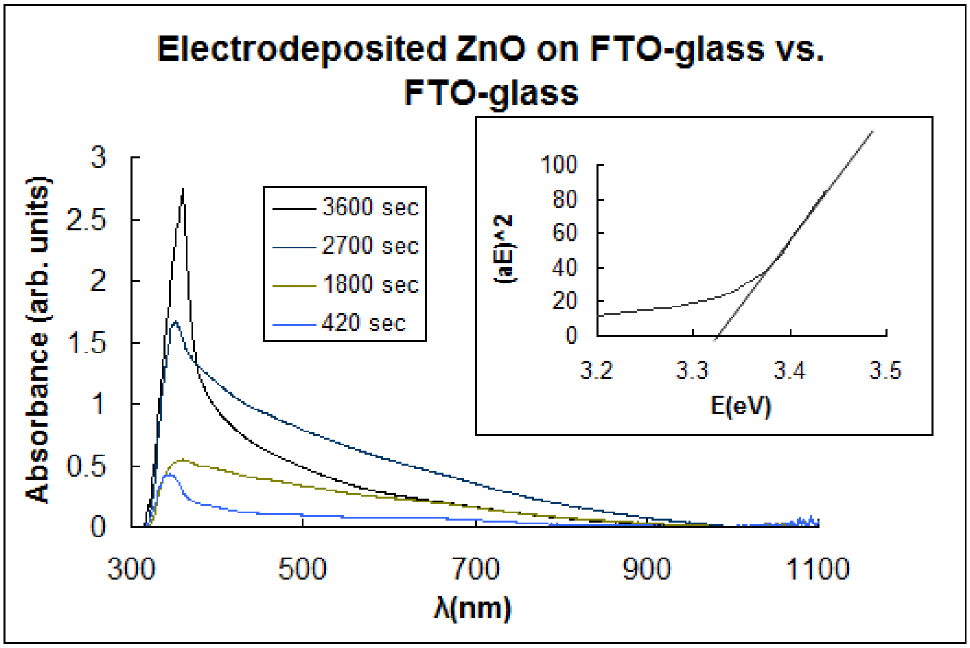

Figure 5.1.3 UV-vis spectra for ZnO films (-1.0V) of differing mean thicknesses, Tauc representations and extrapolation of band gap shown (inset)

5.1.2 α-TiO_2

Polycrystalline anatase(α)-TiO_2 films were successfully deposited on FTO-glass substrates via both ALD and dip-coating in aqueous TiO_2 NP suspensions, confirmed by XRD measurements, as exemplified in Fig. 5.1.4:

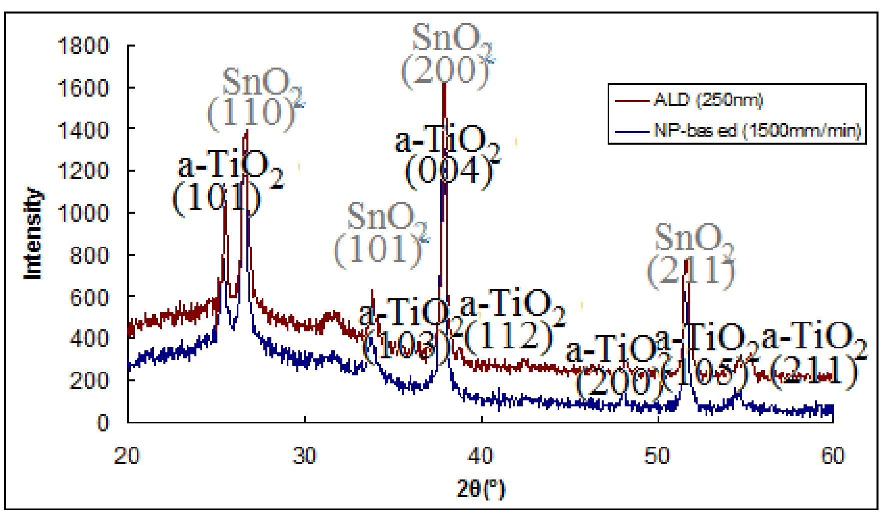

Figure 5.1.4 XRD spectrum (with peaks identified and indexed) of top) ALD- and bottom) NP-suspension dip-coating-deposited-TiO_2 films (~200-250µm) on FTO-glass

Example SEM micrographs of such films are shown in Fig. 5.1.5 below:

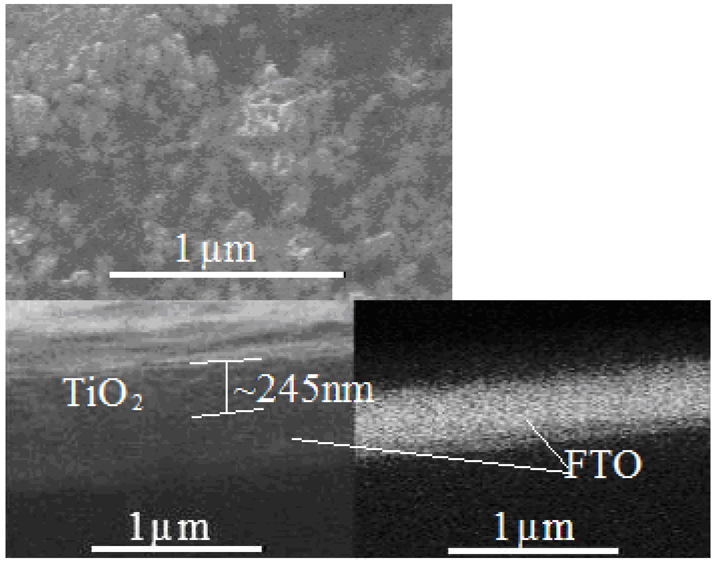

Figure 5.1.5: Top (top) and cross-sectional (SE(left) and BSE(right)) views of an example NP-suspension-based TiO_2 (~245nm) film on FTO-glass

As seen in the micrographs, these polycrystalline TiO_2 films are rough in nature, which is favorable for eta- or sensitized-solar cell applications (discussed previously in Ch.2). The SEM micrographs show, and XRD peak-width measurements run through the Debye-Scherrer equation (Section 4.3) confirm a mean crystallite size of ~39nm, which likely makes sense due to the short anneal time at 'fairly low' temperature (melting point of TiO_2 is >1800^{o}C)[180,181], as well as the lack of a 'correction factor' used in the calculation (i.e. K ~ 0.9 would give 35nm crystallite size, and K~0.82 would give ~32nm crystallites again).

UV-vis of TiO_2 films on FTO-glass is shown in Fig. 5.1.6. Extrapolating the band gap from these measurements yield a direct-band gap indirect-gap Tauc relations (not shown) yield E_g~2.9-3.0eV, which is not the most 'sensible' value for a transparent/'white' material) value of ~3.34eV, which is a bit higher than typically (bulk?) cited values[144], is not in complete disagreement with related work[145]. The 'blue-shifted' band-gap value may be due to size constraints[182], because although Fen, et. al.[144], used smaller (~25nm) TiO_2 particles, their mixture (DeGussa P25), while mostly anatase, also contained a significant fraction (estimated at ~25% by Ohno, et. al.)[183] of rutile (which has a lower band gap (E_g~3.10eV)[144].

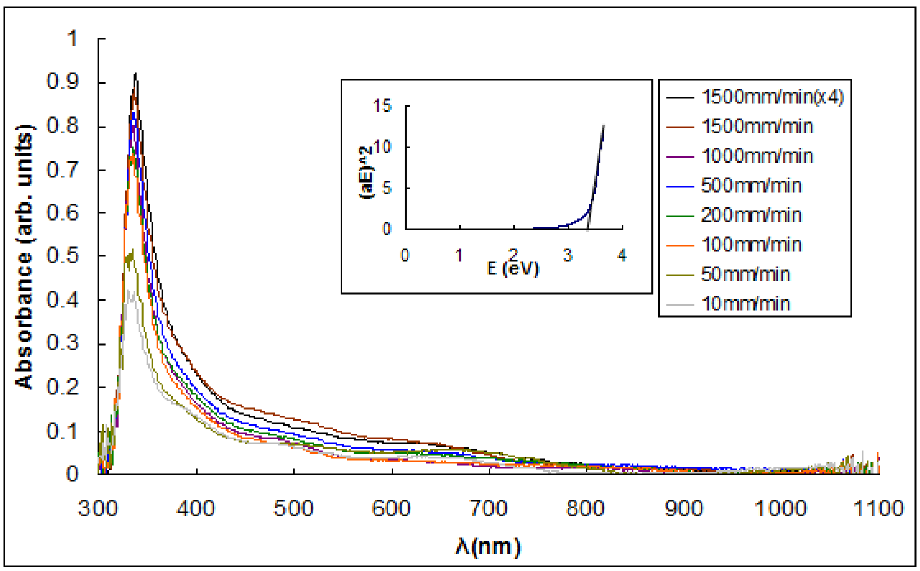

Figure 5.1.6 UV-vis spectra for NP-based TiO_2 films of differing mean thicknesses, Tauc relations and extrapolation of band gap shown (inset)

5.1.3 $BiFeO_3$

Polycrystalline BFO films were successfully dip-coated from BFO-ethyelene glycol-based sols onto FTO-glass. Upon heat treatment, these films were found to be polycrystalline r3c (rhombohedrally-distorted perovskite) structure $BiFeO_3$, as confirmed by XRD (Fig. 5.1.7):

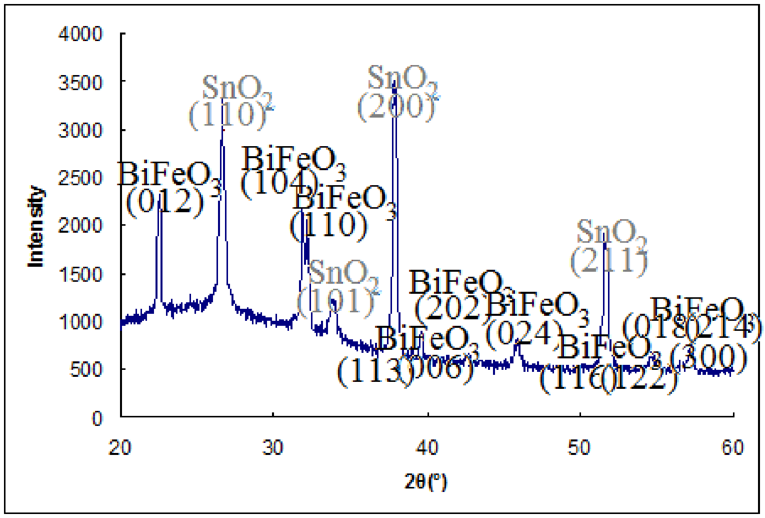

Figure 5.1.7 XRD of BFO on FTO-glass, peaks indexed appropriately

SEM micrographs (Fig. 5.1.8) were also taken of BFO-FTO-glass:

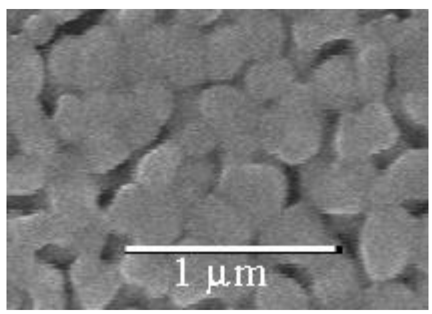

Figure 5.1.8: Representative SEM micrograph of BFO-FTO-glass (top view)

UV-vis was performed on BFO-FTO-glass samples, and band gap was extrapolated and found to be ~2.50eV(direct), again in agreement with the literature[39,100,117,]. Fig. 5.1.9 shows the UV-vis results for BFO on FTO-glass:

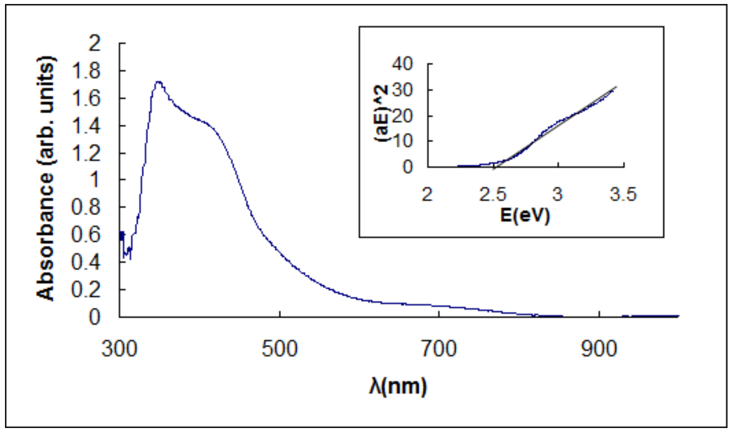

Figure 5.1.9: UV-vis of BFO on FTO-glass (ref. FTO-glass), inset shows Tauc relationship and extrapolated band gap

Ferroelectric hysteresis curves were measured on these films as well, and is shown in Fig. 5.1.10. Due to the fairly high leakage currents, as well as slightly irregular contact area, and potential/visible 'non-uniformities' in sample thickness, E_c and P_r have not been recorded in this work.

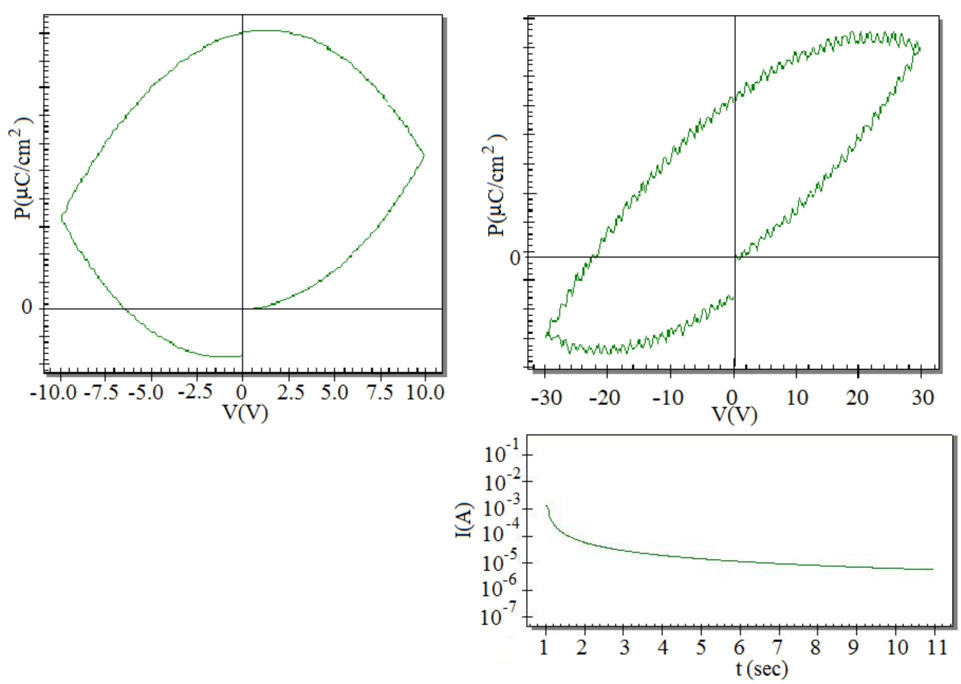

Figure 5.1.10: 'Raw' ferroelectric hysteresis shown by a V vs. P (values approximated as few μC/cm^2) plot for BFO heat treatment film on FTO-glass (top) and leakage current measurements, taken at 5V (bottom)

As seen in Fig. 5.1.10, leakage currents[184] are significant, even at 'low' voltages. With an estimated contact area of ~0.1cm^2 and time of ~10 sec., such would correspond to possibly mC/cm^2 of leakage, which is very significant, considering P_r for BFO is given as ~60μC/cm^2 [100,159]. With significant leakage, attaining a field across the material significant enough to 'switch' it would be rather difficult at best, and likely require higher voltage or low temperature measurements[100]. However, BFO appears to be showing hysteretic behavior, albeit perhaps leaky[184], indicating that such films can likely be polarized for the aforementioned applications.

5.1.4 Attempts at BFO-ZnO

Attempts at BFO sensitizer deposition were initially performed on ZnO-FTO-glass, via BFO-based sol-gel dip-coating and subsequent heat treatment. However, as subsequent XRD spectra imply, several heat treatment conditions failed to yield crystalline BFO (if any BFO) on electrodeposited ZnO-FTO-glass substrates. Table 5.1 summarizes experimental conditions:

Table 5.1: Summary of experimental conditions for attempts to deposit BFO on ZnO-FTO-glass

BFO-ZnO	**Enivronment**	**T1,t1**	**T2,t2**	**T3,t3**	**Comments**
1	furnace, air	400C, 12.5hr	-	-	FTO, ZnO
2	RTA, N2	400C, 5min	-	-	FTO, ZnO
3	furnace, air	400C,30min	450C, 10hr	-	additional peaks @~36.4º,~63º
4	furnace, air	450C, 12.5hr	-	-	
5	RTA, N2	500C, 10min	-	-	
6	furnace, air	500C, 24hr	-	-	
7	furnace, air	400C,30min	625C, 2hr	-	
8	CVD, LP, O2	625C, 3hr	-	-	
9	furnace, air	625C, 2hr	400C, 30min	625C, 2hr	
		(prior to BFO)	(post BFO)		
10	furnace, air	400C,30min	625C, 10hr	-	BFO(on exposed FTO)?
11	furnace, air	400C,30min	625C, 2hr	625C, 10hr	
12	RTA, N2	650C, 5min	-	-	
BFO-TiO_2-ZnO					
13	furnace, air	500C, 30[]min	400C, 30min	625C, 2hr	BFO, ZnO, a-TiO2, other phases
		(prior to BFO)			

Figure 5.1.11 shows the relevant UV-vis absorbance plots for such a system:

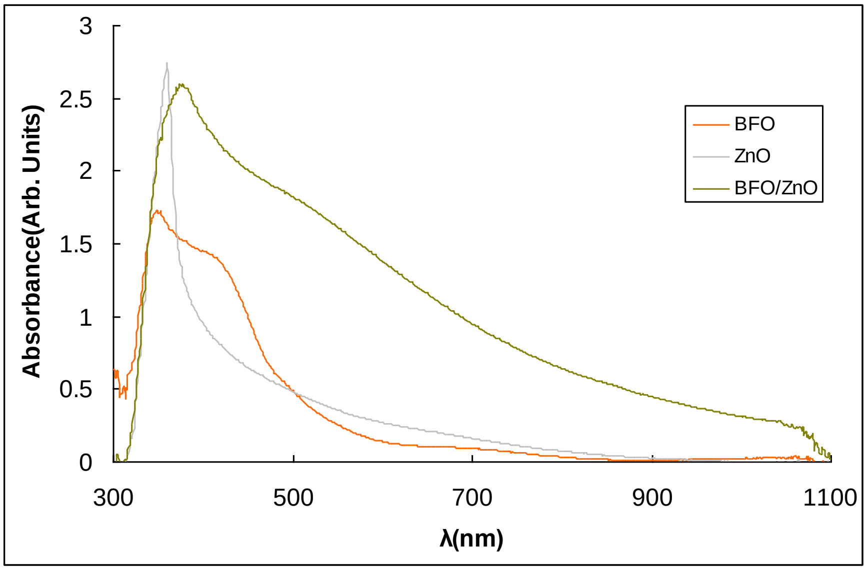

Figure 5.1.11: UV-vis of a) BFO/, b) ZnO/, and c) Bi-Fe-Zn-O/ZnO-FTO-glass vs. FTO-glass (anneal conditions: furnace, air; 400°C, 30min; 625°C, 2hr)

Both visual examination (Figure 5.1.12) of the samples and UV-vis seem to indicate a combination of BFO and ZnO present, as the Bi-Fe-Zn-O/ZnO-FTO-glass spectrum does appear to be a 'hybrid' of sorts of the spectra for the separate BFO- and ZnO-FTO-glass, though perhaps the increased absorption a/o (perhaps more likely due to the coloration of the film being orange rather than red, brown, or black) reflectance imply issues with or differences in the absorber material which occurs and actual BFO.

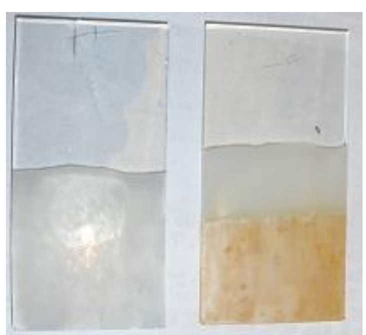

Figure 5.1.12: Photographs of a) ZnO/ and b) Bi-Fe-Zn-O/ZnO/FTO-glass (anneal conditions: furnace, air; 400°C, 30min; 625°C, 2hr[])

Light-harvesting efficiency calculations/estimations based on absorbance are shown in Fig. 5.1.13 below for UV-vis analyzed ZnO-based samples.

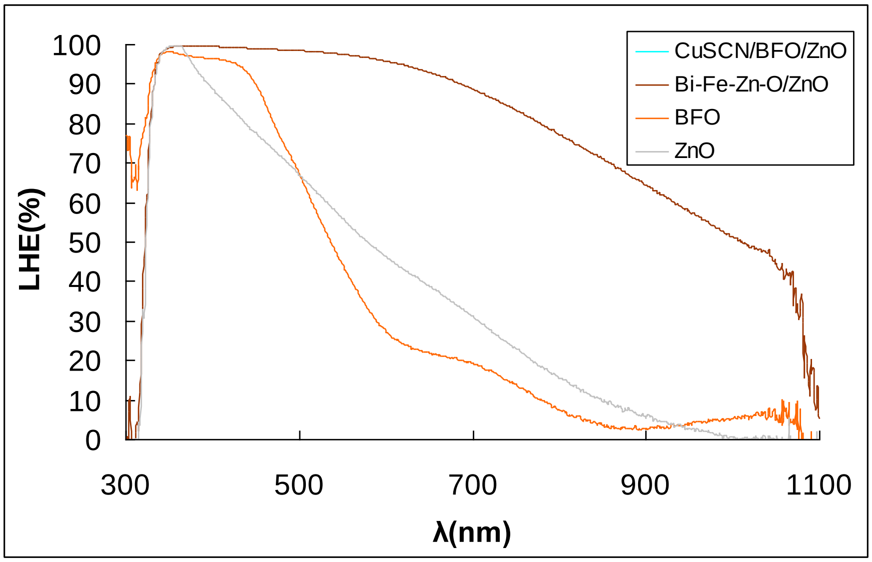

Figure 5.1.13: Light-harvesting efficiencies for a) ZnO/, b) BFO/, and c) Bi-Fe-Zn-O/ZnO/FTO-glass samples

These LHE values are likely overestimates due to internal reflectance, particularly enhanced by the ZnO grain size's (on the order of a few hundred nanometers to a bit over a micron) affects on light scattering[35], being 'on par with' or a bit over the wavelengths of light used in the experiment. Spalling/cracking of the film, as well as the 'tile patterns' and 'intratile splits' seen in some regions of such films (Fig. 5.1.14 to follow) may also contribute to internal reflectance. The UV-vis absorbance measurements taken in absorbance mode likely measure transmittance and may not 'inherently' account for reflectance, particularly diffuse scattering and reflectance from internal light scattering. However, such internal reflectance and light-scattering features increase the probability of light being absorbed before exiting the material[33,56,68,75]. Moreover, the data indicates, as expected, that both BFO, and likely also the achieved absorber material have higher LHE values (due to their less-wide band gaps than ZnO) in the UV and visible region of the spectrum than solely a ZnO photoanode would. Also, as expected, an added absorber/sensitizer material enhances light-harvesting for the same reasons when coupled with a transparent/transluscent/opaque white photoanode material, for similar reasons.

SEM micrographs (Fig. 5.1.14) indicate a somewhat similar-looking absorber morphology, at least in spots, in places to that found on BFO-FTO-glass samples (ref. Fig. 5.1.8):

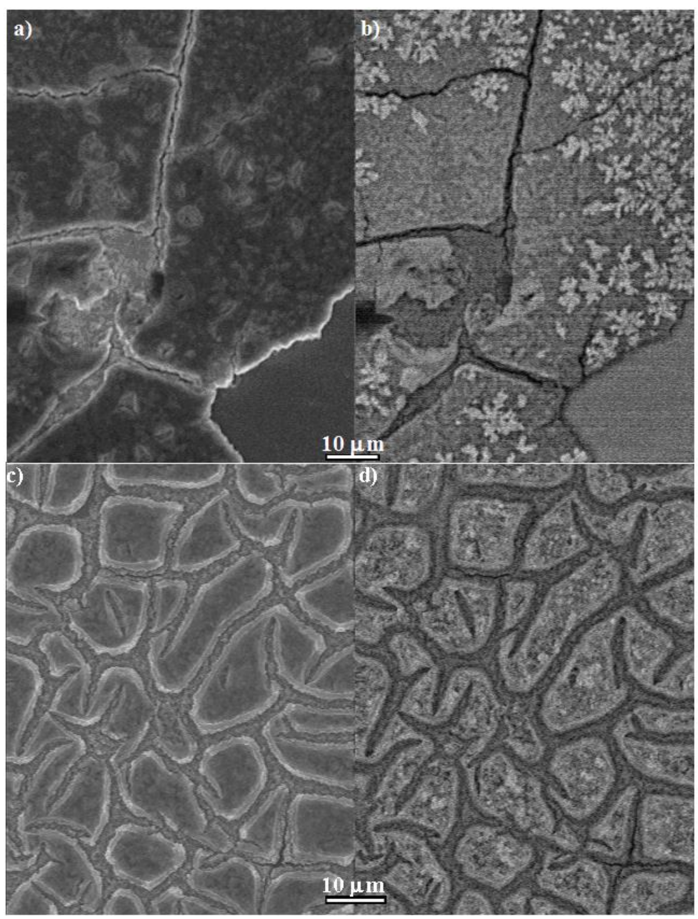

Figure 5.1.14 SEM micrographs of Bi-Fe-Zn-O/ZnO-FTO-glass in a,c) SE and b,d) BSE modes(anneal conditions: furnace, air; 400^{o}C, 30min; 625^{o}C, 2hr[])

As shown in the micrographs, the absorber, possibly along with some or all of the ZnO, forms a ‘mosaic-like’ pattern a/o begin to crack or ‘spall’ off (which may cause the increased apparent absorbance/likely reflectance seen in Fig. 5.1.11) the substrate. Moreover, apparent ‘phase separation’ into Bi-rich, etc. phases may be implied by the light and dark regions of BSE images.

XRD spectra (Figure 5.1.15-5.1.17) for various heat treatment conditions and attempts of these and similar samples indicate no crystalline $BiFeO_3$ is present.

Several crystallization attempts at lower temperatures (~400^{o}C-550^{o}C in air) in the furnace did not appear to yield any crystalline absorber, no less BFO. Figure 5.1.15 summarizes these results:

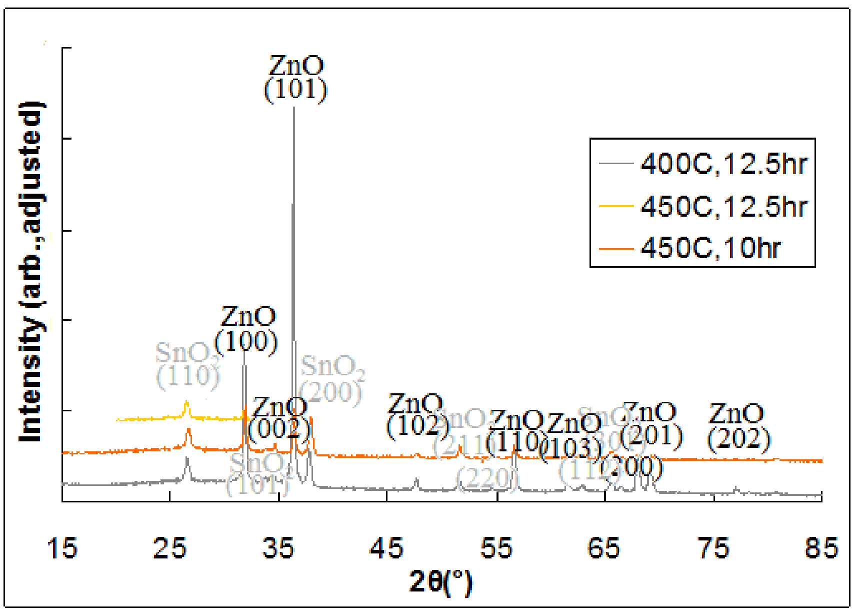

Figure 5.1.15: XRD spectra for furnace heat-treatment conditions that did not yield crystalline sensitizer material

Therefore, increased heat treatment times at various temperatures were also tried. Longer crystallization times, regardless of heat treatment temperature, yielded various Bi- a/o Fe a/o Zn-containing oxide phases, which were not BFO, as indicated in Figure 5.1.16:

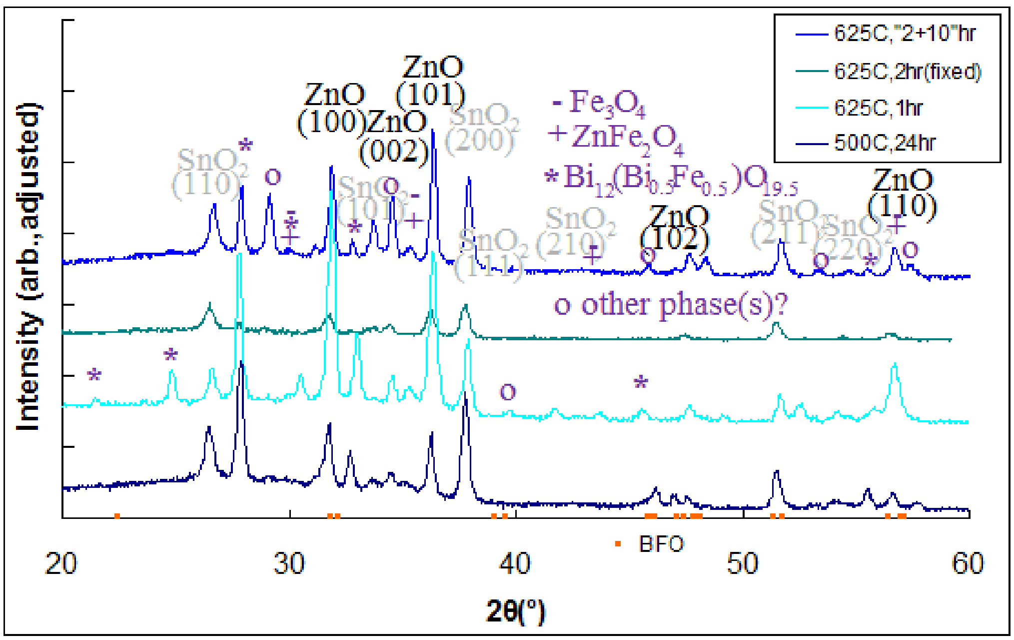

Figure 5.1.16: XRD spectra for furnace-annealed (in air) samples, temperatures and heat treatment times indicated

It would appear that the electrodeposited ZnO either inhibits BFO formation a/o catalyzes the formation of phase-separate Bi-Zn-O a/o Fe-Zn-O a/o other Bi-Fe-O phases a/o Bi-O or Fe-O type phases. Moreover, the noted phases are all cubic, thus ferroelectricity (which requires asymmetry in such crystals) is likely not present in the absorber layer, making these non-BFO 'alternative phases' likely unsuitable for the portion of the proposed work dealing with the effects of ferroelectricity on sensitization. Without ferroelectricity, and with the similar coloration and apparent UV-vis 'character' to BFO, such might function as a good non-polar 'control' sensitizer in the future, however a combination of materials with formation not yet well-understood in the scope of this work may not be the best alternative for such either.

Since furnace anneals often took between an hour and a half and several hours, diffusion of Bi- and Fe- species into the ZnO was also theorized as a problematic possibility. Therefore, similar samples were annealed by N_2-atmosphere RTA for ~5-15min. at a few of temperatures between 400°C and 650°C (higher temperatures cause the FTO-glass substrates to soften a/o melt and warp) to attempt to mitigate such issues, should they be problematic. Results are shown in Figure 5.1.17:

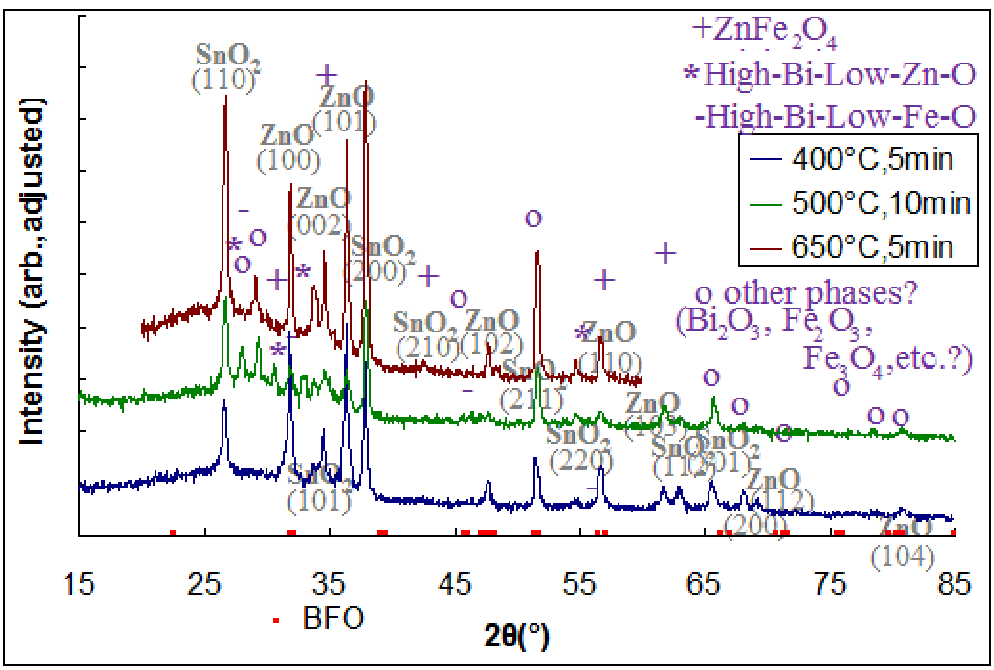

Figure 5.1.17 XRD spectra for RTA-annealed samples, temperatures and times indicated

Again, oftentimes, secondary Bi- a/o Fe- a/o Zn-containing oxide phases were formed (few possible cubic ternaries indexed), and no crystalline $BiFeO_3$ was seen, so diffusion was not likely a major factor in the lack of BFO formation. Also, again worth noting, the 400°C heat treatment appeared to yield no crystalline phases containing significant amounts Bi- or Fe-.

The issue does not appear to be one involving any reaction, combination, phase change, etc. between ZnO and FTO-glass due to typical heat treatment conditions. Comparison between XRD of ZnO-FTO-glass prior- and post-heat treatment (run at 'typical' heat treatment conditions for other BFO/wide-gap semiconductor/FTO-glass or BFO/FTO-glass samples in this work) in air in the furnace at 400°C for 30min, 625°C for ~1hr (Fig. 5.1.18) shows no obvious composition/chemical or phase changes occurring in ZnO/FTO-glass after exposure to the heat treatment conditions.

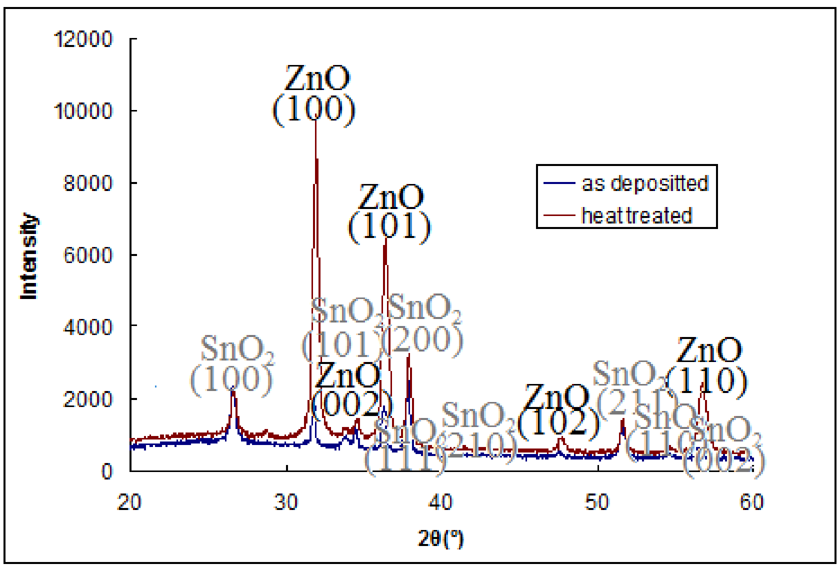

Figure 5.1.18 XRD of ZnO/FTO-glass prior to (blue) and post (red) previously noted heat treatment conditions

Several other issues could cause such problems with the potential BFO/ZnO system, with BFO-absorber layer produced via sol-gel dip-coating. These two materials could be, at elevated temperatures (BFO/ZnO devices were made via other routes[105] previously not requiring heat treatment or crystallization steps), strictly incompatible. To assess this theory, one would have to try dip-coating ZnO substrates or coated substrates produced by methods other than electrodeposition in similar BFO-sols, and if similar BFO formation inhibition or secondary phases were evident, this situation would in fact be the case.

Electrodeposited ZnO may, for reasons such as surface chemistry/termination, also be at the ‘heart’ of the problem, in which case, one could investigate chemical surface termination of such films via a technique such as FTIR, and compare it to the termination of ZnO produced by other means, and subsequently perform similar BFO-dip-coats, heat treats, and XRD analysis to compare.

Perhaps for the BFO-ZnO system, high surface area (due to desirable roughness a/o porosity in the electrodeposited films) catalyzes the formation of secondary Bi/Zn- a/o Fe/Zn-, etc. based oxide phases. Finding an electrodeposition route to deposit ‘fully dense’ (or at least moreso) ZnO films a/o using a different processing route (such as MOVPE or ALD) to make dense, smoother ZnO films and performing similar dip-coating, heat treatment, and XRD analyses would shed light on this possibility too. Similar experiments may also indicate if crystallite size of the rough ZnO present leads to increased Gibbs-Thomson solubility of ZnO in the Bi/Fe-based sol, and hence the formation of secondary phases. However, as evidenced by the micrographs in Fig. 5.1.2, electrodeposited ZnO has a wide distribution of grain/crystallite sizes present, indicating that for Gibbs-Thomson solubility to be the main issue, the crystallites in these films would almost entirely, at least, have to be below a certain critical radius (because no BFO is evident, that would indicate all sol-based products are participating in ZnO-dissolution). Work on films with more uniform grain/crystallite sizes, as well as single-crystal substrates, would provide some indication as to the likelihood of this scenario.

Also, pH-mediated surface etching or dissolution (perhaps also facilitated by roughness/porosity, increased surface area a/o crystallite size) of ZnO and subsequent heat-treating could also be present and problematic. ZnO is fairly pH sensitive, and rather soluble in both acidic and basic pH environments, not far outside the 6-8 range. The pH of the ethylene-glycol $Bi(NO_3)_3/Fe(NO_3)_3$ sol, when measured via pH paper and pH meter (Thermo), is found to be ~0.1(meter)-2(pH 1-12 paper), indicating that at the very least pH a/o surface etching, dissolution a/o reactions may be problematic. ‘Bulk’/’fast’ etching of ZnO in the sol, however, seems unlikely, because the orange coloration indicating the Bi-Fe-O-containing layer (Fig. 5.1.12) still appears to be atop an opaque white layer (as seen from behind the substrates as well, and as opposed to viewing BFO simply on glass, which is appears a more translucent orange with ‘fringes’ of color from non-uniformities in deposition thickness). Moreover, XRD peaks of ZnO are not highly diminished post attempted BFO deposition. Visual examination of the samples (ref. Fig. 5.1.14) from the front, though orange post dip-coating and heat treatment, is still opaque like ‘plain’ ZnO-FTO-glass samples appear. Also, from behind, white, opaque ZnO is still evident, visible through the glass substrate. Therefore bulk dissolution or etching of ZnO is unlikely, but surface dissolution or etching may not be out of the question. Changing the pH of the sol, or depositing BFO on electrodeposited ZnO-FTO-glass by a different method (such as MOCVD[100] or sputtering[103]).

Or, simply or in conjunction with one or more of the above theories (such as surface termination chemistry, reaction/dissolution, etc.), perhaps ZnO, for structural reasons (i.e. wurtzite/hexagonal vs. tetragonal (i.e. as for SnO_2 or α-TiO_2[155]))[151] a/o lattice parameter/size, or even perchance stoichiometry-related reasons causes the favorable nucleation of alternative Bi-Fe-O a/o Bi-O a/o Fe-O, etc. phases, catalysis of the formation of such phases, a/o inhibition of BFO formation a/o crystallization during exposure to at least temperatures over 500^{o}C (perhaps the apparent lack of crystalline BFO or any significant amounts of crystalline absorber at the lower temperatures may be somehow related as well) in air for hours or N_2 for shorter periods of time.

However, some apparent possible/initial success appeared to be had upon heat treating BFO-ZnO-FTO-glass in an O_2 (albeit low pressure) environment in a quartz-tube furnace (Fig. 5.1.19):

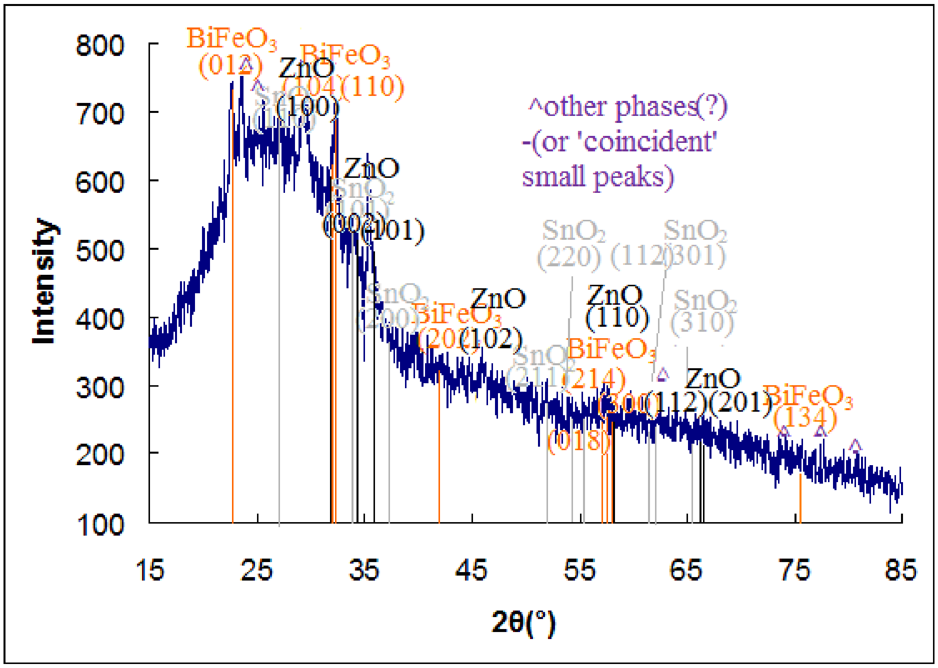

Figure 5.1.19: XRD spectrum for BFO/ZnO/FTO-glass placed in a quartz tube reactor at low-pressure (likely a few torr) at 625°C for ~3hr

As indicated by XRD results, BFO is apparently present along with ZnO on this sample. However, samples had to be cut/broken 'lengthwise' in order to fit them in the tube furnace/reactor. Moreover, some 'second phase(s)' are likely present in addition to BFO. Perhaps further investigations into the effects of vacuum or low-pressure anneals and O_2 partial pressure on BFO formation on ZnO/FTO-glass are warranted in the future.

5.1.5 $BiFeO_3$-TiO_2

BFO-films were deposited via dip-coating onto TiO_2 films on FTO-glass, and subsequently heat treated. XRD for such is show below in Fig. 5.1.20:

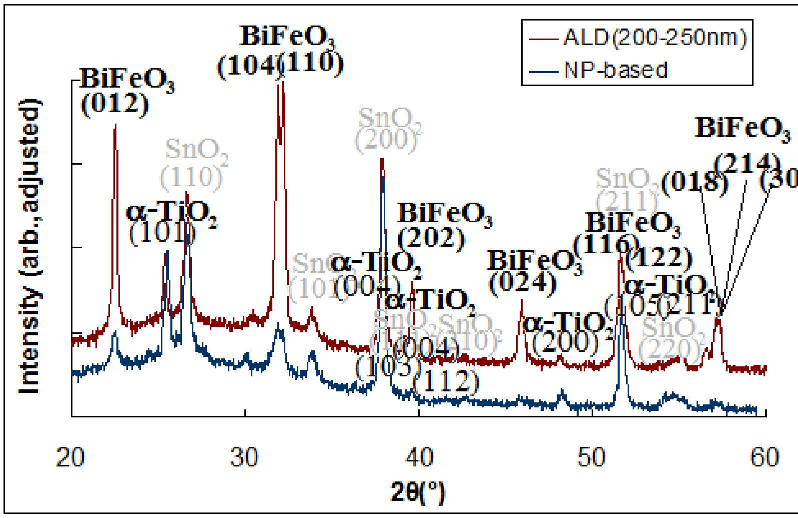

Figure 5.1.20: 'Representative' XRD spectrum for BFO/TiO_2/FTO-glass

SEM micrographs (Fig. 5.1.21) were taken of these combination films, with both SE and BSE detection, in order to properly distinguish one from the other.

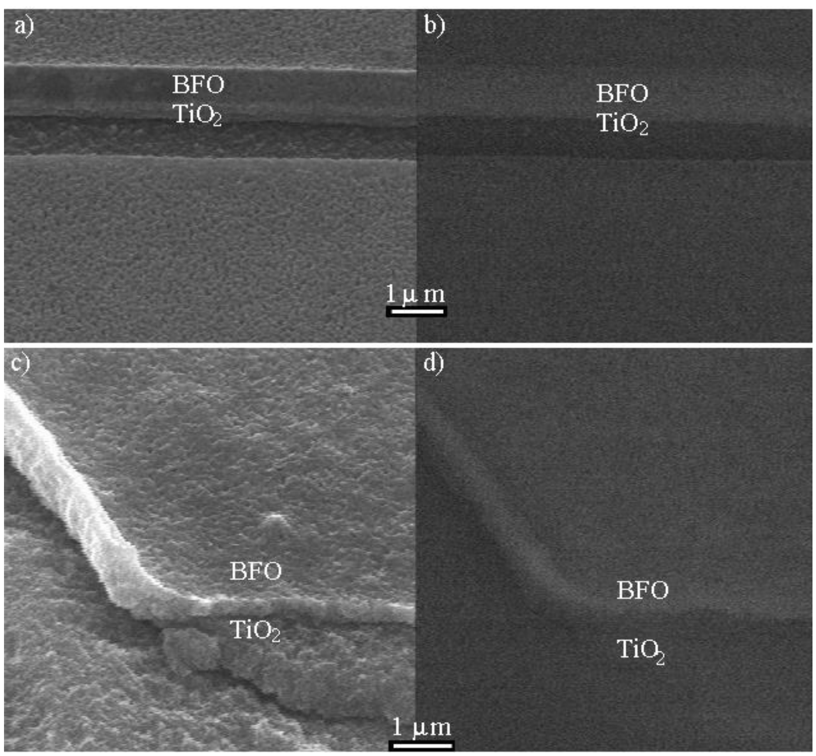

Figure 5.1.21: Exemplary (tilt-view) SEM micrographs (a,c: SE, b,d: BSE) from a BFO/TiO_2/FTO-glass samples (a+b: ALD-TiO_2, c+d: NP-TiO_2

As is evident in the micrographs, the BFO formed a similar 'brainy-like' texture on the TiO_2 films, as it had on top of FTO previously. No phase separation regions are evident from the BSE images, and based on these images and XRD in Fig. 5.1.19, the BFO layer appears to be fairly strictly BFO. Moreover, it has a rough morphology, which may be favorable for internal reflectance and light-scattering[33,56,68,75]. Furthermore, the BFO layer appears to at least conform with, if not at least to some extent penetrate into, the TiO_2 photoanode matrix.

UV-vis measurements were done on combination BFO-TiO_2-FTO-glass samples (Fig 5.1.22), and compared to the UV-vis spectra of their individual components

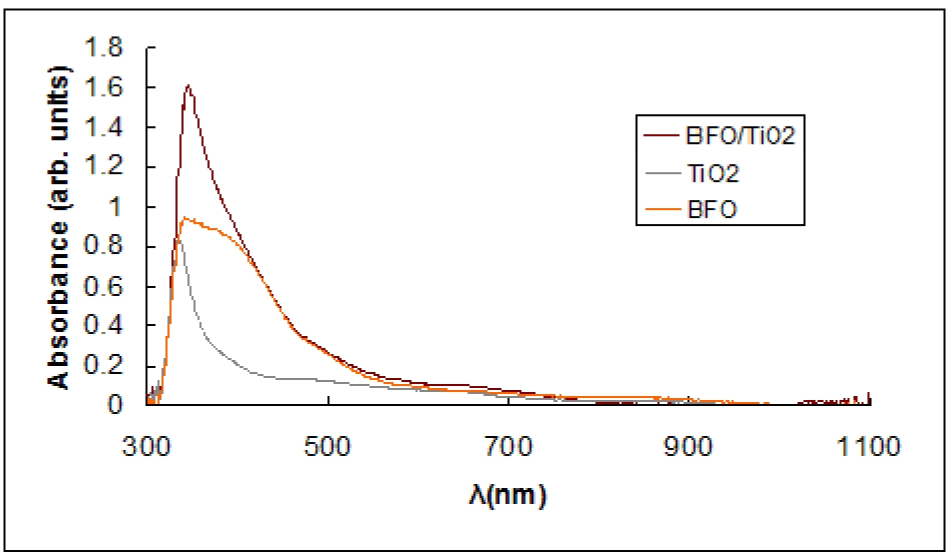

Figure 5.1.22: UV-vis spectra of (a) TiO_2/(dip-coated 1500mm/min), (b) BFO/ (1000mm/min), and (c) BFO/TiO_2/FTO-glass (1500[(?)]mm/min TiO_2, 200mm/min BFO).

As is evidenced in the above figure, and expected, the UV-vis spectrum for the combined materials shows a 'hybridization' of spectral features from both TiO_2 and BFO.

CuSCN films were fairly successfully deposited from n-propyl sulfide solution onto FTO-glass. Upon heat treatment, these films were found to be polycrystalline CuSCN, albeit inconclusive as to which crystal structure is "dominant" (orthorhombic, likely 'mixed' with at least one other) in the mixture, as a few seem possibly present, as shown in the following XRD spectrum (Fig. 5.1.23):

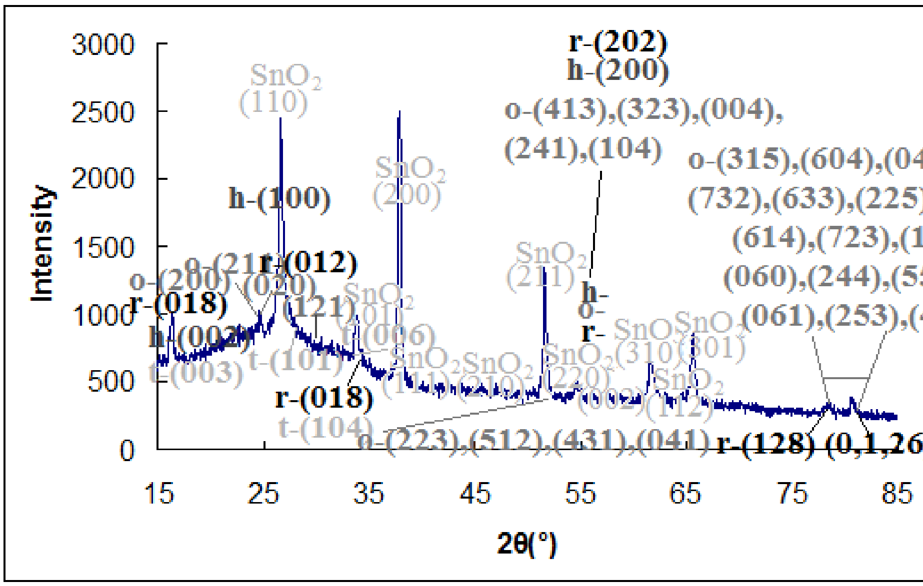

Figure 5.1.23 XRD of CuSCN/FTO-glass, peaks indexed appropriately (from JADE and ref.[141])

UV-vis was performed on CuSCN-TiO_2-FTO-glass samples (referenced to a similar thickness, etc. TiO_2/FTO-glass sample), and band gap was extrapolated and found to be ~3.35eV, a bit less than typically noted in the literature[74,76,77,108,141,150,168], possibly because of slight mismatch in thickness between TiO_2 on the sample and that on the reference. Fig. 5.1.24 shows the UV-vis results for CuSCN on FTO-glass:

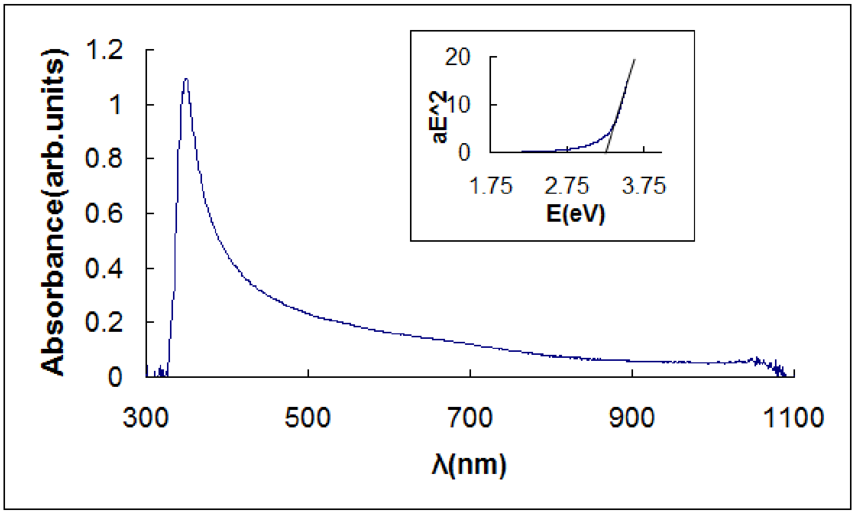

Figure 5.1.24: UV-vis of CuSCN/TiO_2/FTO-glass vs. TiO_2/FTO-glass

CuSCN films were deposited on ZnO/, TiO_2/, Bi-Fe-Zn-O/ZnO/, and BFO/TiO_2/FTO-glass samples as described previously (Section 3.6). XRD for such is show below in Fig. 5.1.25:

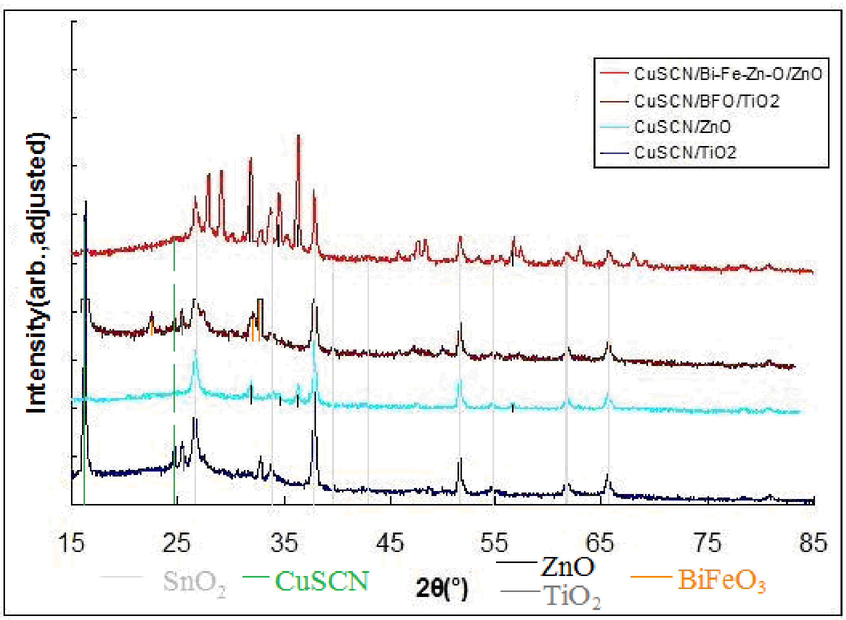

Figure 5.1.25: XRD spectra for CuSCN/TiO_2/, CuSCN/ZnO/, CuSCN/Bi-Fe-Zn-O/ZnO, and CuSCN/BFO/TiO_2/FTO-glass samples (distinct 'characteristic peaks' [apparent[(?)]] noted)

In addition to the expected SnO_2 peaks, both the wide gap semiconductor and the CuSCN are evident in the spectra for the 'absorberless' (bi-layer) samples, as well as CuSCN, BFO, and the expected wide gap semiconductor in the 'full' (tri-layer) structures.

SEM micrographs (Fig. 5.1.26) were taken of CuSCN/BFO/TiO_2 combination films, with both SE and BSE detection, in order to properly distinguish one from the other.

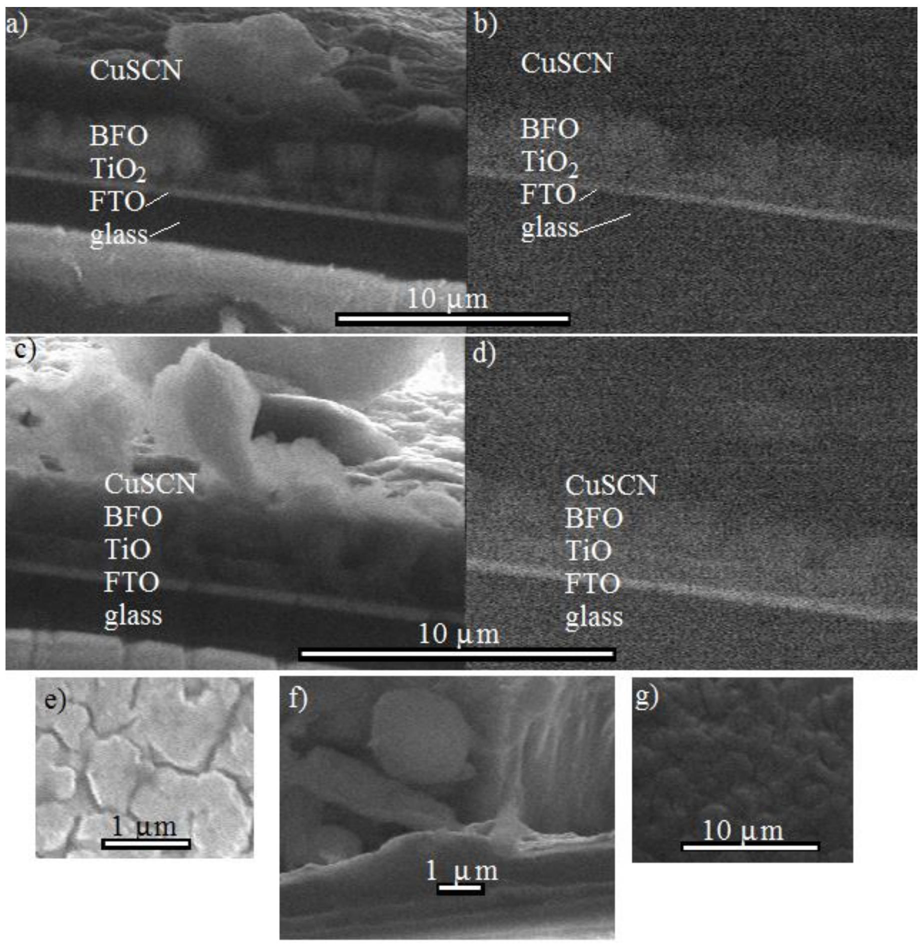

Figure 5.1.26: Exemplary SEM micrographs from a CuSCN/BFO/TiO_2/FTO-glass sample. cross sectional (a-d,f; a,c,f: SE; b,d: BSE), top view (e), and tilt-view (g) micrographs shown

Layers in the CuSCN/BFO/TiO_2/FTO-glass sample are clearly visible in the micrographs, with composition differences indicated by BSE. Although TiO_2 is light-weight in comparison to $BiFeO_3$ and FTO, etc., it appears to 'light up' some in BSE images, perhaps indicating some BFO 'infiltration' into the TiO_2 matrix under it. Also, these micrographs show the roughness and cracking of the CuSCN layer, as well as some degree of thickness variation with location on the sample, etc. Such has the potential not only to lead to light-scattering/diffuse reflectance within a sample (not necessarily unfavorable)[33,56,68,75] (and indicated later by Fig. 5.1.28), but may also lead to issues with the contacting of and electrical measurements on such devices[185].

Similarly, UV-vis measurements were done on combination CuSCN/TiO_2/, and CuSCN/BFO/TiO_2/FTO-glass samples (Fig 5.1.27), and compared to the UV-vis spectra of their individual components.

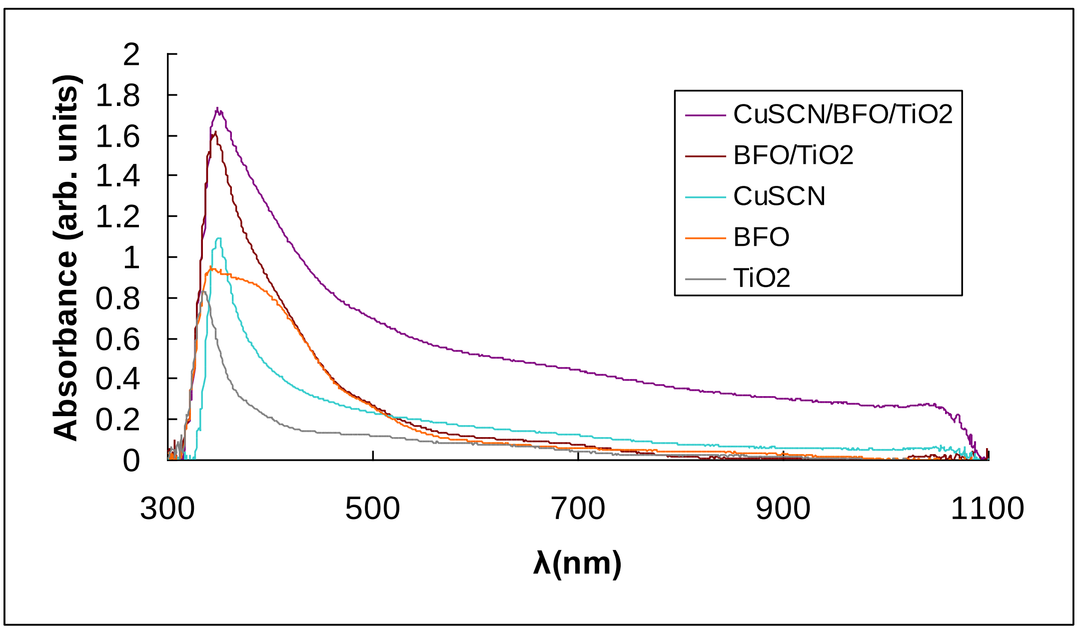

Figure 5.1.27: UV-vis spectra of (a) TiO_2/, (b) BFO/, (c) CuSCN/TiO_2(ref.TiO_2)/, (d) BFO/TiO_2, and (e) CuSCN/BFO/TiO_2/FTO-glass synthesized via a combination of the "as listed" parameters above (referenced to FTO-glass except where noted otherwise)

Again, as expected, the UV-vis spectrum for the CuSCN on TiO_2 shows a 'hybridization' of spectral features of their individual components.

Light-harvesting efficiencies were also calculated/estimated for TiO_2-based samples, as shown in Fig. 5.1.28:

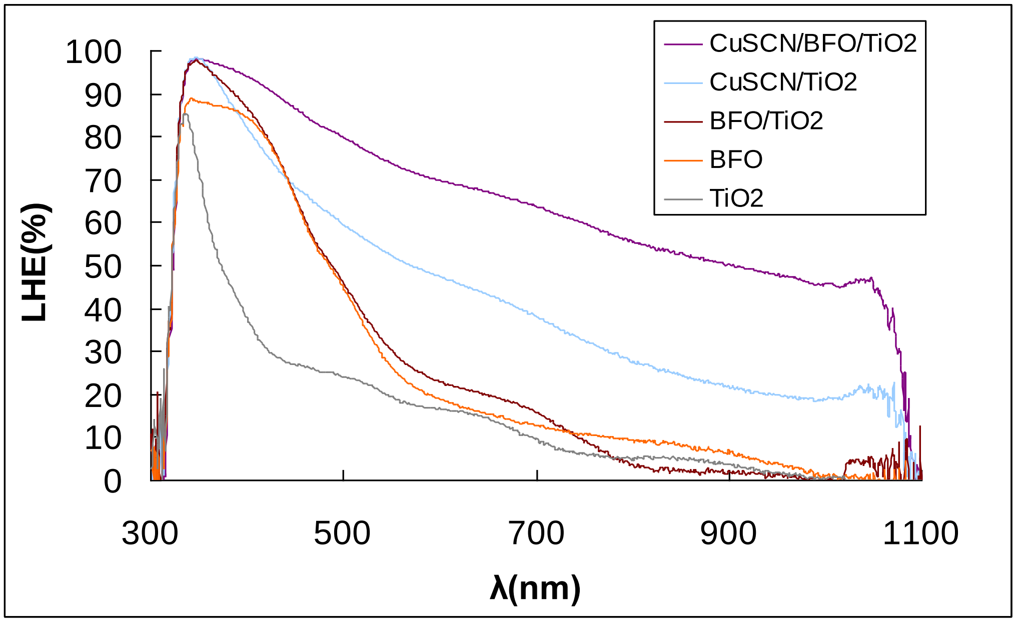

Figure 5.1.28: Light-harvesting efficiencies for a) TiO_2/ b) BFO/, c) CuSCN/TiO_2/, d) BFO/TiO_2/, and e) CuSCN/BFO/TiO_2/FTO-glass

Again, such high values are likely overestimates, as issues arise with the UV-vis measurement of absorbance likely relying on transmittance and not accounting for much reflectance. The reflectance sources, similar to the Bi-Fe-Zn-O/ZnO example previously (Fig. 5.1.14), are likely the roughness of the photoanode roughness (though apparently to less of an extent with the TiO_2 than the ZnO, though quantitatively due to differences in grain sizes and likely in density, these two in this work are not particularly comparable in this regard). Also, the roughness/nonuniformity, morphology, film thickness, and perchance grain size of the CuSCN film may also contributes significantly to internal reflectance. However, they do indicate, at least qualitatively, a likely significant contribution of the BFO absorber (top/purple curve) over simply having an absorberless transparent/translucent (i.e. 'wide' band gap) photoanode, or an essentially p-n-based solar cell comprised of two transparent/translucent materials.

5.2 Device Characterization

Preliminary IV-measurements of Au/Ti-contacted-Bi-Fe-Zn-O/ZnO/FTO-glass (measured across the Bi-Fe-Zn-O layer) were taken, and shown in Fig. 5.2.1:

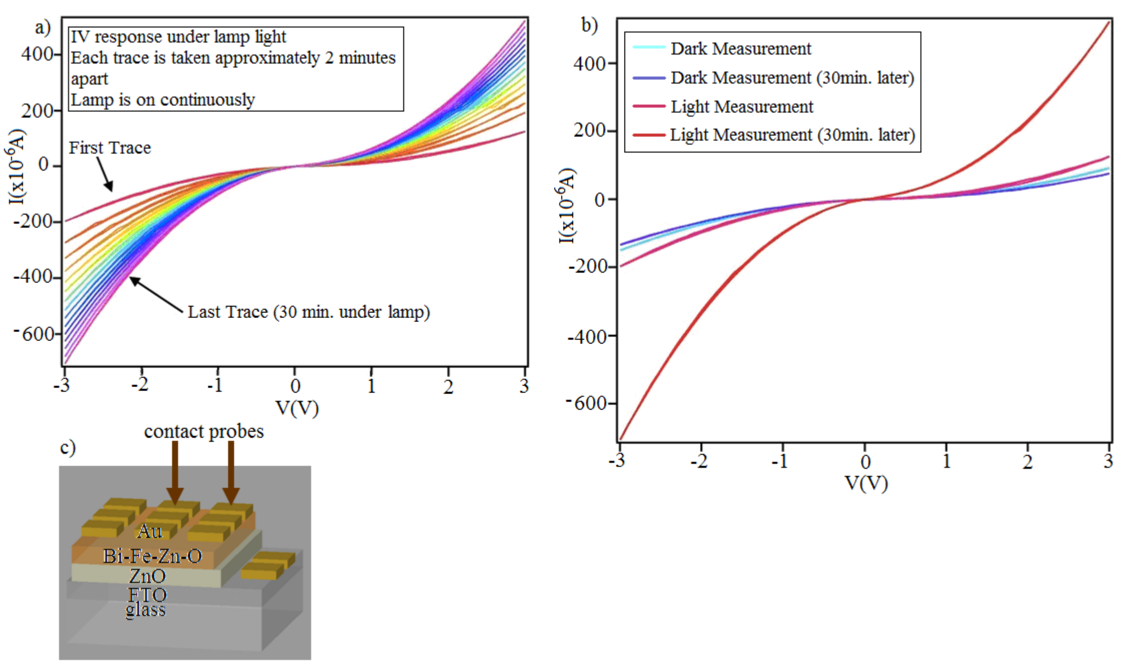

Figure 5.2.1: a,b) IV-measurements taken on Au-Ti/Bi-Fe-Zn-O/ZnO/FTO-glass, c) contacted as shown

Though such devices do not show the desired rectifying/diode behavior expected for photovoltaics (albeit these devices lack a hole conductor or electrolyte), they do exhibit a significant light response. Persistent photocurrent (not shown), as well as the time evolved increased current response, may be due to carrier 'traps' within the film, perhaps due to cracking/spalling, for both inter- and intra-'tile' fracture, surface states due to the high surface area/rough nature of the films, and likely their interface(s), a/o due to impurities and/or phase separation present in such devices[191,192] (discussed earlier in section 5.1.4).

Contacting a Bi-Fe-Zn-O/ZnO/FTO-glass device as expected (i.e. measuring through the device from the FTO on one side to the metal on top of the absorber layer on the other, Fig. 5.2.2b) and measuring (Fig. 5.2.2) shows asymmetric, non-linear behavior, closer to the expected rectifying behavior, perhaps with the non-linear 'tail' on the negative bias side representing breakdown. Apparently, as indicated by the ~0A current at 0V, though this device may be a photodetector, as it responds to light somewhat, it does not show any significant photovoltaic effects, possibly because of the lack of 'circuit-completing'

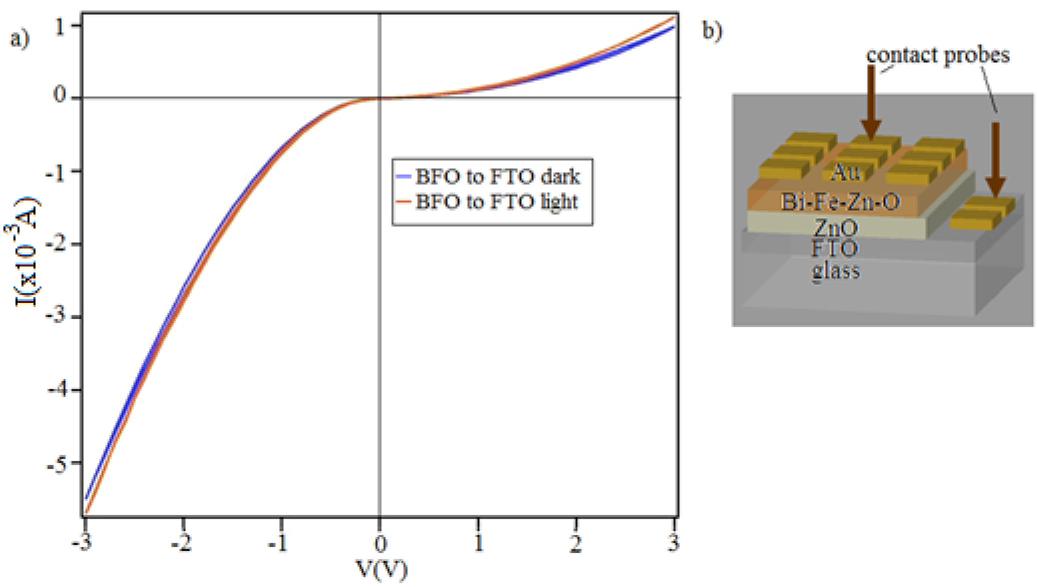

Figure 5.2.2: a) IV-measurements taken on Au-Ti/Bi-Fe-Zn-O/ZnO/FTO-glass, b) contacted as shown

Preliminary IV-measurements were also taken on a Ag-paint-contacted $CuSCN/BFO/TiO_2$/FTO-glass sample, shown in Fig. 5.2.3:

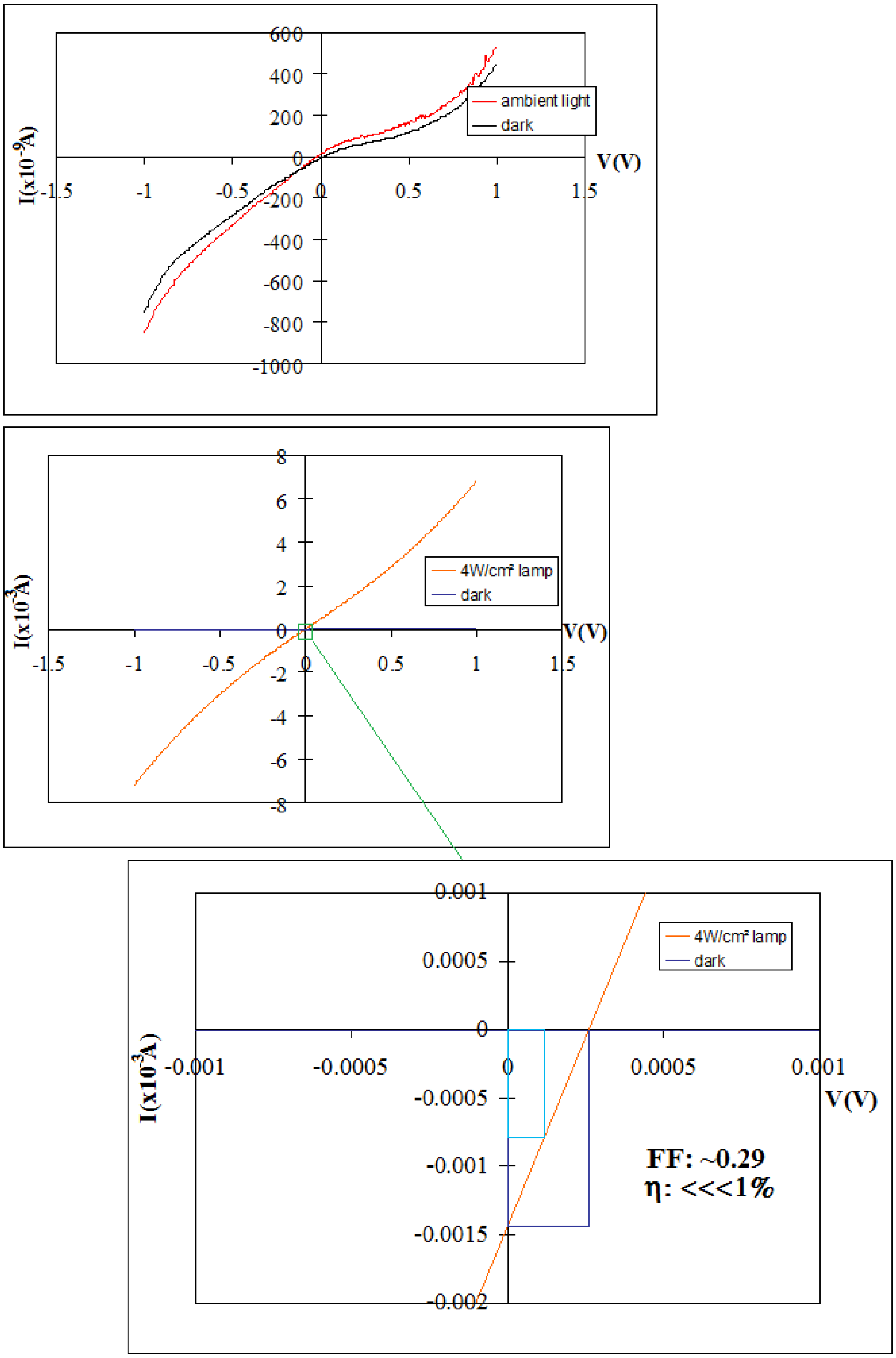

Figure 5.2.3: IV-characteristics of Ag/CuSCN/BFO(as-synthesized/'unpoled')/TiO_2/FTO-glass

Again, rectifying behavior is not seen, but a slight light response, even in just ambient light (as opposed to a solar simulator or more intense lighting) appears to be enough to facilitate some type of response, albeit this behavior is more characteristic of general metal-semiconductor-metal devices[185], as opposed to diodes or typical PV devices. Low current output may be a consequence of poor electrical contact, either between the Ag-paint and the CuSCN a/o the CuSCN and the sensitized-photoanode-substrate/sample. Under ~4W/cm^2 illumination, a significant light response (~4 orders of magnitude) has been seen. Moreover, a slight photovoltage is apparent under such light, as would be expected. The device has a low but reasonable/'decent' fill factor, but, however, V_{oc} and η are quite low. Leakage current (perhaps due to BFO) may also possibly 'present' in these 'devices'.

The non-linear, non-rectifying behavior exhibited by this particular device maybe a consequence of the choice of metallic contact in this case (i.e. Ag-paint more likely to be conformal and is quicker to apply than sputtered or evaporated metals)[185]. Au and Ni have been found to be viable contacts with CuSCN, due to their high work-function values (i.e. > 5eV)[150], and hence contacting with such does not create a Schottky barrier (φ_b) between the metal and p-CuSCN[150,185]. However, using previously noted parameters for CuSCN[74,76,77,108,141,150,168] Ag (φ~4.73eV) gives φ_b of ~0.42-0.7eV, as given by using eqn. 5.2.1[150,186,188]:

$$\varphi_{b,p} = E_g - (\varphi_m - \chi_p) \qquad \textbf{(5.2.1)}^{150,186,188}$$

where $\varphi_{b,p}$ is the Schottky barrier between a metal/conductor and p-type semiconductor, φ_m is the contact metal's work function, and χ_p is the p-type semiconductor's electron affinity.

On the other side, with FTO (φ~4.7eV)[150] on the presumably n-type TiO_2, eqn. 5.2.2[186,188] applies:

$$\varphi_{b,n} = \varphi_m - \chi_n \qquad \textbf{(5.2.2)}^{186,188}$$

where $\varphi_{b,n}$ is the Schottky barrier between a conductor/metal and a n-type semiconductor, and χ_n is the n-type semiconductor's electron affinity.

giving φ_b of ~0-0.8eV (likely pending the doping level, etc. of the TiO_2)[189] when the requisite parameters for FTO[150] and TiO_2[145,150] are used. Though it would seem, based on the calculations and the IV-curve that there is a Schottky/blocking contact on the n-type side of the Ag/CuSCN/BFO/TiO_2/FTO-glass device, further measurements of the doping level of the TiO_2, and perhaps similar information about the FTO, used may be needed to further verify such a conclusion.

However, having blocking contacts on both sides of the device explains the fairly symmetric, non-linear, non-rectifying IV-characteristic of the device[185].

CHAPTER 6: CONCLUSIONS

Despite having not successfully fabricated any BFO-absorber-based PV devices, several useful pieces of information and helpful conclusions can be drawn.

Both ZnO and TiO_2 are two wide-gap semiconductors that can be easily and fairly inexpensively deposited on FTO-glass substrates, with a rough a/o porous morphology desirable for light trapping/scattering in DSSC or eta-solar cells[33,56,68,75].

$BiFeO_3$, a multiferroic material[100] with a band gap of ~2.5eV, is optically active in visible light, and is found to at least qualitatively enhance the light harvesting efficiency of wide-gap photoanodes it may be coupled with to form devices. Its rough as-heat-treated-post-deposition morphology may 'lend itself' well to favorable light-scattering/trapping effects within PV devices containing such[33,56,68,75]. $BiFeO_3$ deposited via the sol-gel method used, in this work, appears to have current leakage issues upon polarization, which may be dealt with via coating the BFO layer with an insulating oxide[189] or attempting a different synthesis route such as sputtering[105] or PLD[101,184], to eventually test the effects of ferroelectricity on an absorber material eta-SC-type device on charge separation and transport. Also, because it lacks toxic heavy metals (Pb, Se, Cd, etc.) often found in eta-absorbers a/o quantum dots, it may also be a more environmentally-friendly sensitizer material in terms of precursors, production, maintenance, etc.

Heat treating ZnO-based BFO-sol-coated samples at conditions typically utilized[117,138,139] for BFO crystallization, when done in N_2 or air, from sol-gel precursor yields either no crystalline absorber, BFO or otherwise (at $T<500^oC$, whether for a few minutes or several hours) or crystalline 'second'/'alternate' phases (at $T>500^oC$, for a few minutes or several hours), many candidates of which are not ferroelectric due to cubic symmetry[35]. Such may be a consequence of chemical reaction, solubility, BFO crystallization a/o final formation inhibition, thermodynamic or kinetic favorability of the 'alternate' phases over BFO, crystal-structure/lattice parameter differences, stoichiometry, surface termination/chemistry, or some combination thereof. Promising results in low-pressure

O_2 annealing were seen, though some ‘second phase’ appears to be present as well, BFO is seen along with ZnO and SnO_2 as desired/expected, and further experiments in O_2 annealing temperature, time, pressure, and flow rate may in fact yield successful BFO/ZnO/FTO-glass samples synthesized via electrodeposition of ZnO and sol-gel dip-coating of BFO. Also, BFO deposition routes such as sputtering[105], which do not require such ‘intense’ heat treatments, and have yielded results in the literature, may be reasonable alternatives as well. Bi-Fe-Zn-O/ZnO films were also found to quite often crack, split, or spall off FTO-glass substrates.

α-TiO_2 was successfully deposited on FTO-glass via both ALD and NP-suspension-dip-coating. A rough morphology was achieved, particularly by the latter process. BFO-sol was successfully deposited on α-TiO_2, and crystallized via typical heat treatments for such[117,138,139], as indicated by XRD, UV-vis, and SEM.

CuSCN deposited via solution deposition in this work formed a rough, cracking, non-uniform film, which could be potentially problematic for electrical contacting and measurements. Greater control over this deposition process in terms of uniformity and thickness may be needed in the future, or a different means of depositing CuSCN such as electrodeposition[62,141], may be used.

Devices fabricated from Bi-Fe-Zn-O and characterized via IV-measurements showed a light response, likely due to an optically-active (albeit not crystalline BFO) sensitizer, as well as time-evolved current increases, and persistent photocurrent, perhaps as a consequence of ‘traps’ for carriers being present due to the alternative absorber phase or phases in addition to the cracked/tiled nature of the films[191,192]. Also, such devices did not show the desired/expected rectifying behavior commonly characteristic of PV devices.

A device fabricated from CuSCN/BFO/TiO_2/FTO-glass contacted with Ag-paint exhibited a light response in preliminary IV-characterization, albeit without rectifying behavior. The non-linear, symmetric response of such a device, which resembles metal-semiconductor-metal device behavior rather than diode-like/PV characteristics, may be caused by the presence of two blocking contacts on the device, when one blocking (Schottky) and one Ohmic contact would be favorable[185].

CHAPTER 7: FUTURE RECOMMENDATIONS

7.1 Immediate Future Research and Development

In the immediate future for the success of the project, the ferroelectric behavior of the BFO absorber layer, both ‘alone’ and within a device structure, must be quantitatively characterized, so that one can ‘pole’ the material and analyze and characterize the effects of ferroelectric polarization on a PV-absorber/sensitizer layer, which is the truly novel implication in such work. Using an alternate synthesis route[101,105,184] for BFO may be a better ‘starting point’ for such work, although leakage could perhaps be mitigated (albeit a higher applied field than usual still required) by insulating the BFO with an insulating oxide layer such as HfO_2[188]. Experiments on facilitating the sol-gel BFO synthesis route on ZnO, particularly relating to O_2 or vacuum anneals, may also prove useful and 'doable' (if at all) in the 'not so distant future'. Overall, the issues relating to combining and heat treating ZnO and BFO should perhaps be investigated as well, as described previously in section 5.1.4.

The issue of BFO current leakage (likely caused by 'charge defects' such as oxygen vacancies, etc., and possibly 'second phases' where present in addition to BFO)[193-195] and electrical conductivity has been addressed in the literature via 'doping' of the material by both aliovalent (such as Ni^{2+} (p-type, increased conductivity)[193] or Ti^{4+}, V^{5+} (n-type, increased resistivity/decreased leakage)[193,194]) or isovalent (La^{3+}, etc., various reasons)[194,195] likely substitution of some Bi^{3+} or Fe^{3+} atoms in BFO. In addition, dopants, particularly in the case of La^{3+}, added to BFO have led to improved remnant polarization (which may translate to a higher 'built in' electric field within the material), also likely beneficial. Research on the effects of doping on leakage[193-195], FE-behavior[195], band gap/optical properties[196], etc.. Moreover, assessment absorber/photoanode a/o hole-conductor/absorber material 'compatibility' should likely also continue be assessed for both intrinsic and doped-BFO, as well as the feasibility and viability of incorporating dopants into whichever deposition process(es)[100,101,117,138,139,184,193-196] may be utilized. Furthermore the polarization/domain structure post-synthesis and post-poling could be analyzed a/o confirmed via a Raman spectroscopy/mapping[197,198] or piezoresponse force microscopy (PFM) done using an atomic force microscope (AFM) probe (which also yields piezoelectric hysteresis data)[91,199,201], depending on the domain size, film thickness, a/o desired resolution.

'Cleaner' hole conductor (CuSCN) deposition is also necessary, whether via solution deposition[62,] or electrodeposition[62,141], for better uniformity, 'cleaner'/'better' electrical contacting, and perhaps better efficiencies or at least more accurate/reproducible/repeatable device electronic characterization and measurements. Other hole conductors[62,65-67] may also be of interest to investigate on such devices in the near future, however CuSCN is already 'predicted' to have proper band alignment[76,108,141,142] with BFO/TiO_2 or BFO/ZnO photoanodes, so parameters such as band gap, electron affinity, and work-function for different hole-conductors would need to be obtained, and similar assessments/predictions made as to their band alignment[141,142], likely prior to experiments or devices of this sort utilizing such.

7.2 Further Research and Development

Once the preliminary/pioneering work on FE-sensitized eta-PV-devices is completed, one can work on a number of things, such as (further) alternative deposition routes for the various layers, nanostructured/architecture device morphologies and the effects thereof, and better tuning the absorber/sensitizer material in terms of band gap a/o ferroelectric properties. For instance, Xu, et. al. have shown that $BiMnO_3$ (E_g~1.1eV) and BFO can form an alloy/solid solution, with tunable absorbance onset/band gap from ~1.1-2.7eV, a 'good range' considering the visible and near IR portions of the electromagnetic spectrum[196]. Moreover, such films have been shown to exhibit and retain their ferroelectric character over a range of compositions[200]. Mn^{3+} substitution is even believed to increase breakdown voltage in such materials, albeit with a 'trade-off' of increased leakage current densities[200], and at least an apparent increase E_c[200], meaning increased voltage (i.e. likely more power and perhaps a 'higher voltage' voltage source required) to 'switch' the polarization of the material, both of the latter of which would then also have to be addressed. Though likely due to leakage issues, ferroelectricity in $BiMnO_3$ has been difficult to show[201], it has been recently measured by Grizalez, et. al.[202], furthering the feasibility of using $BiMnO_3$ in conjunction with BFO films, whether via a single, favorable alloy composition, or a graded film composite, as a(n) absorber/sensitizer in eta-SC devices. Studies on apparent E_c changes with respect to insulator type and thickness (for the insulating film, knowing dimensions and material resistivity, assuming a conformal, uniform film, give one some idea of the series resistance contributed by it, and hence the expected voltage drop across it at a given current can be estimated, and, knowing the total voltage applied, the effective voltage and hence field E across the FE layer can be calculated/estimated as well) on 'leaky-film-containing' systems would also be useful.

Aside from changes in photoanode, at least somewhat analyzed in this work and further proposed in Ch. 7.1, sensitizer (discussed just prior in this section), and hole conductor (addressed in 7.1), changes in device structure/architecture can be addressed as well. If/when a thin-film 'system' or set of 'systems' containing a n-type photoanode/FE-sensitizer/p-type hole conductor setup has been reasonably established, comparable devices made of similar materials composed of either porous template[54-56,91,203]('inside out') or nanowire a/o hierarchical-nanostructure[57-61]('regular order') nanoarchitectured devices (Fig. 7.2.1) can be constructed and evaluated.

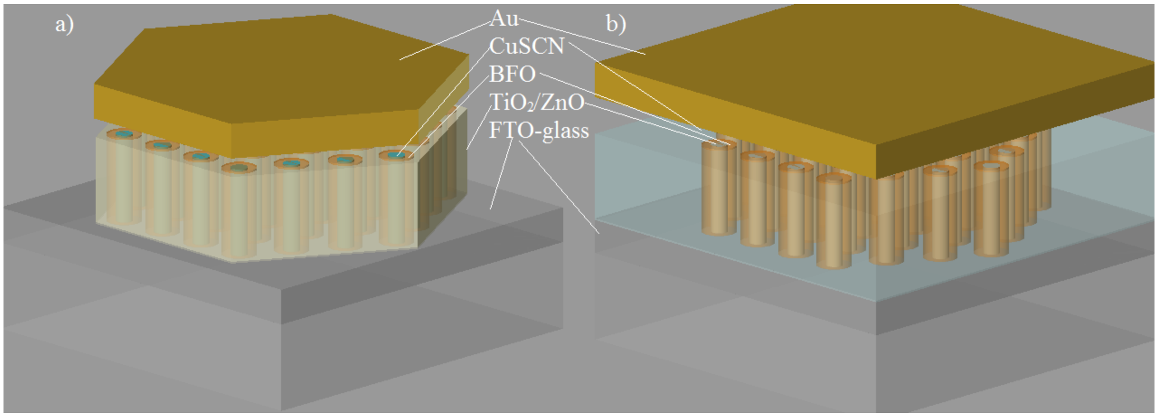

Figure 7.2.1: Example schematic hypothetical future device architectures with a) 'inside out' and b) 'regular order' designs

Both porous templates and nanowire-based architectures allow for the possible synthesis of thin, curved ferroelectric 'sensitizer' shells incorporated into eta-PV devices. Finite curvature effects have been found to mitigate the effects of a depolarizing field on thin-film ferroelectrics, and furthermore possibly yield a 'favorable polarization direction' as synthesized (i.e. even absent an applied coercive E-field)[91,203,204]. Furthermore, any changes caused by changing the 'ordering' of the materials in nanostructured devices can be investigated. Finally the 'effects' of 'orthogonalizing', at least to some extent, charge transport and absorption (as mentioned previously in section) can be investigated for deliberately/orderly nanostructured/arrayed devices, and compared to the available information on their 'thin film'/'sandwich' structure counterparts, for potential improvements in or optimization of light absorption, trapping, charge transport, and overall efficiency[107].

7.3 Scalability

FTO-glass can be purchased in small pieces or panels of a few hundred mm x a few hundred mm[205]. Dip-coating and electrodeposition appear to be relatively inexpensive, reasonably controllable (in terms of thickness and morphology), simple deposition routes for wide-band-gap semiconductor photoanodes in DSSC. Sol-gel dip-coating and solution deposition routes for BFO, as well as potentially electrodepositing this layer[140] (albeit such is done thus far in acidic solution, which is likely unfavorable for bare ZnO to be placed in) are viable, scalable processes as well. ‘Doctor blading’ is a technique common on the ‘larger scale’, particularly in the printing industry[206], and may also be used for TiO_2 suspension film thickness control[165,166], if not for BFO, etc. as well. Since p-CuSCN as a hole conductor can be deposited by solution deposition (though on a large scale especially, one may want to avoid the used of n-propyl sulfide due to price and odor) or electrodeposition[62,141], it ‘follows suit’ in terms of simplicity if used for ‘scale-up’ production of such devices. Metallic contacts can be applied via sputtering or some other physical vapor deposition process, and masking can be used to create patterned contacts, though precious metals will still likely contribute much of the expense to such fabrication on a large-scale.

List of References

[1] United States Department of Energy (US DoE) Energy Information Administration (EIA), “International Energy Outlook 2009”

[2] Carlin, J., “Environmental Externalities in Electric Power Markets: Acid Rain, Urban Ozone, and Climate Change” US DoE EIA CNEAF Featured Article (SEPT 2002) <http://www.eia.doe.gov/cneaf/pubs_html/rea/feature1.html> Accessed 25MAR2010.

[3] Renewable Energy Trust, “What Are Emissions?” <http://www.masstech.org/cleanenergy/important/envemissions.htm> Accessed 23MAR2010.

[4] Keller, C.F., “Global warming: a review of this mostly settled issue” Stochastic Env. Res./Risk Assessment **23**(5), 2009(online first 08AUG2008).

[5] Bernard, Susan M., Samet, Jonathan M., Grambsch, A., Ebi, K.L., Romieu, I., “The Potential Impacts of Climate Variability and Change on Air Pollution-Related Health Effects in the United States” Environ. Health Perspect. **109**(2), 2001.

[6] Likens, G. (Lead Author); Environmental Protection Agency (Content source); Davis, W., Zaikowski, W., and Nodvin, S.C. (Topic Editors). 2010. "Acid rain." In: Encyclopedia of Earth. Eds. Cutler J. Cleveland (Washington, D.C.: Environmental Information Coalition, National Council for Science and the Environment). [First published in the Encyclopedia of Earth October 9, 2006; Last revised January 2, 2010; Retrieved March 25, 2010]. <http://www.eoearth.org/article/Acid_rain> Accessed 25MAR2010.

[7] Malsch, I., “Thin Films Seek a Solar Future” The Industrial Physicist **9**(2), 2003.

[8] United States Department of Energy (US DoE) Energy Information Administration (EIA), “Renewable and Alternative Fuels” <http://www.eia.doe.gov/fuelrenewable.html> Accessed 25MAR2010.

[9] Arvizu, D. E., National Renewable Energy Laboratory, “Renewable Energy Technology Opportunities: Responding to Global Energy Challenges” Clean-Tech Investors Summit, 23JAN2007. <http://www.nrel.gov/director/pdfs/clean_tech_jan07_final.pdf> Accessed 29MAR2010.

[10] Arvizu, D.E., National Renewable Energy Laboratory, “The Promise of Solar Electricity”, 22OCT2008. <http://www.nrel.gov/director/pdfs/ks_aee-2008-1022.pdf> Accessed 29MAR2010.

[11] Roberts, B. National Renewable Energy Laboratory, “Dynamic Maps, GIS data, and Analysis Tools: “Photovoltaic Solar Resource of the United States” <http://www.nrel.gov/gis/solar.html> Accessed 26MAR2010.

[12] Land Art Generator Initiative, “SURFACE AREA REQUIRED TO POWER THE WORLD WITH ZERO CARBON EMISSIONS AND WITH SOLAR ALONE” <http://www.landartgenerator.org/images/PosterSolar.jpg> Accessed 29MAR2010.

[13] Diaz, J., “How Many Solar Panels Would It Take to Power The Entire World?” GIZMODO, 01SEPT2009 <http://gizmodo.com/5350191/how-many-solar-panels-would-it-take-to-power-the-entire-world> Accessed 26MAR2010

[14] Netstate.com, “Texas: The Geography of Texas” <http://www.netstate.com/states/geography/tx_geography.htm>

[15] Martinot, E., Mastny, L. (editor), Rosbotham, L. (editor), Suding, P. (coordinator), Sonntag-O’Brien, V. (coordinator), Lempp, P. (coordinator), El-Ashry, M.(chair), Renewable Energy Policy Network for the 21st Century (REN21), “Renewables 2007: Global Status Report” <http://www.ren21.net/pdf/RE2007_Global_Status_Report.pdf> Accessed 26MAR2010.

[16] Martinot, E.(author), Sawin, J.L.(author), Lempp, P.(secretariat), Mastny, L.(editor), Welker, B.(editor), El-Ashry, M.(chair), Renewable Energy Policy Network for the 21st Century (REN21), “RENEWABLES GLOBAL STATUS REPORT 2009 Update” <http://www.ren21.net/pdf/RE_GSR_2009_Update.pdf> Accessed 29MAR2010.

[17] BusinessGreen Staff, “Global PV market to hit $32bn by 2012” BusinessGreen.com <http://www.businessgreen.com/business-green/news/2206609/global-pv-market-hit-32bn-2012> Accessed 29MAR2010.

[18] BusinessGreen Staff, “Solar to take on coal within three years” BusinessGreen.com <http://www.businessgreen.com/business-green/news/2206331/solar-coal-within-three-years> Accessed 29MAR2010.

[19] Luque, A.(editor), Hegedus, S.(editor), *Handbook of Photovoltaic Science and Engineering*, John Wiley & Sons, Inc., 2003.

[20] Advanced Energy, “Comparison of Various PV Technologies: Part I” PV Sun Times Q2, 2009 <http://www.advanced-energy.com/en/PV_Sun_Times.html> Accessed 08JUN2010.

[21] Honsberg, C., Bowden, C. “PVCDROM|pveducation.org” <http://pvcdrom.pveducation.org/index.html> Accessed 26JUN2010.

[22] University of New South Wales (UNSW), School of Photovoltaic and Renewable Energy, “Third Generation Photovoltaics” <http://www.pv.unsw.edu.au/Research/3gp.asp> Accessed 29MAR2010

[23] Energy Alternatives India, “The second generation of Solar Cells: Thin-Film PV” 24JUL2010 <http://eai.in/blog/2010/06/the-second-generation-of-solar-cells-thin-film-pv.html> Accessed 25AUG2010

[24] Grätzel, M., “Dye-sensitized solar cells” *J. Photochem. Photobiol*. **4**(2), 2003.

[25] Shockley, W., Queisser, H.J., “Detailed Balance Limit of Efficiency of p-n Junction Solar Cells” *J. Appl. Phys.* **32**(3), 1961.

[26] Katz, E.A., “Multi-Junction III-V Concentrator Solar Cells: Lessons with Ultra-High Flux of Real Sunlight”, Lecture, Drexel University, Department of Materials Science and Engineering (MSE), Seminar Series, Fall 2009 (08DEC2009).

[27] Cheney, T., “Solarmer breaks organic solar PV cell conversion efficiency record, hits NREL-certified 7.9%” Photovoltaics International, 02DEC2009 <http://www.pvtech.org/news/_a/solarmer_breaks_organic_solar_pv_cell_conversion_efficiency_record_hits_nre/> Accessed 25AUG2010

[28] Chiba, Y., Islam, A., Watanabe, Y., Komiya, R., Koide, N., Han, L. “Dye-Sensitized Solar Cells with Conversion Efficiency of 11.1%” *Jap. J. Appl. Phys*. **45**(25), 2006.

[29] Zyga, L. “Porphyrin Dimers Increase Efficiency of Dye-Sensitized Solar Cells” PhysOrg.com, 30OCT2009 <http://www.physorg.com/news176112834.html> Accessed 25AUG2010.

[30] Grätzel, M. “The artificial leaf, molecular photovoltaics achieve efficient generation of electricity from sunlight” Coord.Chem.Rev. **111**(6), 1991.

[31] Grätzel, M., Kalayanasundaram, K., “Artificial photosynthesis: Efficient dye-sensitized photoelectrochemical cells for direct conversion of visible light to electricity”, Curr. Sci. **66**(10), 1994.

[32] Green, M.A., Wenham, S. R., “Novel parallel multijunction solar cell” Appl. Phys. Lett. **65**(23), 1994.

[33] Könenkamp, R., Hoyer, P., Wahi, A., "Heterojunctions and devices of colloidal semiconductor films and quantum dots" *J. Appl. Phys.* **79**(), 1996.

[34] Kaiser, I., Ernst, K., Fischer, Ch.-H., Könenkamp, R., Rost, C., Sieber, I., Lux-Steiner, M.Ch., "The eta-solar cell with $CuInS_2$: A photovoltaic cell concept using an extremely thin absorber (eta)" *Sol. Energ. Mater.* **67**(1-4), 2001.

[35] Barsoum, M.W. "Fundamentals of Ceramics" Taylor and Francis, New York, 2003.

[36] Spanier, J.E. "Inorganic Nanowires" Drexel University, Chemistry Dept. 19NOV2009.

[37] Dissemination of IT for the Promotion of Materials Science (DoITPoMS) "Ferroelectric Materials" University of Cambridge <http://www.doitpoms.ac.uk/tlplib/ferroelectrics/printall.php?question=3&type=1> Accessed 25AUG2010.

[38] May, S. Complex Oxides "mini-course" [informal], Drexel University, Winter+Spring 2010.

[39] Choi, T., Lee, S., Choi, Y.J., Kiryukhin, V., Cheong, S.-W., "Switchable Ferroelectric Diode and Photovoltaic Effect in $BiFeO_3$" *Science* **324**(63), 2009.

[40] Yang, S.Y., Seidel, J., Byrnes, S.J., Shafer, P., Yang, C.-H., Rossell, M.D., Yu, P., Chu, Y.-H., Scott, J.F., Ager, J.W. III, Martin, L.W., Ramesh, R., "Above-bandgap voltages from ferroelectric photovoltaic devices" *Nature Nanotech*. Advance online publication, 2010.

[41] Desilvestro, J., Grätzel, M., Kavan, L., Moser, J., "Highly Efficient Sensitization of Titanium Dioxide" *J. Am. Chem. Soc.* **107**(10), 1985.

[42] Grätzel, M. "Recent Advances in Sensitized Mesoscopic Solar Cells" *Acct. Chem. Res.* **42**(11), 2009.

[43] Lenzmann, F.O., Kroon, J. M., "Recent Advances in Dye-Sensitized Solar Cells" *Adv. Optoelectronics* **2007**, 2007.

[44] Vogel, R., Pohl, K., Weller, H., "Sensitization of highly porous, polycrystalline TiO_2 electrodes by quantum sized CdS" *Phys. Chem. Lett.* **174**(3-4), 1990.

[45] Vogel, R., Hoyer, P., Weller, H., "Quantum-Sized PbS, CdS, Ag_2S, Sb_2S_3, and Bi_2S_3 Particles as Sensitizers for Various Nanoporous Wide-Bandgap Semiconductors" *J. Phys. Chem.* **98**(12), 1994.

[46] Hotchandani, S., Kamat, P.V., “Charge-Transfer Processes in Coupled Semiconductor Systems. Photochemistry and Photoelectrochemistry of the Colloidal CdS-ZnO System” *J. Phys. Chem.* **96**(16), 1992.

[47] Kamat, P.V., “Quantum Dot Solar Cells. Semiconductor Nanocrystals as Light Harvesters” *J. Phys. Chem. C* **112**(48), 2008.

[48] Lee, Y.-L., Huang, B.-M., Chien, H.-T., “Highly Efficient CdSe-Sensitized TiO_2 Photoelectrode for Quantum Dot-Sensitized Solar Cell Applications” *Chem. Mater.* **20**(22), 2008.

[49] Shalom, M., Albero, J., Tachan, Z., Martínez-Ferrero, E., Zaban, A., Palomares, E. “Quantum Dot-Dye Bilayer-Sensitized Solar Cells: Breaking the Limits Imposed by the Low Absorbance of Dye Monolayers” *J. Phys. Chem. Lett.* **1**(7), 2010.

[50] Kongkanand, A., Tvrdy, K., Takechi, K., Kuno, M., Kamat, P.V., “Quantum Dot Solar Cells. Tuning Photoresponse through Size and Shape Control Of CdSe-TiO_2 Architecture” *J. Amer. Chem. Soc.* **112**(30), 2008.

[51] Larramona, G., Choné, C., Jacob, A., Sakaura, D., Delatouche, B., Péré, D., Cieren, X., Nagino, M., Bayón, R., “Nanostructured Photovoltaic Cell of the Type Titanium Dioxide, Cadmium Sulfide Thin Coating, And Copper Thiocyanate Showing High Quantum Efficiency” *Chem. Mater.* **18**(6), 2006.

[52] Grätzel, M. “Photoelectrochemical cells” *Nature* **414**(6861), 2001.

[53] Tennakone, K., Perera, V.P.S., Kottegoda, I.R.M., Kumara, G.R.R. “Dye-sensitized solid state photovoltaic cells based on composite zinc oxide/tin (IV) oxide films” *J. Phys. D: Appl. Phys.* **32**(4), 1999.

[54] Adachi, M., Okada, I., Ngamsinlapasathian, S., Murata, Y., Yoshikawa, S., “Dye-sensitized Solar Cells Using Semiconductor Thin Film Composed of Titania Nanotubes” *Denki Kagaku oyobi Kogyo Butsuri Kagaku* **70**(6), 2002 (similar/also available at <http://www.electrochem.org/dl/ma/201/pdfs/1046.pdf> Accessed 26AUG2010)

[55] Uchida, S., Chiba, R., Tomiha, M., Masaki, N., Shirai, M., “Application of Titania Nanotubes to a Dye-sensitized Solar Cell” *Kagaku oyobi Kogyo Butsuri Kagaku* **70**(6), 2002.

[56] Zhu, K., Neale, N.R., Miedaner, A., Frank, A.J., “Enhanced Charged Collecting and Light Scattering in Dye-Sensitized Solar Cells Using Oriented TiO_2 Nanotube Arrays” *Nano Lett.* **7**(1), 2007.

[57] Law, M., Green, L.E., Johnson, J.C., Saykally, R., Yang, P., "Nanowire dye-sensitized solar cells" *Nature Mater.* **4**(6), 2005.

[58] Sauvage, F., Di Fonzo, F., Li Bassi, A., Casari, C.S., Russo, V., Divitini, G., Ducati, C., Bottani, C.E., Comte, P., Grätzel, M. "Hierarchical TiO_2 Photoanode for Dye-Sensitized Solar Cells" *Nano Lett.* **10**(7), 2010.

[59] Xu, F., Dai, M., Lu, Y., Sun, L. "Hierarchical ZnO Nanowire-Nanosheet Architectures for High Power Conversion Efficiency in Dye-Sensitized Solar Cells" *J. Phys. Chem. C* **114**(6), 2010.

[60] Zhang, Q., Chou, T.P., Russo, B., Jeneke, S.A., Cao, G., "Aggregation of ZnO Nanocrystallites for High Conversion Efficiency in Dye-Sensitized Solar Cells" *Angew. Chem. Int. Ed.* **47**(13), 2008.

[61] Tan, B., Wu, Y., "Dye-Sensitized Solar Cells Based on Anatase TiO_2 Nanoparticle/Nanowire Composites" *J. Phys. Chem. B* **110**(32), 2006.

[62] Liduo Wang, B.L., Kang, B., Wang, P., Qui, Y., "Review of recent progress in solid-state dye-sensitized solar cells" *Sol. Energ. Mater.* **90**(5), 2006.

[63] Tennakone, K., Kumara, G.R.R.A., Kumarasinghe, A.R., Wijayantha, K.G.U., Sirimane, P.M., "A dye-sensitized nano-porous solid-state photovoltaic cell" *Semicond. Sci. Technol.* **10**(12), 1995.

[64] Meng, Q.-B., Takashi, K., Zhang, X.-T., Sutanto, I., Rao, T.N., Sato, O., Fujishima, A., Watanabe, H., Nakamori, T., Uragami,M., "Fabrication of an Efficient Solid-State Dye-Sensitized Solar Cell" *Langmuir* **19**(9), 2003.

[65] Kaneko, M., Hoshi, T., Kaburagi, Y., Ueno, H., "Solid type dye-sensitized solar cell using polysaccharide containing redox electrolyte solution" *J. Electroanal. Chem.* **572**(1), 2004.

[66] Yum, J.-H., Chen, P., Grätzel, M., Nazeeruddin, M.K., "Recent Developments in Solid-State Dye-Sensitized Solar Cells" *Chem. Sus. Chem.* **1**(8-9), 2008.

[67] Snaith, H.J., Moule, A.J., Klein, C., Meerholz, K., Friend, R. H., Grätzel, M. "Efficiency Enhancements in Solid-State Hybrid Solar Cells via Reduced Charge Recombination and Increased Light Capture" *Nano Lett.* **7**(11), 2007.

[68] Ernst, K., Belaidi, A., Könenkamp, R., "Solar cell with extremely thin absorber on highly structured substrate" *Semicond. Sci. Technol.* **18**(6), 2003.

[69] Siebentritt, S., Ernst, K., Fischer, C., Könenkamp, R., "CdTe and CdS as extremely thin absorber materials in an η-solar cell" *Proc. 14th European Photovolt. Sol. Energ. Conf.,* Barcelona, 1997.

[70] Soga, T. *Nanostructured Materials for Solar Energy Conversion*, Elsevier, 2006.

[71] Rost, C., Ernst, K., Siebentritt, S., Könenkamp, R., Lux-Steiner, M.C., *Proc. 2nd. World Conf. & Exhibition Photovolt. Sol. Energ. Conv.*, Vienna, 1998.

[72] Möller, J., Fischer, C.H., Siebentritt, S., "$CuInS_2$ as an extremely thin absorber in an eta solar cell" *Proc. 2nd. World Conf. & Exhibition Photovolt. Sol. Energ. Conv.*, Vienna, 1998.

[73] Qiu, J., Jin, Z., Qian, J., Shi, Y., Wu, W., "Influence of post-heat treatment on the properties of $CuInS_2$ thin films deposited by an ion layer gas reaction (ILGAR)" *J. Cryst. Growth* **282**(3-4), 2005.

[74] Rost, C., Sieber, I., Siebentritt, S., Lux-Steiner, M.C., Könenkamp, R., "Spatially distributed p-n heterojunction based on nanoporous TiO_2 and CuSCN" *Appl. Phys. Lett.* **75**(5), 1999.

[75] Taretto, K., Rau, U., "Modeling Extremely Thin Absorber Solar Cells for Optimized Design" *Prog. Photovolt. Res. Appl.* **12**(8), 2004.

[76] Tena-Zaera, R., Katty, A., Bastide, S., Lévy-Clément, C.. O'Regan, B., Muñoz-Sanjosé, V., "ZnO/CdTe/CuSCN, a promising heterostructures to act as inorganic *eta*-solar cell" *Thin Solid Films* **483**(1-2), 2005.

[77] Lévy-Clément, C., Tena-Zaera, R., Ryan, M.A., Katty, A., Hodes, G., "CdSe-Sensitized p-CuSCN/Nanowire n-ZnO Heterojunctions" *Adv. Mater.* **17**(12), 2005.

[78] Kieven, D., Dittrich, T., Belaidi, A., Tornow, J., Schwarzburg, K., Allsop, N., Lux-Steiner, M., "Effect of internal surface area on the performance of ZnO/In_2S_3/CuSCN solar cells with extremely thin absorber" *Appl. Phys. Lett.* **92**(15), 2008.

[79] Günes, S., Saricifftci, N. S., "Hybrid solar cells" *Inorganica Chim. Acta.* **361**(3), 2008.

[80] Nanu, M., Schoonman, J., Gooesens, A., "Solar-Energy Conversion in $TiO_2/CuInS_2$ Nanocomposites" *Adv. Func. Mater.* **15**(1), 2005.

[81] Krunks, M., Kärber, E., Katerski, A., Otto, K., Oja Acik, I., Dedova, T., Mere, A. "Extremely thin absorber layer solar cells on zinc oxide nanorods by chemical spray" *Sol. Energ. Mater.* **94**(7), 2010.

[82] Busch, G. "Early history of ferroelectricity" *Ferroelec.* **74**(1), 1987.

[83] Valasek, J., “The early history of ferroelectricity” *Ferroelec.* **2**(1), 1971.

[84] Haertling, G., “Ferroelectric Ceramics: History and Technology” *J. Am. Ceram. Soc.* **82**(4), 2004.

[85] Valasek, J. “Piezo-electric and Allied Phenomena in Rochelle Salt” *Rochelle Salt* **17**(4), 1921.

[86] Cross, L.E., Newnham, R.E., “History of Ferroelectrics” *Ceramics and Civilization, Vol. III, High-Technology Ceramics-Past, Present, and Future*, American Ceramic Society, 1987.

[87] Wadhawan, V.K., *Introduction to ferroic materials*, CRC Press, 2000.

[88] Randall, C.A., Newnham, R.E., Cross, L.E., “History of the First Ferroelectric Oxide, $BaTiO_3$”

[89] Haertling, G.H., “Ferroelectric thin films for electronic applications” *J. Vac. Sci. Technol.* **9**(3), 1990.

[90] Song, Y.-J., “Ferroelectric Thin Films for High Density Non-volatile Memories” *PhD Dissertation* (adv. Dr. Seshu Desu, Virginia Polytechnic Institute (Materials Science and Engineering), 13AUG1998.

[91] Nonnenmann, S.S. “Integrated non-planar ferroelectric nanostructures” *PhD Dissertation* (adv. Dr. Jonathan Spanier), Drexel University (Materials Science and Engineering), 26APR2010.

[92] Junquera, J., Ghosez, P., “Critical thickness for ferroelectricity in perovskite ultrathin films” *Nature* **422**(6931), 2003.

[93] Brody, P.S., Crowne, F., “Mechanism for the high voltage photovoltaic effect in ceramic ferroelectrics” *J. Elect. Mater.* **4**(5), 1975.

[94] Brady, J.J., Moore, W.H., “Actinoelectric Effects in Tartaric Acid Crystals” *Phys. Rev.* **55**(3), 1939.

[95] Fridkin, V.M. “Bulk Photovoltaic Effect in Noncentrosymmetric Crystals” *Crystallogr. Rep.* **46**(4), 2001.

[96] Yang, S.Y., Seidel, J., Byrnes, S.J., Shafer, P., Yang, C.-H., Rossell, M.D., Yu, P., Chu, Y.-H., Scott, J.F., Ager, J.W. III, Martin, L.W., Ramesh, R., “Above-bandgap voltages from ferroelectric photovoltaic devices” *Nature Nanotech.* (published online), 2010.

[97] Glass, A.M., von der Linde, D., Negran, T.J, “High-voltage photovoltaic effect and the photorefractive process in $LiNbO_3$” *Appl. Phys. Lett.* **25**(4), 1974.

[98] Qin, M., Yao, K., Liang, Y.C., “High efficient photovoltaics in nanoscaled ferroelectric thin films” *Appl. Phys Lett.* **93**(12), 2008.

[99] Yao, K., Gan, B.K., Chen, M., Shannigrahi, S., “Large photo-induced voltage in a ferroelectric thin film with in-place polarization” *Appl. Phys. Lett.* **87**(21), 2005.

[100] Catalan, G., Scott, J.F., “Physics and Applications of Bismuth Ferrite” *Adv. Mater.* **21**(24), 2009.

[101] Wang, J., Neaton, J.B., Zheng, H., Nagarajan, V., Ogale, S.B., Liu, B., Viehland, D., Vaithyanathan, V., Schlom, D.G., Waghmare, U.V., Spaldin, N.A., Rabe, K.M., Wuttig, M., Ramesh, R., “Epitaxial $BiFeO_3$ Multiferroic Thin Film Heterostructures” *Science* **299**(5613), 2003.

[102] Basu, S.R., Martin, L.W., Chu, Y.H., Gajek, M., Ramesh, R., Rai, R.C., Xu, X., Musfeldt, J.L. “Photoconductivity in $BiFeO_3$ thin films” *Appl. Phys. Lett.* **92**(9), 2008.

[103] Li, S., Lin, Y.-H., Zhang, B.-P., Li, J.-F., Nan, C.-W., “$BiFeO_3$/TiO_2 core-shell structured nanocomposites as visible-active photocatalysts and their optical response mechanism” *J. Appl. Phys.* **105**(5), 2009.

[104] Ji, W., Yao, K., Liang, Y.C., “Bulk Photovoltaic Effect at Visible Wavelength in Epitaxial Ferroelectric $BiFeO_3$ Thin Films” *Adv. Mater.* **22**(15), 2009.

[105] Wu, J., Lou, X., Wang, Y., Wang, J., “Resistive Hysteresis and Diodelike Behavior of $BiFeO_3$/ZnO Heterostrure” *Electrochem. Solid St. Lett.* **13**(2), 2010.

[106] Kundys, B., Viret, M., Colson, D., Kundys, D.O., “Light-induced size changes in $BiFeO_3$ crystals” *Nat. Mater.*, online publication [25JUL2010], 2010.

[107] Allen, J.E., conversations [informal] about ‘orthoganlizing’ absorption and transport in nanostructured solar cells (during BNL-SULI internship), Summer 2009.

[108] Padawer, I., “Synthesis and Characterization of CdSe-Coated ZnO Nanowires for Extremely Thin Absorber Solar Cells” *MS Thesis* (adv. Dr. Jason Baxter), Drexel University (Chemical and Biological Engineering), 29MAY2009.

[109] Liu, X.-Z., Huang, Z., Li, K-X., Li, H., Li, D.-M., Chen, L.-Q., Meng, Q.-B., “Recombination Reduction in Dye-Sensitized Solar Cells by Screen-Printed TiO_2 Underlayers” *Chin. Phys. Lett.* **23**(9), 2006.

[110] Wienke, J., Krunks, M., Lenzmann, F., “$In_x(OH)_yS_z$ as recombination barrier in TiO_2/inorganic absorber heterojunctions” *Semicond. Sci. Tech.* **18**(9), 2003.

[111] Taretto, K., Rau, U., “Influence of built-in voltage in optimized extremely thin absorber solar cells” *Thin Solid Films* **480-481**, 2005.

[112] Redfield, D., “Multiple-pass thin film silicon solar cell” *Appl. Phys. Lett.* **25**(11), 1974.

[113] Taretto, K., Rau, U., Werner, J.H., “Closed-form expression for the current/voltage characteristics of *pin* solar cells” *Appl. Phys. A* **77**(7), 2003.

[114] Kittel, C., *Introduction to Solid State Physics* 8th ed., Wiley & Sons, United States, 2005.

[115] Yang, S.Y., Zhan, Q., Yang, P.L., Cruz, M.P., Chu, Y.H., Ramesh, R., Wu, Y.R., Singh, J., Tian, W., Scholom, D.G., “Capacitance-voltage characteristics of $BiFeO_3/SrTiO_3$/GaN heteroepitaxial structures” *Appl. Phys. Lett.* **91**(2), 2007.

[116] Thomas, N.W., “A new framework for understanding relaxor ferroelectrics” *J. Phys. Chem. Solids* **51**(12), 1990.

[117] Wang, X., Zhang, Y., Wu, Z., “Magnetic and optical properties of multiferroic bismuth ferrite nanoparticles by tartaric acid-assisted sol-gel strategy” *Mater. Lett.* **64**(3), 2010.

[118] Yang, S.-Y., “Complex Metal Oxide Thin Film Growth By Metalorganic Chemical Vapor Deposition” *PhD Dissertation*, University of Maryland, 2005.

[119] Bera, D., Kuiry, S.C., Seal, S. “Synthesis or Nanostructured Materials Using Template-Assisted Electrodeposition” *Journal of Materials* **56**(1), 2004.

[120] Zheng, M.J., Zhang, L.D., Li, G.H., Shen, W.Z., “Fabrication and optical properties of large-scale uniform zinc oxide nanowire arrays by one-step electrochemical deposition technique” *Chem. Phys. Lett.* **363**(1-2), 2002.

[121] Mahalingam, T., John, V.S., Raja, M., Su, Y.K., Sebastian, P.J., “Electrodeposition and characterization of transparent ZnO thin films” *Sol. Energ. Mater.* **88**(2), 2005.

[122] Wellings, J.S., Chaure, N.B., Heavens, S.N., Dharmadasa, I.M., “Growth and characterisation of electrodeposited ZnO thin films” *Thin Solid Films* **516**(12), 2008.

[123] Zhitomirsky, I., Petric, A., Niewczas, M., “Nanostructured Ceramic and Hybrid Materials via Electrodeposition” *Journal of Materials* **54**(9), 2002.

[124] Schlesinger, M., "Electrochemistry Encyclopedia -- Electroplating" <http://electrochem.cwru.edu/encycl/art-e01-electroplat.htm> *Ernest B. Yeager Center for Electrochemical Sciences, Chemical Engineering Department, Case Western University* Accessed 24SEPT2010.

[125] Baxter, J.B., Walker, A.M., van Ommering, K., Aydil, E.S., "Synthesis and characterization of ZnO nanowires and their integration into dye-sensitized solar cells" *Nanotechnology* **17**(11), 2006.

[126] Cambridge Nanotech, "ALD | Atomic Layer Deposition Materials | Cambridge NanoTechCambridge Nanotech" <http://www.cambridgenanotech.com/ald/aldmaterials.php> Accessed 04OCT2010.

[127] Cambridge NanoTech, "Cambridge NanoTech Corporate Overview" (pictures based on animation by FrameWork Media) from AUG2009 <http://www.cambridgenanotech.com/cnpruploads/Cambridge%20NanoTech%20Web%20Overview.pdf> Accessed 04OCT2010.

[128] Cambridge NanoTech, "TiO_2 grown with Titaium isopropoxide $Ti(O^iPr)_4$ and H_2O" *Cambridge NanoTech – Confidential* viewed 19OCT2010.

[129] Dimitriev, Y., Ivanova, Y., Iordanova, R., " History of Sol-Gel Science And Technology (Review)" *J. Univ. Chem. Technol. Metall.* **43**(2), 2008.

[130] Hench, L.L., West, J.K., "The Sol-Gel Process" *Chem. Rev.* **90**(1), 1990.

[131] Shih, W.-H., "3.4.5 Sol-Gel Process" from *Lecture Notes:* Chapter 3 for *MatE 345: Ceramics Processing*, Drexel University, Winter Term, 2008.

[132] Brinker, C.J., Hurd, A.J., "Fundamentals of sol-gel dip-coating" *J. Phys. III France* **4**(7), 1994.

[133] Liu, J., Kuo, Y.-T., Klabunde, K.J., Rochford, C., Wu, Judy, Li, J., "Novel Dye-Sensitized Solar Cell Architecture Using TiO_2-Coated Vertically Aligned Carbon Nanofiber Arrays" *ACS Appl. Mater. Interfaces* **1**(8), 2009.

[134] Kuwabara, T., Sugiyama, H., Yamaguchi, T., Takahasi, K., "Inverted type bulk-heterojunction organic solar cell using electrodeposited titanium oxide thin films as electron collector electrode" *Thin Solid Film* **517**(13), 2009.

[135] Hemissi, M., Amardjia-Adnani, H., Plenet, J.C., "Titanium oxide thin layers deposed by dip-coating method: Their optical and structural properties" *Curr. Appl. Phys.* **9**(4), 2009.

[136] Di Fonzo, F., Casari, C.S., Russo, V., Brunella, M.F., Li Bassi, A., Bottani, C.E., "Hierarchically organized nanostructured TiO_2 for photocatalysis applications" *Nanotech.* **20**(1), 2009.

[137] Song, M.Y., Kim, D.K., Ihn, K.J., Jo, S.M., Kim, D.Y., "Electrospun TiO_2 for dye-sensitized solar cells" *Nanotech.* **15**(12), 2004.

[138] Park, T.-J., Mao, Y., Wong, S.S., "Synthesis and characterization of multiferroic $BiFeO_3$ nanotubes" *Chem. Commun.* **24**(), 2004.

[139] Park, T.-J., Papaefthymioiu, G.C., Viescas, A.J., Moodenbaugh, A.R., Wong, S.S., "Size-Dependent Magnetic Properties of Single-Crystalline Multiferroic $BiFeO_3$ Nanoparticles" *Nanolett.* **7**(3), 2007.

[140] Gujar, T.P., Shinde, V.R., Kulkarni, S.S., Pathan, H.M., Lokhande, C.D., "Room temperature electrodeposition and characterization of bismuth ferric oxide (BFO) thin films from aqueous nitrate bath" *Appl. Surf. Sci.* **252**(10), 2006.

[141] Ni, Y., Jin, Z., Fu, Y., "Electrodeposition of p-Type CuSCN Thin Films by a New Aqueous Electrolyte With Triethanolamine" *J. Am. Ceram. Soc.* **90**(9), 2007.

[142] Seeger, K., *Semiconductor Physics: an introduction*, 7th Ed. Springer, Berlin/New York, 1999.

[143] Fraser, D.A., *The physics of semiconductor devices*, 3rd Ed. Oxford: Clarendon Press, 1983.

[144] Luo, F., Wang, L., Qiu, Y., "Comparison between P25 and anatase-based TiO_2 quasi-solid state dye sensitized solar cells" *Chinese Sci. Bulletin* **53**(6), 2008.

[145] Könenkamp, R., Word, R.C., Godinez, M., "Electroluminescence in nanoporous TiO_2 solid-state heterojunctions" *Nanotech.* **17**(8)**,** 2006.

[146] Wang, Z.L., Song, J., "Piezoelectric Nanogenerators Based on Zinc Oxide Nanowire Arrays" *Science* **312**(10), 2006.

[147] Yang, H., Luo, H.M., Wang, H., Usov, I.O, Suvorova, N.A., Jain, M., Feldmanm, D.M., Dowden, P.C., DePaula, R.F., Jia, Q.X., "Rectifying current-voltage characteristics of $BiFeO_3$/Nb-doped $SrTiO_3$ heterojunction" *Appl. Phys. Lett.* **92**(10), 2008.

[148] Orendorez, A., Wüsten, J., Ziegler, C., Gnaser, H., "Photoelectron spectroscopy of nanocrystalline anatase TiO_2 films" *Appl. Surf. Sci.* **252**(1), 2005.

[149] Ju, S., Kim, S, Mohammadi, S., Janes, D.B., Ha, Y.-G., Facchetti, A., Marks, T.J., "Interface studies of ZnO nanowire transistors using low-frequency noise and temperature measurements" *Appl. Phys. Lett.* **92**(2), 2008.

[150] Gavrilov, S.A., Dronov, A.A., Shevyakov, V.I., Belov, A.N., Poltoratskii, E.A., "Ways to Increase the Efficiency of Solar Cells with Extremely Thin Absorption Layers" *Nanotech. Russ.* **4**(3-4), 2009.

[151] MDI JADE 7.0 XRD Analysis Software and Database, CRF, Drexel University

[152] Winter, M., WebElements, "WebElements Periodic Table of the Elements | Zinc | zinc oxide" <http://www.webelements.com/compounds/zinc/zinc_oxide.html> Accessed 05OCT2010.

[153] Wellings, J.S., Samantilleke, A.P., Warren, P., Heavens, S.N., Dharmadasa, I.M., "Comparison of electrodeposited and sputtered intrinsic and aluminum-doped zinc oxide thin films" *Semicond. Sci. Technol.* **23**(12), 2008.

[154] Chatman, S., Emberley, L., Poduska, K.M., "Significant Carrier Concentration Changes in Native Electrodeposited ZnO" *ACS Appl. Mater. Interfaces* **1**(10), 2009.

[155] Barthelmy, D., Mineralogy Database "jPOWD Applet for Brookite mineral structure data" <http://webmineral.com/jpowd/JPX/jpowd.php?target_file=Brookite.jpx> Accessed 05OCT2010. (noted based on Meagher E P , Lager G A , The Canadian Mineralogist, 17 (1979) p.77-85, Polyhedral thermal expansion in the TiO2 polymorphs: Refinement, of the crystal structures of rutile and brookite at high temperature, Sample at 25 degrees C)

[156] Barthelmy, D., Mineralogy Database "jPOWD Applet for Rutile mineral structure data" <http://webmineral.com/jpowd/JPX/jpowd.php?target_file=Rutile.jpx> Accessed 05OCT2010. (noted based on Wyckoff R W G , Crystal Structures , 1 (1963) p.239-444, Second edition. Interscience Publishers, New York, New York)

[157] Barthelmy, D., Mineralogy Database "jPOWD Applet for Anatase mineral structure data" <http://webmineral.com/jpowd/JPX/jpowd.php?target_file=Rutile.jpx> Accessed 05OCT2010. (noted based on Horn M , Schwerdtfeger C F , Meagher E P , Zeitschrift fur Kristallographie , 136 (1972) p.273-281, Refinement of the structure of anatase at several temperatures, Sample: T = 25 C, Locality: Legenbach quarry, Binnatal, Switzerland)

[158] Morgan, B.J., Watson, G.W., "Intrinsic n-type Defect Formation in TiO_2: A Comparison of Rutile and Anatase from GGA+U Calculations" *J. Phys. Chem. C* **114**(5), 2010.

[159] Singh, S.K., Ishiwara, H., "Micro-structure and ferroelectric properties of $BiFeO_3$ thin films formed on Pt-coated r-plane sapphire substrates" *J. Electroceram.* **16**(4), 2006.

[160] Katz, S., McIntyre, P., Paul C. McIntyre Research Group "McIntyre Group Webpage, Stanford University – 'Ferroelectric Thin Films'" <http://www.stanford.edu/group/mcintyre/Ferro.html> Accessed 05OCT2010.

[161] O'Regan, B., Lenzmann, F., Muis, Wienke, J., "A Solid State Solar Cell Fabricated with Pressure-Treated P25-TiO_2 and CuSCN: Analysis of Pore filling and IV Characteristics" *Chem. Mater.* **14**(12), 2002.

[162] Madjidi, H. and Baxter, J.B. [informal] 'Standard' cleaning procedure for FTO-glass substrates, NEAT Laboratory, Chemical And Biological Engineering, Drexel University.

[163] McPeak, K.M., "Chemical Bath Deposition of Semiconductor Thin Films & Nanostructures in Novel Microreactors" (sp. ref.) *PhD Dissertation* (adv. Dr. Jason Baxter), Drexel University (Chemical and Biological Engineering), 03SEPT2010.

[164] Kontos, A.I., Kontos, A.G., Tsokleris, D.S., Bernard, M.-C., Spyrellis, N., Falaras, P., "Nanostructured TiO_2 films for DSSCS prepared by combining doctor-blade and sol-gel techniques" *J. Mater. Proc. Technol.* **196**(1-3), 2008.

[165] Arabatzis, I.M., Stergiopoulos, T., Bernard, M.C., Labou, D., Neophytides, S.G., Falaras, P., "Silver-modified titanium dioxide thin films for efficient photodegradation of methyl orange" *Appl. Catal. B: Environ.* **42**(2), 2003.

[166] Arabatzis, I.M., Antonaraki, S., Stergiopoulos, T., Hiskia, A., Papaconstantinou, E., Bernard, M.C., Falaras, P. "Preparation, characterization and photocatalytic activity of nanocrystalline thin film TiO_2 catalysts towards 3,5-dichlorophenol degradation" *J. Photochem. Photobiol. A : Chem.* **149**(1-3), 2002.

[167] Kang, T.-S., Smith, A.P., Taylor, B.E., Durstock, M.F., "Fabrication of Highly-Ordered TiO_2 Nanotube Arrays and Their Use in Dye-Sensitized Solar Cells" *Nano Lett.* **9**(2), 2009.

[168] Kumara, G.R.R.A, Konno, A., Senadeera, G.K.R., Jayaweera, P.V.V., De Silva, D.B.R.A., Tennakone, "Dye-sensitized solar cell with the hole collector p-CuSCN deposited from a solution in n-propyl sulphide" *Sol. Energ. Mater.* **69**(2), 2001.

[169] Vehoff, T., “X-Ray Physics” Journal club for Organic Electronics research group (adv. Adrienko, D.), Max Planck Institute (Polymer Research), 15AUG2007 <http://www.mpip-mainz.mpg.de/~andrienk/journal_club/xray.pdf> Accessed 07OCT2010.

[170] May, S. [‘informally shared’], Debye-Scherrer equation and Instrumental line broadening, from Lecture slides on X-Ray Diffraction (XRD) from MatE 515: Experimental Techniques (Fall 2009).

[171] Tena-Zaera, R., Ryan, M.A., Katty, A., Hodes, G., Bastide, S., Levy-Clement, C., “Fabrication and characterization of ZnO nanowires/CdSe/CuSCN eta-solar cell” *C.R. Chimie* **9**(5-6), 2006.

[172] An, B.-K., Mulherin, R., Langley, B., Burn, P., Meredith, P., “Ruthenium complex-cored dendrimers: Shedding light on efficiency trade-offs in dye-sensitized solar cells” *Organic Electr.* **10**(7), 2009.

[173] Tachibana, Y., Hara, K., Sayama, K., Arakawa, H., “Quantitative Analysis of Light-Harvesting Efficiency and Electron-Transfer Yield in Ruthenium-Dye-Sensitized Nanocrystalline TiO_2 Solar Cells” *Chem. Mater.* **14**(6), 2002.

[174] Rusu, R.S., Rusu, G.I., “On the Electrical and Optical Characteristics of CdO Thin Films” *J. Optoelect. Adv. Mater.* **7**(2), 2005.

[175] Pankove, J.I. *Optical Processes in Semiconductors*, Dover, New York, 1975. courtesy of Google Books <http://books.google.com/books?id=HHM9Vo0DYZAC&dq=Optical+Processes+in+Semiconductors&source=gbs_navlinks_s> Accessed 06OCT2010.

[176] Rani, S., Sanghi, S., Agarwal, A., Khasa, S., “Influence of Nb_2O_5 on the optical band gap and electrical conductivity of $Nb_2O_5{\cdot}BaO{\cdot}B_2O_3$” *IOP Conf. Ser.-Mater. Sci.+Eng.* **2**(1), 2009.

[177] Nam, C.-Y., conversations and brief lesson [informal] about photovoltaic devices and I-V characterization (during BNL-SULI internship), Summer 2009.

[178] Bera, S.C., Singh, R.V., Garg, V.K., “A Temperature Dependent PIN Diode Model For Simple Temperature Invariant Attenuator Circuits” *Microwave Journal* **48**(2), 2005.

[179] Google search/calculator result “Planck’s constant in eV/nm”

[180] Wikipedia “Titanium dioxide” <http://en.wikipedia.org/wiki/Titanium_dioxide> Accessed 06OCT2010.

[181] Winter, M., WebElements "WebElements Periodic Table of the Elements | Titanium | titanium dioxide" <http://www.webelements.com/compounds/titanium/titanium_dioxide.html> Accessed 07OCT2010.

[182] Shih, W.-H., "Laboratory II: Aqueous Synthesis of CdS and ZnS Quantum Dots (1 week)" *MatE 345: Ceramics Processing*, Drexel University, Winter Term 2009.

[183] Ohno, T., Sarukawa, K., Tokieda, K., Matsumura, M., "Morphology of a TiO_2 Photocatalyst (Degussa, P-25) Consisting of Anatase and Rutile Crystalline Phases" *J. Catalysis* **203**(1), 2001.

[184] Spanier, J.E. [informal] conversations+email about leakage currents and effects on polarization and dielectric/hysteresis behavior in BFO, etc., Drexel University, Fall Term, 2010.

[185] McGuckin, T. [informal] conversations about contacting requirements and issues relating to metallization on CuSCN in eta-/DSSC-type devices, Mesoscaled Materials Laboratory, Materials Science and Engineering, Drexel University, Fall 2010.

[186] Ayalew, T., "3.1.6.2 Schottky Contact" *from online dissertation* JAN2004; <http://www.iue.tuwien.ac.at/phd/ayalew/node56.html> Accessed 16OCT2010.

[187] Nave, R., "Work Functions for Photoelectric Effect" (from Tipler, Llwellyn, 3rd ed.) <http://hyperphysics.phy-astr.gsu.edu/hbase/tables/photoelec.html> Accessed 16OCT2010.

[188] Wikipedia "Ohmic contact" <http://en.wikipedia.org/wiki/Ohmic_contact> Accessed 16OCT2010

[189] Snaith, H.J., Grätzel, M., "The Role of a "Schottky barrier" at an Electron-Collection Electrode in Solid-State Dye-Sensitized Solar Cells" *Adv. Mater.* **18**(14), 2006.

[190] Gallo, E. [informal] conversations about preventing leakage in BFO film-based PV devices, Mesoscaled Materials Laboratory, Materials Science and Engineering, Drexel, University, Summer 2010.

[191] Gallo, E. [informal] conversations about IV-characterization of BFO(?)/ZnO/FTO-glass devices, Mesoscaled Materials Laboratory, Materials Science and Engineering, Drexel, University, Fall 2010.

[192] McGuckin, T. [informal] conversations about persistent photocurrent in BFO(?)/ZnO/FTO-glass devices, Mesoscaled Materials Laboratory, Materials Science and Engineering, Drexel, University, Fall 2010.

[193] Qi, X., Dho, J., Tomov, R., Blamire, M.G., MacManus-Driscoll, J.L., "Greatly reduced leakage current and conduction mechanism in aliovalent-ion-doped $BiFeO_3$" *Appl. Phys. Lett.* **86**(6), 2005.

[194] Yu, B., Li, M., Liu, J., Guo, D, Pei, L., Zhao, X., "Effects of ion doping at different sites on electrical properties of multiferroic $BiFeO_3$ ceramics" *J. Phys. D: Appl. Phys.* **41**(6), 2008.

[195] Yan, J., Hu, G.D., Chen, X.M., Wu, W.B., Yang, C.H., "Ferroelectric properties, morphologies, and leakage currents, or $Bi_{0.97}La_{0.03}FeO_3$ thin films deposited on indium tin oxide/glass substrates" *J. Appl. Phys.* **104**(7), 2008.

[196] Xu, X.S., Ihlefeld, J.F., Lee, J.H., Ezekoye, O.K., Vlahos, E., Ramesh, R., Gopalan, V., Pan, X.Q., Schlom, D.G., Musfeldt, J.L., "Tunable band gap in $Bi(Fe_{1-x}Mn_x)O_3$ films" *Appl. Phys. Lett.* **96**(19), 2010.

[197] Presser, V., Schuster, B.-E., Casu, M.B., Heinemeyer, U., Schreiber, F., Nickel, K.G., Chassé, T., "Raman polarization studies of highly oriented organic thin films" *J. Raman. Spectroscopy* **40**(12), 2009.

[198] Deluca, M., Bermejo, R., Grünbichler, H., Presser, V., Danzer, R., Nickel, K.G, "Raman spectroscopy for the investigation of indentation-induced domain texturing in lead zirconate titanate piezoceramics" *Scripta Materialia* [in press], 2010.

[199] Hong, S., Klug, J.A., Park, M., Imre, A., Bedzyk, M.J., No, K., Petford-Lord, A., Auciello, O., "Nanoscale piezoresponse studies of ferroelectric domains in epitaxial $BiFeO_3$ nanostructures" *J. Appl. Phys.* **105**(6), 2009.

[200] Singh, S.K., Ishiwara, H., Maruyama, K., "Room temperature ferroelectric properties of Mn-substituted $BiFeO_3$ thin films deposited on Pt electrodes using chemical solution deposition" *Appl. Phys. Lett.* **88**(26), 2006.

[201] Scott, J.F., "Nanoferroelectrics: statics and dynamics" *J. Phys. Condens. Matter* **18**(17), 2006.

[202] Grizalez, M., Martinez, E., Caicedo, J., Heiras, J., Prieto, P., "Occurrence of ferroelectricity in epitaxial $BiMnO_3$ thin films" *Microelectronics Journal* [in press/online at: <http://www.cenm.org/productos/articulos/articulos/054.pdf > Accessed 21OCT2010], 2010.

[203] Nonnenmann, S.S., Leafer, O.D., Gallo, E.M., Coster, M.T., Spainer, J.E., "Finite Curvature-Mediated Ferroelectricity" *Nano Lett.* **10**(2)[published online], 2010.

[204] Spanier, J.E. [informal] conversations+email about finite curvature effects on a thin ferroelectric films and potential applications to BFO-'sensitized'-SCs, etc., Drexel University, Fall/Winter(?) Term, 2010.

[205] TradeBoss.com, "Xinyan Technology Ltd" <http://www.tradeboss.com/default.cgi/action/viewcompanies/companyid/175106/> Accessed 21OCT2010.

[206] Koenig, E., Hilpert, M., Messmer, K., "Method and Device for Printing Solar Cells By Screen Printing" *Patent App.* No. 0165661, 2009; from Patentdocs <http://www.faqs.org/patents/app/20090165661> Accessed 12OCT2010.